Master's thesis

NTNU
Norwegian University of Science and Technology
Faculty of Engineering
Department of Geoscience and Petroleum

Sanyam Ghimire

Analysis of the measured pore pressure and hydraulic data from Roskrepp hydropower plant

Master's thesis in Hydropower Development
Supervisor: Krishna Kanta Panthi
Co-supervisor: Kaspar Vereide
June 2023

NTNU
Norwegian University of
Science and Technology

Sanyam Ghimire

Analysis of the measured pore pressure and hydraulic data from Roskrepp hydropower plant

Master's thesis in Hydropower Development
Supervisor: Krishna Kanta Panthi
Co-supervisor: Kaspar Vereide
June 2023

Norwegian University of Science and Technology
Faculty of Engineering
Department of Geoscience and Petroleum

NTNU
Norwegian University of
Science and Technology

NTNU
Norwegian University of
Science and Technology

Department of
Geoscience and Petroleum

Your ref.: MS/I24T72/IGP/SGKKP Date: 16.01.2023

TGB4945 ENGINEERING GEOLOGY - MSc thesis
for
HPD student Sanyam Ghimire

Analysis of the measured pore pressure and hydraulic data from Roskrepp hydropower plant

Background

Most of the hydropower plants in Norway are operated in real-time with variable load (hydro-peak) following the development in the market situation. The plant operation with variable load results in periodic fluctuation of the pore pressure in the rock mass. The pore pressure fluctuation in the rock mass may cause hydraulic fatigue in the long run which may form new cracks (joints) leading to block failure over the time. In recent years, frequent block falls have been registered in many hydropower plants confirming the phenomenon of hydraulic fatigue.

In view of this, a prototype real-time pore-water pressure monitoring system in the rock mass was installed in 2018 at downstream end of the headrace tunnel at Roskrepp hydropower plant. The registered data until 2020 have been analyzed by Dr. Bibek Neupane in his PhD research. Now, more data are available which needed to be analyzed to assess on the overall trend of the pore pressure fluctuation in the rock mass so that the concept of long-term hydraulic fatigue is explained further.

MSc thesis task

This MSc thesis aims to conduct further assessment of pore pressure data from Roskrepp hydropower plant. The MSc thesis work will comprise the following tasks:

- Brief review on the concept used in the design of waterway system in Norway. Present recent development in the operation scenario of hydropower plants in Norway in a dynamic power market.
- Brief review of the properties of discontinuities in the rock mass and their hydraulic behaviour. Discuss the theory and principles of fatigue.
- Analyse the recorded pore pressure and hydraulic data of boreholes of Roskrepp hydropower plant and evaluate selected time periods with start-stop sequences.

- Simulate response of boreholes during transients based on data measured by real-time instrumentation.
- Evaluate transient induced blocks movements due to long-term operational fatigue of joints using UDEC simulations.
- Discuss the findings and conclude the thesis work.

Relevant computer software packages

The candidate shall use relevant computer hardware and software applicable to the tasks.

Background information for the study

- Relevant information such as reports, maps, information, and data given to the candidate by supervisors.
- Scientific papers, reports, and books in rock engineering, hydraulic and hydropower.

Supervisors

Professor Krishna K. Panthi is the main supervisor. The operator of Roskrepp power plant, Sira-Kvina kraftselskap, is the co-operating partner. Adjunct Associate Professor Kaspar Vereide is co-supervisor and the contact person from Sira-Kvina.

The project work has started on 9th January 2023 and to be completed by 11th June 2023.

The Norwegian University of Science and Technology (NTNU)
Department of Geoscience and Petroleum

January 16, 2023

Dr. Krishna K. Panthi
Professor of geological engineering, main supervisor

Note: This MSc task must be inserted in the MSc thesis after cover page

Abstract

There is change in operational regime of hydropower power plants in Norway after deregulation of energy markets and recent integration of renewable and unregulated energy sources such as wind and solar in an energy mix. Hydropower being a regulated system, their operators adjust production level based on demand and supply trends to get benefit from variable power prices. This causes an increase in the number of load changes in hydropower plants causing frequent pressure transients in the waterway system. The frequent pressure pulsations induce cyclic loading on rock mass resulting in rock mass fatigue over the long run and may contribute to increased instances of block falls.

This study is focused on understanding the effect of frequent start and stop sequences of hydropower in unlined pressure tunnels. For this purpose, it utilizes data from pore water pressure monitoring system which was installed at the downstream end of headrace tunnel at Roskrepp hydropower plant. This study describes a framework for accessing raw pressure data, evaluating Hydraulic Impact (HI) and Maximum Pressure Difference (MPD), and quantifying the impact of transients based on HI and MPD. HI was introduced earlier, whereas MPD is a new term proposed in this study to quantify the hydraulic stress exerted on the surrounding rock mass due to pressure transients in unlined hydropower tunnels. The monitoring of pressure data over the years clearly shows that the frequent load changes due to transient in the waterway could cause a considerable effect in the rock mass and constituent joint system. A delayed response to pressure from boreholes with respect to the tunnel is seen in all start and stop sequences and is considered as the main reason for instability arising due to transients. The response of pore pressure in boreholes is greatly influenced by the condition and properties of joint, its geometry and wall properties.

Results show that start sequence induces more HI and MPD than stop sequence. Numerically, the start sequence produces three times as much as HI than the stop sequence over the study period. It is seen that there are changes in operation pattern of hydropower and decrease in shutdown duration after late 2019 which has increased both HI and MPD in all boreholes. The study indicates that a faster shutdown duration induces more stress in the rock mass surrounding the tunnel. The HI can be as high as five times when the shutdown duration is decreased by 50 %.

A Machine Learning approach is attempted to predict the borehole pressure using LSTM method. The model works satisfactorily with MSE of 0.0055 and R2 of 0.82. However, this

approach cannot be used to evaluate the impact of transient at the moment and is potential prospect for future research work.

Analysis in UDEC program is carried out to evaluate the block movement due to change of roughness parameters of rock joints by transient induced cyclic loadings. Analysis indicates that there is increase in total and shear displacement of block when the roughness characteristics of rock joints are degraded due to cyclic fatigue of rock joints.

Finally, this study recommends minimizing the shutdown duration so that the impact caused by start and stop of hydropower in rock joints of unlined tunnels and shaft could be minimized, enhancing their lifetime. It is recommended to increase the number of instrumentation programs in other projects particularly where block falls are expected to better improve the understanding of transient induced instabilities in unlined pressure tunnels. This study also recommends implementing a more conservative design approach, particularly in tunnels with weak rock masses and projects that involve frequent load changes.

Acknowledgements

I would like to express my humble gratitude Krishna Kanta Panthi for his consistent advice, constructive suggestions, motivations, and encouragements. I heartily appreciate his warm and welcoming nature for fruitful discussion which has greatly contributed to shaping this manuscript. I gratefully acknowledge Kaspar Vereide for his guidance, and supportive attitude throughout the study period.

I express my sincere gratitude to Pawan Shrestha for his motivation and inspiration who helped me to know the practical applications and implications of Rock Mechanics during my early days as a Hydropower Engineer in Nepal. I am grateful to Bibek Neupane for his follow-up, advice, guidance, and timely responses to my queries through emails and meetings.

A special acknowledgment goes to Sira-Kvina kraftselskap for generously providing the necessary data to conduct the study. This study would not have been possible without their cooperation.

I record my deep-felt gratitude for my parents who motivated me all the time. I would also like to extend my thanks to my friends in Trondheim, who created a warm and supportive environment during my studies. Special thanks to my friends around my reading space who helped me a lot to assimilate with them when I was new at the department. I must acknowledge that this list is inevitably incomplete, and I sincerely apologize for any inadvertent omissions of those who have cooperated with me in this endeavor.

Trondheim, June 2023

Sanyam Ghimire

Table of Contents

Abstract i

Acknowledgements iii

Table of Contents iv

List of Acronyms vii

List of Figures viii

List of Tables x

1 Introduction 1

1.1 Background for study 2

1.2 Problem Description 2

1.3 Objectives and Scope 4

1.4 Coordination Schema of Research 5

1.5 Organization of Study 6

2 Hydropower tunnels in Norway 7

2.1 Introduction 7

2.2 Design concept 8

2.3 Block fall events 12

2.4 Past and present operation scenario 13

3 Theory 16

3.1 Rock Mass Properties 16

3.1.1 Uniaxial Compressive Strength 17

3.1.2 Deformation modulus 18

3.1.3 Joint Stiffness 19

3.1.4 Rock Stresses 19

3.1.5 Shear Strength 20

3.1.6 Joint Dilation 22

3.1.7 Discontinuties and their properties 23

3.2 Modified cubical law:.....25
3.2.1 Joint character.....26
3.3 Numerical Modelling.....26
3.4 Surge Tank.....29
3.5 Signal Processing.....31
3.5.1 Nyquist criterion.....31
3.5.2 Butterworth Filter.....32
3.5.3 Fast Fourier Transform (FFT).....33
3.6 LSTM.....33
4 Fatigue in rock mass.....35
5 Hydropower case project.....39
5.1 Brief on Roskrepp HPP.....39
5.2 Instrumentation Location.....41
5.3 Instrumentation and Data acquisition.....44
6 Analysis and interpretation of acquired data.....47
6.1 Analysis.....47
6.1.1 Overview of Analysis.....47
6.1.2 Finding Peaks for data extraction.....48
6.1.3 Natural frequency of oscillation.....50
6.1.4 Shutdown.....54
6.1.5 Quantifying the impact.....56
6.1.6 Method of calculating HI and MPD.....59
6.2 Results.....60
6.2.1 Pore pressure response.....60
6.2.2 Start and stop sequence.....64
6.2.3 Effect of Shutdown duration.....66
6.2.4 Effect of initial water head.....70

6.2.5 Correlation analysis 71
6.3 Machine Learning for predicting borehole pressure 73
7 Numerical analysis by UDEC simulation 75
7.1 Model set-up 75
7.1.1 Choice of cross-section and model design 75
7.2 Material Properties and Parametric Assessment 77
7.3 Modelling 79
7.4 Results 81
8 Discussion 84
8.1 Behavior of boreholes 84
8.2 Joint Characteristics 85
8.3 Natural, Cutoff and Sampling frequency 85
8.4 Effect of Water hammer and mass oscillation 86
8.5 Predicting borehole pressure 87
8.6 UDEC modelling 87
8.7 Fatigue Process 89
8.8 Design Practice 91
8.9 Operational requirements 92
9 Conclusions and recommendations 93
9.1 Conclusions 93
9.2 Limitations 94
9.3 Recommendations 95
References 97
Personal Communication 106

List of Acronyms

BH	Bore Hole
DEM	Discrete Element Method
FEM	Finite Element Method
FEM	Finite Element Method
FFT	Fast Fourier Transformation
FoS	Factor of Safety
HI	Hydraulic Impact
Hz	Hertz
IRENA	International Renewable Energy Agency
JRC	Joint Roughness Coefficient
LSTM	Long Short Term Memory
MIV	Main Inlet Valve
ML	Machine Learning
MO	Mass Oscillation
MPD	Maximum Pressure Difference
MSE	Mean Square Error
NSE	Nash Sutcliffe Efficiency
UDEC	Universal Distinct Element Code
WH	Water Hammer

List of Figures

Figure 1-1: Framework of study 5

Figure 2-1: Layout of waterway and powerhouse in Norwegian hydropower schemes..... 7

Figure 2-2: Development of unlined pressure tunnels and shafts in Norway..... 8

Figure 2-3: Parameters used in rule of thumb design criteria for unlined pressure shaft and tunnels. 9

Figure 2-4: L/H ratios of unlined pressure shafts vs inclination of valley side, β 10

Figure 2-5: Example of rock fall which may be due to dynamic pressure from transients 13

Figure 2-6: Increase in market share (Energy production) of renewables in Norway..... 14

Figure 3-1: The commonly used rock joint shear strength criteria..... 22

Figure 3-2: Joint roughness types 24

Figure 3-3: Schematic representation of discontinuties properties in a rock mass..... 25

Figure 3-4: Schematic profile of surge tank along with waterway system. 30

Figure 3-5: High, Low and Band pass filter 33

Figure 3-6: Schematic representation of Long Short Term Memory (Lees et al., 2022) 34

Figure 4-1: S-N material for different rock samples..... 35

Figure 4-2: Brazilian disc specimens of Brisbane tuff after failure..... 36

Figure 4-3: CT scan images of cracked chevron-notched Brazilian disc 36

Figure 4-4: Fatigue failure in rock joint of sandstone samples..... 37

Figure 5-1: Location Map of Roskrepp Hydropower Plant along with geological setting..... 39

Figure 5-2: Series of interconnected hydropower system including Roskrepp hydropower... 40

Figure 5-3: Details of instrumentation location..... 41

Figure 5-4: 3D laser scanned isometric view showing location of borehole..... 42

Figure 6-1: Formulated methodology flowchart for data extraction 48

Figure 6-2: Dataset of 2021-05 without extracted peaks. 49

Figure 6-3: Dataset of 2021-05 after extraction. 49

Figure 6-4: Results of FFT analysis applied in mass oscillation. 51

Figure 6-5: Time period of mass oscillation over the study period. 52
Figure 6-6: Results of FFT analysis applied only in water hammer surge wave. 53
Figure 6-7: Shutdown duration and the initial pressure head 55
Figure 6-8: Shutdown duration over the years. 56
Figure 6-9: Response of pore pressure of all the boreholes and tunnel 57
Figure 6-10: Schematic figure representing quantification parameters for impact of transients in rock mass. 58
Figure 6-11: Cutoff frequencies used for quantifying impact. 59
Figure 6-12: Water pressure data of tunnel and boreholes in a typical stop sequence 61
Figure 6-13: Cumulative hydraulic impact for boreholes and tunnel pressure. 62
Figure 6-14: Cumulative maximum pressure difference for boreholes and tunnel pressure. 62
Figure 6-15: Water pressure data of tunnel and boreholes in a typical start sequence 63
Figure 6-16: Water pressure data of tunnel and boreholes in a typical start sequence 64
Figure 6-17: Hydraulic Impact of boreholes in start and stop sequences for BH1, BH2 and BH4. 66
Figure 6-18: Typical stop sequence before late 2019 and after late 2019. 67
Figure 6-19: Hydraulic impact by mass oscillation and water hammer of stop sequences 68
Figure 6-20: Maximum pressure difference by mass oscillation and water hammer of stop sequences 69
Figure 6-21: Hydraulic Impact for boreholes vs initial water head. 70
Figure 6-22: Maximum pressure difference for boreholes vs initial water head 71
Figure 6-23: Correlation between different variables of transients. 72
Figure 6-24: Period used for calibration and validation used in LSTM method. 73
Figure 6-25: Prediction of BH2 pressure using LSTM model 74
Figure 7-1: Geometry creation in UDEC. 76
Figure 7-2: Vector plot showing displacements in the UDEC model 81
Figure 7-3: Displacement in vertical direction vs Number of Cycles 82
Figure 7-4: Plot indicating shear displacement in joints in the UDEC model 83

Figure 8-1: Schematic representation of 4 types of boreholes.....84

List of Tables

Table 1-1: Coordination schema of the thesis work 5

Table 5-1: Joint orientation at project location.....41

Table 5-2: Joint characteristic at instrumentation location in the tunnel.....43

Table 5-3: Characteristics of boreholes 44

Table 7-1: Apparent spacing and dip of J1 and Jf used in UDEC modelling. 77

Table 7-2: Properties of intact rock in UDEC 78

Table 7-3: Overview of joint properties used in UDEC modelling. 78

Table 7-4: Values of joint roughness used in parametric study.....80

Table 8-1: Bore hole type and there response due to MO and WH.....85

1 Introduction

Hydropower has been the source of electricity since the late 19th century. In Norway, the first hydropower project was constructed in 1891. Over the years, hydropower projects have been developed in diverse geological and topographical settings with various layouts. In Norway, most of the hydropower projects utilize unlined pressure tunnels as the primary waterway system, spanning a total length of over 4300 kilometers and operating at high heads, with the highest at 1047 meters (Panthi & Basnet, 2018). The high waterhead exerts high water pressure around the tunnels. The tunnels are designed to withstand the pressure exerted by the water to the surrounding rock mass of tunnel and support and lining are only provided where it is deemed necessary where the rock mass cannot withstand the internal water pressure. The design of high-pressure unlined tunnels uses maximum water head as parameter for design and does not consider occasionally occurring pressure transients which might have impact on long-term stability of tunnels.

In the past, most hydropower plants in Norway were primarily designed as base load energy supply systems. Deregulation of the energy market in Norway in 1991 (Bye & Hope, 2005) brought changes in the operation patterns of hydropower projects. Additionally, with the increasing presence of renewable and unregulated energy sources like solar and wind in the energy market, supply and demands changes the operational regime of hydropower plants, leading to base load hydropower systems being operated as peaking projects.

As a result, there is greater pressure on hydropower systems to regulate the energy mix and provide flexibility. This flexibility is achieved by swiftly starting or stopping the turbines to match the changing demand and supply in the energy market. Hydropower, being a regulated source of electricity, can offer flexibility in supply to balance the system for short or extended periods. Consequently, the future operation of hydropower is expected to be dynamic, characterized by frequent and significant changes in load of larger magnitudes. The fluctuation in the operation pattern of hydropower by more frequent and stronger changes in loads induces pressure transients in the waterway of hydropower and may pose stability issues in the long run.

In this context, there are increased threats to unlined tunnels due to block falls resulting from rock mass fatigue induced by increased dynamic operation (Bråtveit et al., 2016; Neupane, Panthi, et al., 2021). Therefore, a better understanding of transient and its impact on surrounding rock mass due to increased loading by transients is deemed necessary. There is

also a need to understand the response of the pore pressure of the rock mass during transients and its relation with other variables of power plant operations and the destabilizing forces caused by it.

1.1 Background for study

The supervising professor of this study conducted site visits to various tunnels in Norway and observed small blocks falling from the tunnel walls and roof (pers. com. Panthi, 2023). These block falls were unique and not believed to be caused by general stability issues. It was reported that new joints were formed locally, leading to the removal of blocks and subsequent failures in multiple locations. These cases were suspected to result not only from pre-existing joints but also from the cyclic loading behavior in the hydropower waterway system. To investigate the effects of frequent start-stop sequences, a real-time pore water pressure monitoring system was installed in the rock mass of the waterway system at the Roskrepp hydropower plant in 2018. Dr. Bibek Neupane analyzed the recorded data from 2018 to 2020 as part of his PhD research. Additional data is now available and needs to be analyzed to assess the overall trend of pore pressure fluctuations in the rock mass, providing further insights into the concept of long-term hydraulic fatigue. The analysis of the instrumented data aims to identify any changes recorded in the pore water pressure so that the concept of long-term hydraulic fatigue is explained further.

1.2 Problem Description

With the implementation of energy laws, integration of non-regulated, renewable, and volatile energy sources, as well as external factors such as war and economic embargoes, there is a growing demand for regulation and flexibility in the energy system. In Norway, 75% of electricity sources are flexible by the virtue of hydropower (Energifakta, 2021) so, the use of hydropower for flexibility and regulation in the system is increasing. This has resulted in frequent start and stop of the turbines and also increased the number of transient events in most of the hydropower plants in Norway.

The study from Neupane, Vereide, et al., (2021) shows that, on average, there are 200 to 400 start/stop events happening per turbine per year and these events are on increasing trend. Currently, there are 150 to 200 significant load changes occurring per year for turbines smaller than 50MW and it is projected that these load changes will increase by 30-45% between 2025 and 2040 for the power plants studied. In this context, the transient in hydropower is certainly in increasing trend which will induce more cyclic loading in surrounding rock mass of tunnel.

These transient induced cyclic load may cause threat to long-term instability due to cyclic fatigue (Neupane, Panthi, et al., 2021).

Most of the hydropower have been rehabilitated, upgraded or/and modernized after initial commissioning to increase the installed capacity via increasing the number of turbine or constructing newer powerhouse (Bråtveit et al., 2016). The upgradation of plants includes changing hydropower from generic to pumped storage or increasing discharge and velocity of water in the tunnel that changes the dynamic behavior of hydraulic system. However, the upgradation generally doesn't include upgradation of tunnel support system which consequently alters the response of tunnel to water pressure in surrounding rock mass.

The impacts of frequent and rapid changes of pore pressure in connection with block falls in hydro tunnel system is not known properly (Bråtveit et al., 2016). There is a lack of research on the effects of cyclic load from water transients in hydropower and its implications in unlined pressure tunnels (Neupane, 2021). It is even challenging to quantify the impact of transient on rock mass numerically as this is a new field of research. Furthermore, there is a need to develop a proper methodology for effectively analyzing raw pore water data obtained from instrumentation stations and quantifying the impact of transients on the rock mass. So, it is utmost necessary to investigate these topics in the research.

The previous study conducted by Neupane, (2021) focused solely on the analysis of the impact of transients during the stop sequence. However, it is deemed necessary to include the analysis of the start sequence as well in order to comprehensively understand the overall hydraulic impact resulting from both start and stop sequences.

The change in pressure due to transients in waterway is known and can be solved using the Method of Characteristics or Finite Difference Method (Wylie & Streeter, 1978). However, the changes in pore water pressure within the tunnel walls are highly unpredictable and depend on the variable characteristics of joints and the geological conditions of the tunnel. Making a reasonable assumption about the pore pressure based on the available data would provide valuable guidance for future research in this area.

According to the state-of-the-art design criteria for unlined tunnels (Palmström & Broch, 2017), minor rock falls are deemed acceptable as long as they do not have a notable impact on frictional loss or result in tunnel blockage. Design of unlined pressure tunnels includes confinement criteria assisted by rock stress measurement with validated 3D numerical modelling. However, these methods do not consider the mass oscillation and water hammer

effect in the tunnels. In a study conducted by Helwig, (1987), the depth at which significant transient pressures are transmitted to the surrounding rock mass was investigated. The results indicated that the impact of water hammer is limited to a relatively shallow zone in close proximity to the tunnel. Therefore, this aspect is not considered in the design of pressure requirements. So, it is necessary to analyze the phenomena of transient behavior to further understand its influence in unlined pressure tunnels.

Cyclic fatigue has been identified as cause of transient induced block falls due to cyclic loading (Neupane, Panthi, et al., 2021). The resulting stress changes due to cyclic loading causes deformation of joints (Olsson & Barton, 2001). To assess the long-term operational fatigue of joints, it is important to know the extent of block deformation using a numerical model. Additionally, analyzing the deformation of blocks can provide an impression of stability of the rock mass surrounding the tunnel.

1.3 Objectives and Scope

The objectives of this study are as follows:

1. To analyze the recorded pore pressure and hydraulic data of boreholes of Roskrepp hydropower plant.
2. To simulate response of borehole during transients based on available dataset.
3. To evaluate transient induced block movement due to long-term operational fatigue of joints by using UDEC software.

1.4 Coordination Schema of Research

This study maintained coherency by adhering to the coordination schema presented in Table 1-1. Overall framework of the study is illustrated in Figure 1-1.

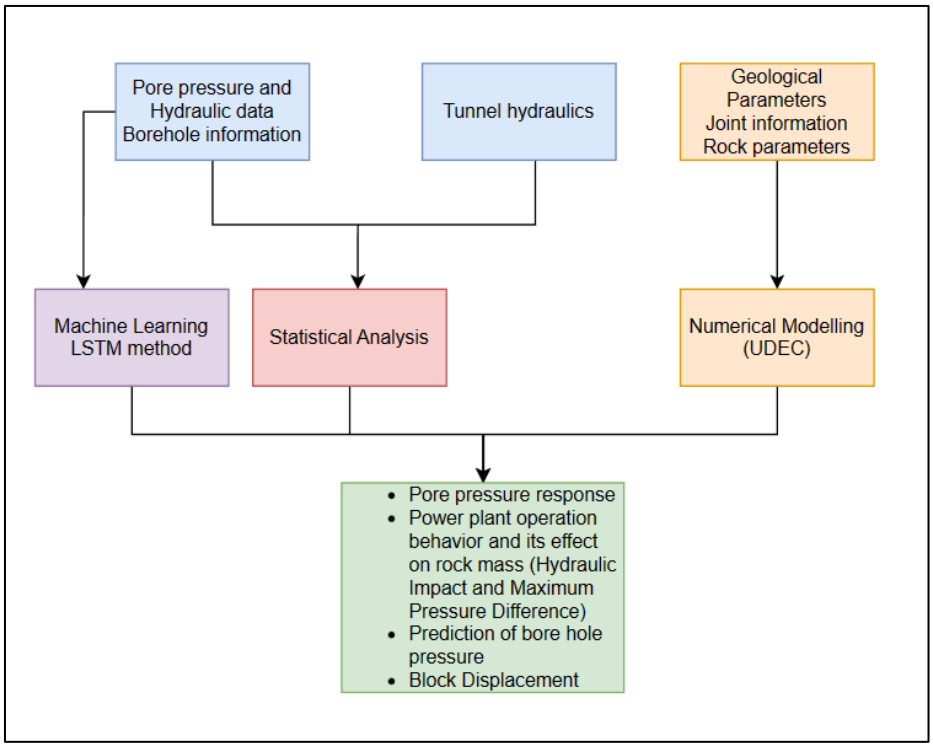

Figure 1-1: Framework of study

Table 1-1: Coordination schema of the thesis work

Key Problems	**Research Questions**	**Objectives**	**Material and Methods**	**Results**
The number of transient events in hydropower is increasing.	How much does transient impact the unlined pressure tunnel?	Analyze the borehole data to evaluate and quantify impact of hydraulic transients in unlined pressure tunnel.	(i)Remove noise from raw data and differentiate between mass oscillation (MO) and water hammer (WH). (ii)Calculate HI and MPD for WH and MO.	HI and MPD can be used as complementary values to quantify the impact of hydraulic transient in unlined pressure tunnel.

No means of predicting borehole pressure available in literature.	How does borehole pressure changes with respect to tunnel water pressure?	Predict the response of borehole using available data.	Predict borehole pressure using the LSTM method based on tunnel water pressure.	The LSTM method provides a fair estimation of borehole pressure, indicating a new direction for future research work.
Transient affects stability of the unlined pressure tunnel.	How much do blocks displace due to transients?	Evaluate transient induced block movement caused by degradation of joint roughness induced by cyclic fatigue.	Make a UDEC model and evaluate displacements due to change in roughness characteristics.	Block movement increases with roughness degradation and joint smoothening. Providing a proxy representation of the impact of long term operational fatigue on the stability of the unlined pressure tunnel.

1.5 Organization of Study

The thesis is organized in the following way:

Chapter 1: Introduction, Problem description and objectives

Chapter 2: Introduction to hydropower tunnels in Norway and its design concept

Chapter 3: Theory about rock mass, Surge tank, Numerical Modelling and Digital Signal Processing

Chapter 4: Literature review on Fatigue in rock mass

Chapter 5: Hydropower Case Project (Roskrepp Hydropower Plant)

Chapter 6: Statistical analysis of Data and quantification of impact due to transients

Chapter 7: Numerical Modelling (UDEC)

Chapter 8,9: Discussion, conclusions, and recommendations

2 Hydropower tunnels in Norway

2.1 Introduction

Unlined pressure tunnels are popular in Norway and other parts of the world due to its cost effectiveness, technical soundness, and timely completion rate (Panthi & Basnet, 2018). In 1906, the first Norwegian underground hydropower tunnel was built for Svelgfoss which started the history of usage of underground space for hydropower in Norway. However, until 1950, a conventional arrangement consisting of a surface powerhouse with a surface, or an underground penstock was used for hydropower depending upon the topography of the area (Figure 2-1a). After the first world war (1914-1918), due to the shortage of steel and uncertainty in delivery and price hike, four Norwegian hydropower stations with unlined pressure shafts were put into operation from years 1919 to 1921 with head varying from 72 to 152 m (Palmström & Broch, 2017). Three out of four projects faced problems during initial water fillings which were solved using extended penstock pipe and grouting (Panthi & Basnet, 2016). Up until 1958, an additional nine pressure shafts without lining were built but all of them had water heads that were below 100 meters.

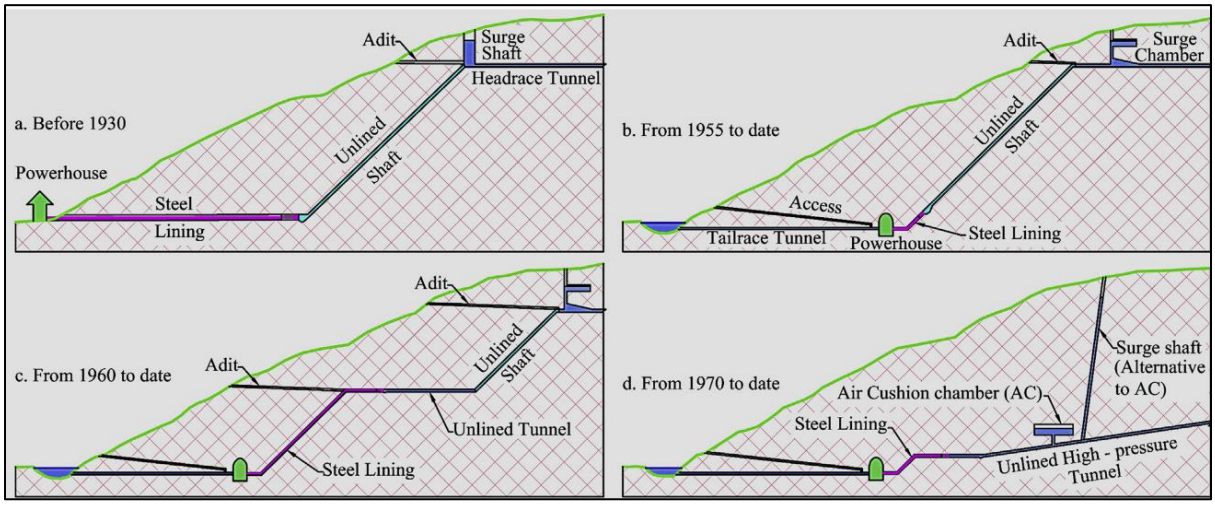

Figure 2-1: Layout of waterway and powerhouse in Norwegian hydropower schemes (Panthi & Basnet, 2018)

Before Tafjord K3 (1930-1955), the design principle of unlined low pressure headrace tunnel was used with high pressure lined penstock shaft and an underground powerhouse. After around 1960, a commonly used design solution in areas with topographical limitations involved a configuration that included a lower shaft along and a portion of the horizontal pressure tunnel located downstream of the unlined pressure shaft lined with steel (Figure 2-1c). Since 1965 the

unlined pressure tunnels have been a customary cost-effective solution for hydropower waterway layout arrangement.

Driva Hydropower project which came into operation in 1973, faced challenges in installing a vented surge chamber. This was due to the highly steep and difficult topography of the area for laying out access road to construction adits and top of surge shaft. This led to an innovative concept of air cushion surge chamber (Selmer-Olsen, 1974) which is an unlined underground cavern generally located very near to powerhouse at upstream portion of penstock shaft (Mosonyi, 1991)(Figure 2-1d). At present, Norway has air cushion surge chambers in 10 of its hydropower schemes as a means of controlling the upsurge oscillation resulting from sudden stoppage of the power plants.

Currently, Norway operates over 80 unlined high-pressure tunnels, which collectively span a total length exceeding 4000 km of head over 150 meters. These tunnels have an almost 99 percent success rate, with the unlined pressure tunnel with the highest head being 1047 meters (Panthi & Basnet, 2018). Figure 2-2 shows the history of development of unlined pressure tunnels and shafts in Norway.

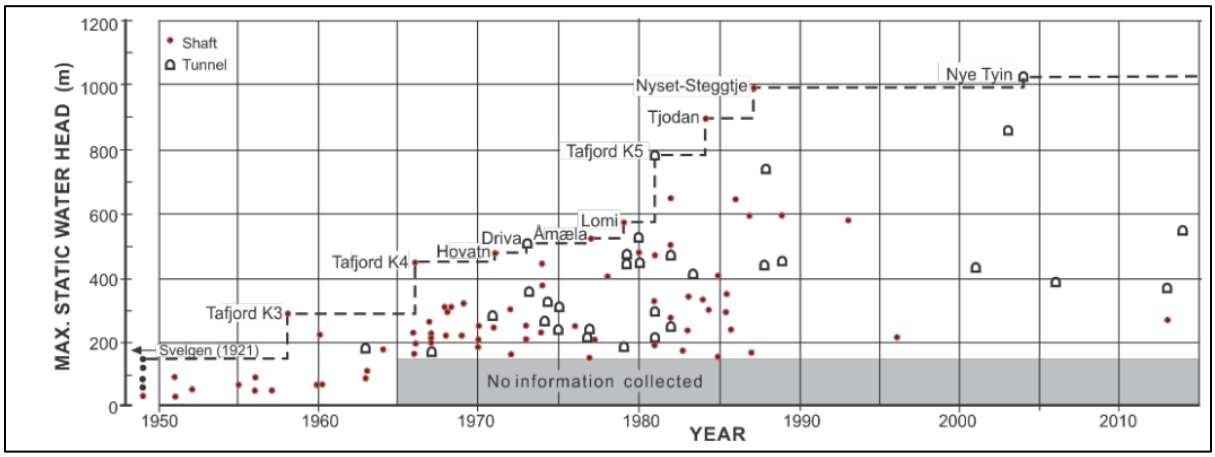

Figure 2-2: Development of unlined pressure tunnels and shafts in Norway (Palmström & Broch, 2017). *The dotted lines indicate increasing maximum head of Norwegian tunnels or shaft. Water head more than 150m is represented.*

2.2 Design concept

Initially the layout of hydropower in Norway included mostly surface structures. Due to difficult topography the penstocks in some of the hydropower had to be placed underground. The penstock were mostly steel lined and concrete was poured into the space between the lining and rock in order to transfer a portion of the water pressure onto the rock (Tøndevold, 2002). There was a need for steel-saving design due to steel shortage after the second world war. So,

it started by omitting the steel lining for some low-pressure schemes and gradually used for unlined shaft and tunnels for higher heads as well. This design concept utilizes the rock mass as a structural component and minimizes the consumption of steel in hydropower waterway.

Before 1968, a rule of thumb was used for designing unlined pressure shafts in Norway. Due to constructional limitations, the inclination of unlined shaft varied between 31º and 47º with most common being 45º (Broch, 1984a). The rule of thumb was expressed as in Equation (2-1) which should be valid for every location in tunnel.

$$h > c.H \qquad (2\text{-}1)$$

Where, h is the vertical depth of the location considered, H is the static water head (in m) at the location and c is a constant, which was 0.6 for valley sides with inclinations up to 35º and increased to 1.0 for valley sides of 60º. However, the valley sides steeper than 60º is bit uncommon in Norway. The parameters for rule of thumb are indicated in Figure 2-3.

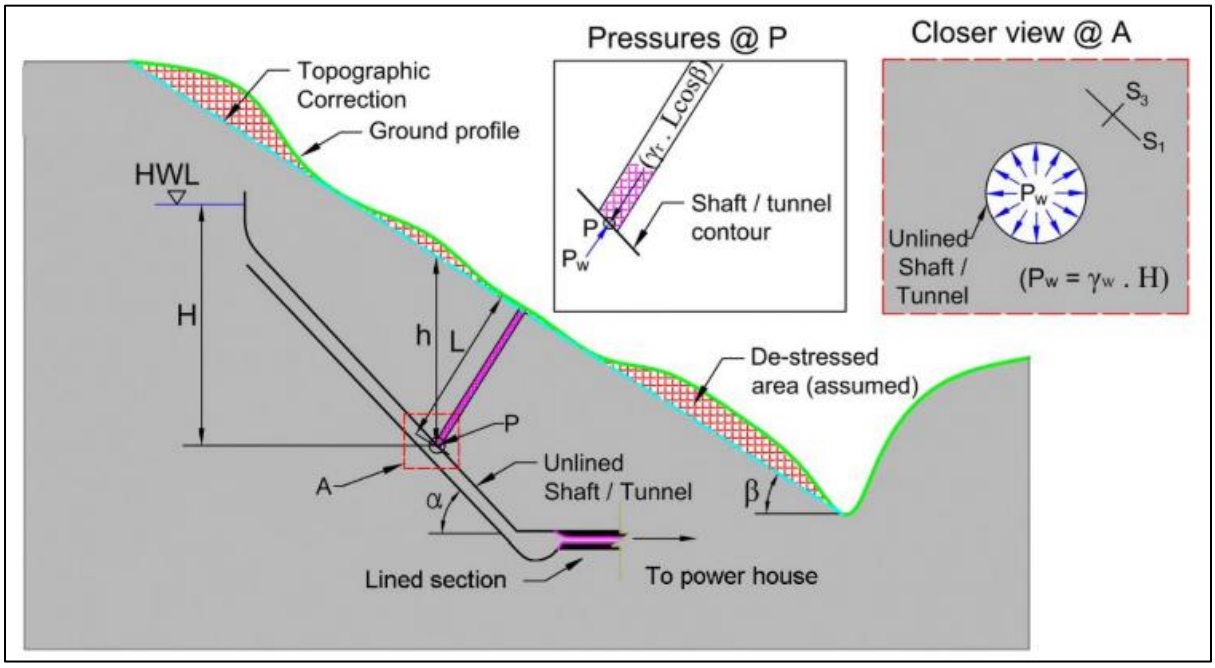

Figure 2-3: Parameters used in rule of thumb design criteria for unlined pressure shaft and tunnels. (S_1 is major principal stress, S_3 is minor principal stress and HWL is the head water level) (Neupane, 2021; Panthi & Basnet, 2021)

A revised rule of thumb came into practice which could cover the shafts slopes steeper than 45º after the failure of unlined pressure shaft at Byrte Hydropower with static water head of 300m which had an uncommon steepness of 60º. The revised rule of thumb (Selmer-Olsen, 1970) is expressed in Equation (2-2).

$$h > \frac{\gamma_w . H}{\gamma_r \cos \alpha} \qquad (2\text{-}2)$$

Where, γ_w is the density of water, γ_r is the density of the rock mass and α is the inclination of the shaft.

In 1970, another failure occurred in Åskora where the unlined tunnel was hydraulically split which led to a new rule of thumb (Equation (2-3)) introduced by Bergh-Christensen & Dannevig, (1971) where the inclination of the valley side was directly taken into account.

$$L > \frac{\gamma_w . H}{\gamma_r \cos \beta} \qquad (2\text{-}3)$$

These Norwegian "start-of-art" confinement criteria with topographic correction suggested by Broch, (1984b) for planning unlined pressure tunnels and shafts are based on equilibrium conditions and take considerations only of gravitational stresses against static water pressure. There was large leakage at Bjerka and Holsbru Hydropower even though they satisfy the criterion (Panthi & Basnet, 2016). The stress field is influenced by topography, geology, and geo-tectonics of the concern area. So, a stress state analysis by for instance 3D FEM numerical modelling is useful for taking account of those factors (Panthi & Basnet, 2018).

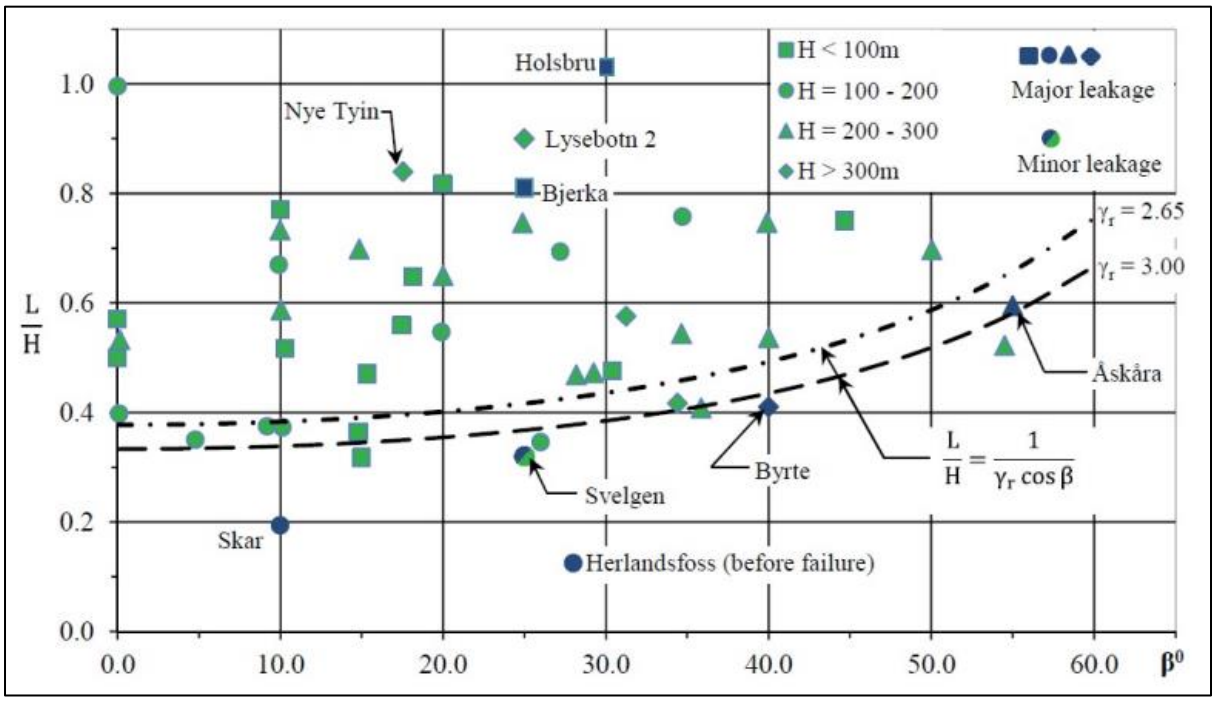

Figure 2-4: L/H ratios of unlined pressure shafts vs inclination of valley side, β (Panthi & Basnet, 2016)

In addition to this, the correct measurement of in-situ stresses at various locations of the project is essential to insure the safe implementation of unlined pressure tunnels. However, it is costly and demanding to carry out physical stress measurement at different locations. A validated rock stress model (Stephansson & Zang, 2012) could be used by integrating some measured stress data for predicting in-situ stresses along the proposed tunnel.

Due to cost effectiveness, unlined pressure tunnels are also used outside Norway (Neupane, 2021). However, there must be some considerations made before opting for an unlined pressure tunnel. From literatures (Basnet & Panthi, 2018; Broch, 1984a; Palmström & Broch, 2017), following design and operational criteria of unlined pressure tunnels and shaft can be outlined.

- The tunnels and shafts should be deep seated to avoid the conditions of hydraulic jacking ensuring in-situ minor principal stress larger than the pressure exerted by water. Valley bottoms generally have high stress concentrations that make Norwegian criterion overly conservative (Rancourt, 2010). Therefore, confinement criteria should be supplemented with rock stress measurements and numerical modelling in the final design.
- The initial water filling of the pressure shaft and tunnels should be done in a controlled way in stages so that any leakage can be detected, and an appropriate action can be taken in time. Similarly, dewatering should also be done in a controlled way to gradually relieve pore water pressure on walls with respect to tunnel pressure.
- Provided that rockfalls in specific sections of the tunnel do not significantly develop and result in increased head loss, the presence of several small blockages spread throughout the tunnel and will not cause any harm or disturbance to the operation of the hydropower.
- There must be follow up after the power production has started and measurement of change in head loss should be registered which may indicate change in roughness of surface or serious collapse in the waterway.

The design guidelines for unlined pressure tunnel design against water hammer an dmass oscillations is limited. Benson, (1989) recommended the Factor of Safety (FoS) against hydraulic jacking in normal operation of 1.3 and 1.1 during surges/mass oscillation. The FoS against water hammer is not available or recommended. Water hammer lasts not even more than few minutes and the water pressure does not have time to propagate deep into the rock mass (Rancourt, 2010). The influence of water hammer has been found to be confined to a relatively shallow area around the tunnel, and this is why it may not have

been considered into the design (Helwig, 1987). Neupane, (2021) stated that the water hammer may have higher influence than mass oscillation in some cases and cannot be ignored. Based on the review of literature, it can be understood that there is a gap of research and knowledge on how the pressure transients travel into the rock mass and its affect in long term stability of the tunnel.

2.3 Block fall events

With the increase of unsteady flow situations and transients due to change in energy markets, there is increased in structural instability in the tunnel systems as rock falls (Bråtveit et al., 2016). As mentioned in earlier section, minor falls and instabilities are acceptable while taking advantage of rock mass as a structural component in tunnel. It is difficult to ascertain the proper link between frequent and abrupt changes in water pressure in hydropower tunnel systems and the block fall event induced by them. These block falls reduce cross-sectional area and increase head loss, consequently loss of energy production and may lead to stoppage of power plant. It was concluded in the study of Bråtveit et al., (2016) that Norwegian hydropower tunnels that have been exposed to hydropeaking have experienced an increase in the frequency of rockfalls by a factor of 3 to 4 with reference to year 1991 with the average size of failed block reduced by 25%. Collection of failures of unlined pressure tunnels were presented in Neupane, (2021) and most of them were from insufficient support, support degradation, insufficient support in weak mass with or without swelling clay, hydraulic jacking, and dynamic power plant operation i.e. due to hydraulic transients. A particular failure case of Svandalsflona hydropower was further investigated and was found that the dynamic impact of water during mass oscillations had led joint infilling material to erode. This resulted in the opening of joints which propagated into the junction of concrete and rock masses over the years of operation. Consequently, the contact of the concrete structure with rock wall weakened over time, resulting in collapse of the structure (Neupane & Panthi, 2018). New block falls have also been reported in some recently inspected hydropower plants and they were suspected to be from cyclic loads due to transients (Figure 2-5, right). All these case studies indicate that the transients induced instabilities in hydropower tunnels are increasing and there is a need for further understanding of this phenomenon.

Figure 2-5: Example of rock fall which may be due to dynamic pressure from transients (left) (Bråtveit et al., 2016). *Right: Block fall seen in Ulset headrace tunnel in 2017* (Neupane, Vereide, et al., 2021)

2.4 Past and present operation scenario

Deregulation of energy markets started in Norway in the 1990s along with the implementation of Electricity act in 1991 aimed at creating competitive market for electricity (Bye & Hope, 2005). After that, the Nordic power market, regarded as one of the most successful power markets was established in 1993 (Bredesen, 2016). The situation at that time was characterized by a surplus of power as the production capacity significantly exceeded the level of power consumption. So, there was a need for competition in the power industry.

Until deregulation, 90 percent power from hydropower plants were typically operated to supply firm power on long-term contracts (Bye & Hope, 2005). Power producers had to supply electricity within their concessionary areas and fulfill their firm power contract commitments by entering into contracts with other power producers. The energy share of other renewables like solar and wind was also very low as compared to hydropower. Those conditions did not offer much flexibility to the energy market.

After the implementation of regulated market, hydropower plants started being operated based on market signals and the balanced based on supply and demand. This means that the hydropower operators must be able to adjust the output of their plants quickly and efficiently, depending on market conditions and other factors such as weather and hydrological conditions. Every day, electricity is bought and sold on a day-ahead market, where producers offer to generate a certain amount of electricity at a specific price, and consumers indicate how much they want to buy at various price ranges. The calculation of the Nord Pool system price is

determined by balancing the demand and supply schedules for each hour, which establishes the equilibrium price in the market (Nordpoolgroup, 2023). This needs rapid adjustment in the discharge in the hydropower consequently increasing the start and stop sequences to produce electricity in varying market.

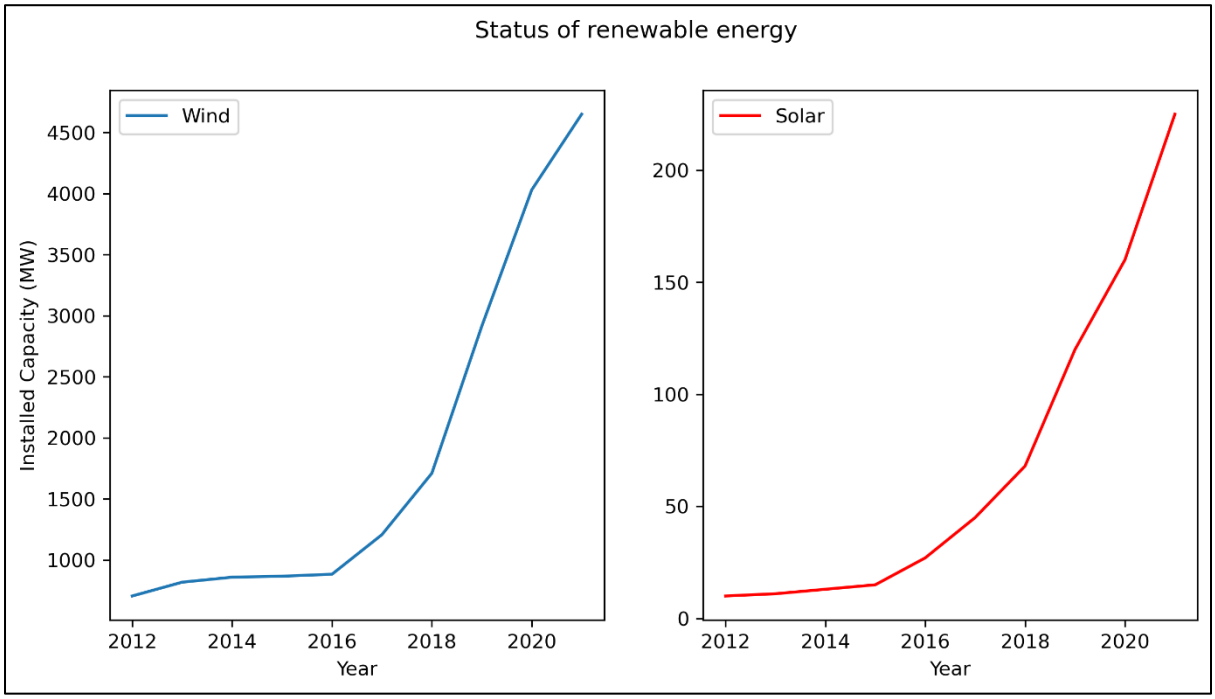

Figure 2-6: Increase in market share (Energy production) of renewables in Norway (IRENA, 2022)

Following the signing of the Paris Agreement in 2015, the global energy market has been undergoing a significant transformation as it moves away from fossil fuels and transitions towards renewable energy sources. Projections indicate a significant increase in the proportion of renewable energy in the electricity sector, expected to rise from 25% in 2017 to approximately 85% by 2050 which is expected to be largely driven by the expansion of solar and wind power generation (IRENA, 2018). It can also be seen from Figure 2-6 that the installed capacity of renewable energy source is drastically increasing from year 2016. The nature of wind and solar power generation presents certain challenges due to their variability. These sources of energy are dependent on specific conditions, such as sunlight and wind, which means they can only generate electricity when those conditions are present. Furthermore, the output of wind and solar power is difficult to dispatch, making it challenging to turn production on and off as needed. Additionally, predicting the amount of electricity that will be produced in the future can be difficult due to the variable nature of these energy sources. Due to the variability of energy sources, there is an increasing demand to improve the flexibility of current

power production and storage systems. Flexibility means capability to quickly adjust operations to maintain a balance between electricity production and consumption, while keeping costs as low as possible. Such flexibility is required both in the short-term, where changes must be made within minutes or seconds to balance the system, and in the long-term, to balance the system over days or weeks. Out of several solutions, regulated hydropower has the potential to provide both short- and long-term flexibility. Norwegian hydropower reservoirs account for roughly 50% of the total energy storage capacity available across all hydropower reservoirs in Europe (Eurelectric, 2011). This highlights the significant role that Norway's hydropower infrastructure plays in the continent's energy system, in terms of providing reliable and flexible energy supply.

The need of making hydropower flexible due to aforementioned reason will increase start and stop sequence of the power plants. It is projected that the average number of start/stop sequences are in increasing trend and would increase by 30-45% between 2025 and 2040 for some studied Norwegian power plants (Neupane, Vereide, et al., 2021). The author stated that there is a high probability that both the number and intensity of load changes will increase considerably in the future. As a result, this will lead to more frequent and stronger transients.

3 Theory

3.1 Rock Mass Properties

The rock is composed of naturally composed aggregate of minerals. The properties of the rock preliminary depend upon amount of minerals and their composition. The mineral composition creates inhomogeneity which is the major factor for anisotropy in rock. Rock mass consists of intact rock and discontinuties. The mechanical and physical properties of rock in its in-situ condition is generally described by the properties of rock mass. Nilsen & Thidemann, (1993) describes the rock mass characteristics in following categories:

Physical properties

Physical features of the rock such as hardness, density, porosity, degree of saturation, wave velocity, heat transfer and expansion etc.

Weathering of rocks

The process of disintegration and decomposition of the rock material is weathering of rocks. The weathering is caused by different ways viz. physical disintegration and by chemical decomposition. Rock mass undergoes mechanical breakdown and fragmentation which is primarily controlled by discontinuities, grain boundaries and mineral cleavages whereas chemical weathering involves decomposition and dissolution of rock mass. Superficial weathering in rock is caused by environmental and climatic factors whereas the weathering process at greater depth is largely influence by chemical weathering and is related to dissolution, oxidation and hydrothermal alteration (Panthi, 2006).

Jointing in rock mass

Properties of rock mass are highly influenced by the characteristics of joints and discontinuities. Tension forces are not transferred by joints like compressive and shear forces. The properties of joints will be discussed in the following sections.

Weakness Zones and Faults

Weakness and fault zones are major discontinuities in the rock mass, and they are generally considered as the weakest link and the preferred pathways for circulation of groundwater. Since they are relatively weaker and conductive section, they may be responsible for block failure during excavation or operation of hydro tunnels. The weakness and faults zone are categorized into two main divisions according to their properties. The first one includes layers of weak and schistose rock within a series of strong rocks and is referred to as zone of weak

rock. The second one includes zones of crushed rock formed by faulting or tectonic events (Nilsen & Thidemann, 1993).

For defining criteria, uniaxial compressive strength and deformation modulus of rock mass is generally estimated to know the strength and deformability of jointed rock mass (Hoek, 2006).

3.1.1 Uniaxial Compressive Strength

When the compressive strength of rock is measured, an intact specimen of rock is used which does not generally constitute of discontinuity as it is difficult to use a whole rock mass as a specimen. Therefore, there is certainly a scale effect when measuring the compressive strength of intact rock and representing the strength of a rock mass as a whole. There are some empirical formulae used to estimate the rock mass strength on the basis of UCS value of intact rock specimen. Some of them are presented from Equation (3-1) to (3-5).

$$\sigma_{cm} = \sigma_{ci} * exp\left[\frac{RMR - 100}{18.75}\right] \quad \text{(Bieniawski, 1993)} \quad \textit{(3-1)}$$

$$\sigma_{cm} = \sigma_{ci} * s^{a} = \sigma_{ci} * \left[exp\left[\frac{RMR - 100}{18.75}\right]\right]^{a} = \sigma_{ci} * \left[exp\left[\frac{RMR - 105}{9}\right]\right]^{a} \quad \text{(Hoek, 1994, 2006)} \quad \textit{(3-2)}$$

$$\sigma_{cm} = 5\gamma * Q_c^{1/3} = 5\gamma * \left[\frac{\sigma_{ci}}{100} * Q\right]^{1/3} \quad \text{(Barton, 2002)} \quad \textit{(3-3)}$$

$$\sigma_{cm} = \frac{\sigma_{ci}^{1.5}}{60} \quad \text{(Panthi, 2006)} \quad \textit{(3-4)}$$

$$\sigma_{cm} = \frac{\sigma_{ci}^{1.6}}{60} \quad \text{(Panthi, 2017)} \quad \textit{(3-5)}$$

Where, σ_{cm} is the unconfined compressive strength of the rock mass in MPa, σ_{ci} is the uniaxial compressive strength of intact rock (50 mm core diameter) in MPa, RMR is the Bieniawaski rock mass rating, s and a are the material constant related to Hoek-Brown failure criterion, GSI is the Geological Strength Index, γ is the density of rock (t/m^3), Q_c is the normalized rock mass quality rating and Q is the rock mass quality rating. To remove the subjectivity Panthi, (2006) suggests the use of σ_{ci} directly for calculating rock mass strength as other methods use highly subjective parameters such as RMR and Q value in calculation. The author suggests using Equation (3-4) for highly schistose and deformed rock mass and Equation (3-5) for strong and

brittle rock mass. The author also found that σ_{ci} is smallest when schistosity plane is inclined at around 30^o to the direction of loading.

3.1.2 Deformation modulus

The deformation modulus of the rock is the ratio of the stress corresponding strain during loading of rock mass including elastic and inelastic behavior. Due to the non-elastic behavior of jointed rock mass, the term "modulus of deformation" is used instead of the modulus of elasticity. However, laboratory test values for the deformation modulus are typically higher than the actual in-situ rock mass. Obtaining the in-situ deformation modulus through large-scale specimen testing is often impractical and costly. As a result, the availability of in-situ deformation modulus values is not available in most cases. So, different authors have presented empirical formula and some of them are listed from Equation (3-6) to (3-10).

$$E_m = 2RMR - 100 \quad \text{(Bieniawski, 1993)} \quad \textit{(3-6)}$$

$$E_m = 10^{\frac{RMR-10}{40}} \quad \text{(Serafim \& Pereira, 1983)} \quad \textit{(3-7)}$$

$$E_m = 10 * \left[\frac{Q * \sigma_{ci}}{100}\right]^{1/3} \quad \text{(Barton, 2002)} \quad \textit{(3-8)}$$

$$E_m = \left[1 - \frac{D}{2}\right]\sqrt{\frac{\sigma_{ci}}{100}}\ 10^{(GSI-10)/40} \quad \text{(Hoek et al., 2002)} \quad \textit{(3-9)}$$

$$E_m = \frac{1}{60} * E_{ci} * \sigma_{ci}^{0.5} \quad \text{(Panthi, 2006)} \quad \textit{(3-10)}$$

Where E_m is the deformation modulus of rock mass, E_{ci} is the intact rock modulus, GSI is the geological strength index, D is the disturbance factor which depends upon blast damage and stress relaxation.

Shear modulus (G) is a similar parameter to modulus of elasticity (E) which describes the relation between shear stress and shear deformation. A third elasticity parameter is bulk modulus (K) which describes the relationship between pressure and volume change (ITASCA, 2011). Both shear and bulk modulus can be calculated using E and poisons ratio (ν) , as shown in Equation (3-11) and (3-12) respectively (Goodman, 1989).

$$G = \frac{E}{2(1+\nu)} \quad \textit{(3-11)}$$

$$K = \frac{E}{3(1-2\nu)} \tag{3-12}$$

3.1.3 Joint Stiffness

When there is uniaxial loading of rock subjected to uniaxial loading containing a single set of uniformly spaced joints oriented perpendicular to the loading direction, Equation (3-13) and (3-14) applies for normal and shear stiffness of joints (ITASCA, 2023a).

$$k_n = \frac{E_m E_{ci}}{s(E_{ci} - E_m)} \tag{3-13}$$

$$k_s = \frac{G_m G_{ci}}{s(G_{ci} - G_m)} \tag{3-14}$$

3.1.4 Rock Stresses

Usually for an engineering design, materials are tested in the laboratory and the stress are ascertained quite appropriately. Unlike this, geological materials are preloaded with in-situ stress which is redistributed when an underground space is excavated thus inducing tangential stresses in the vicinity of opening (Hoek, 2006). This situation is complicated by the presence of structural features like joints, fractures, bedding, and schistosity planes. The combination of stresses perpendicular to the principal stress plane give three major principal stresses in the rock mass. They are called major, minor, and intermediate stresses. Three mutually perpendicular planes where shear stress is zero is called principal stress.

The main origin of in-situ stresses in the rock mass are induced by gravity, plate tectonic, history and topography. The in-situ stress is induced by four stresses which are given in the section below.

Gravitational stress:

Rock stress originated as a virtue of gravity alone and is called gravitational stress. In an elastic rock mass, there is a relationship between vertical and horizontal gravitational stress which is governed by Poisson's ratio. The expression of horizontal and vertical stresses is given in Equation (3-15) and (3-16) respectively.

$$\sigma_{\mathrm{v}} = \gamma \mathrm{h} \tag{3-15}$$

$$\sigma_h = \frac{\nu}{1-\nu}\sigma_{\mathrm{v}} \tag{3-16}$$

Where, σ_v is the vertical stress, σ_h is the horizontal gravitational stress, γ is the specific weight of overlying strata, ν is the Poisson's ratio of elastic rock.

Topographic Stress:

Usually there is negligible topographic stress when tunnelling is done on a plain surface deep underground. However, the topographic effect is induced due to the inclination of the valley side slope and has a very great effect on the rock stress situation. This situation is pronounced for example, in powerhouse where it is located at the bottom of the valley which is also known as valley effect. In such cases, the major principal stress near the surface aligns in a direction that is parallel to the slope of the valley, while the minor principal stress is oriented perpendicular to the slope.

Tectonic stress

There are different continental plates (about 20) which are dynamic and there is subduction or divergence of one plate to another. These causes great thrust or fault and induce tectonic stress (σ_{tec}). Due to the presence of tectonic stress, the horizontal stress is greater than that induced by gravity particularly in shallow and moderate depths as shown in Equation (3-17).

$$\sigma_h = \frac{\nu}{1-\nu}\sigma_v + \sigma_{tec} \qquad (3\text{-}17)$$

Residual stress:

Residual stress is remnant stress which has been locked in the rock material at earlier stages of its geological history. The most prominent example of this category pertains to the stress induced by the contraction of rock melt (magma) during cooling. Residual stresses can also result from the removal of the top layer due to glacial erosion. When vertical stresses are exceptionally high, they are generally attributed to residual stress (Shrestha, 2021).

3.1.5 Shear Strength

Shear strength of rock discontinuity is an important property that holds the rock block in place. When the shear strength of existing rock block is low, it results in structurally controlled block falls in tunnels by sliding and falling popularly known as wedge failure.

The most influential external factor that affects the shear strength is magnitude of effective normal stress acting across the joint. Additionally, the shear strength and deformation characteristics of joint walls can vary significantly depending on whether they are in contact or not, due to the mechanical differences between the two types of joints. When working with

unfilled joints, the roughness and compressive strength of the joint walls play an important role. However, in the case of filled joints, the primary focus is on the physical and mineralogical properties of the material that separates the joint walls (Barton & Choubey, 1977).

There are three commonly used rock joint shear strength criteria viz. Mohr-Coulomb, Patton (Patton, 1966) and Barton and Bandis (Barton & Choubey, 1977). The schematic representation for aforementioned shear strength criteria is illustrated in Figure 3-1.

The Mohr-Coulomb strength criterion is one of the most widely used strength criterion in soil and rock engineering model and design. The shear strength from Mohr-Coulomb criterion is given in Equation (3-18).

$$\tau = c + \sigma_n \tan\phi \qquad (3\text{-}18)$$

Where, τ is the shear strength of joint, c is the cohesion, σ_n is the normal stress and ϕ is the angle of internal friction.

Patton, (1966) suggested another equation for calculating shear strength of joint given in Equation (3-19).

$$\tau = \sigma_n \tan(\phi + i) \qquad (3\text{-}19)$$

Where, angle "i" refers to the angle at which the failure surfaces are inclined in relation to the direction of the applied shearing force.

Barton & Choubey, (1977) provides empirical relationship for shear strength that can be used to describe, fit, extrapolate, and even predict it both for weathered and unweathered joint which is given in Equation (3-20).

$$\tau = \sigma_n \tan\left[JRC\ log_{10}\left(\frac{JCS}{\sigma_n}\right) + \phi_r\right] \qquad (3\text{-}20)$$

Where, JRC is joint roughness coefficient, JCS is joint wall compressive strength and ϕ_r is residual frictional angle. The index testing required for shear strength calculation are Tilt test for ϕ_b (basic friction angle) and conversion to ϕ_r, Schmidt hammer test for obtaining rebound value for weathered joint (r) and unwethered core stick (R). Further explanations, procedure and illustrations of used indexes in Equation (3-20) can be found in Barton, (2013).

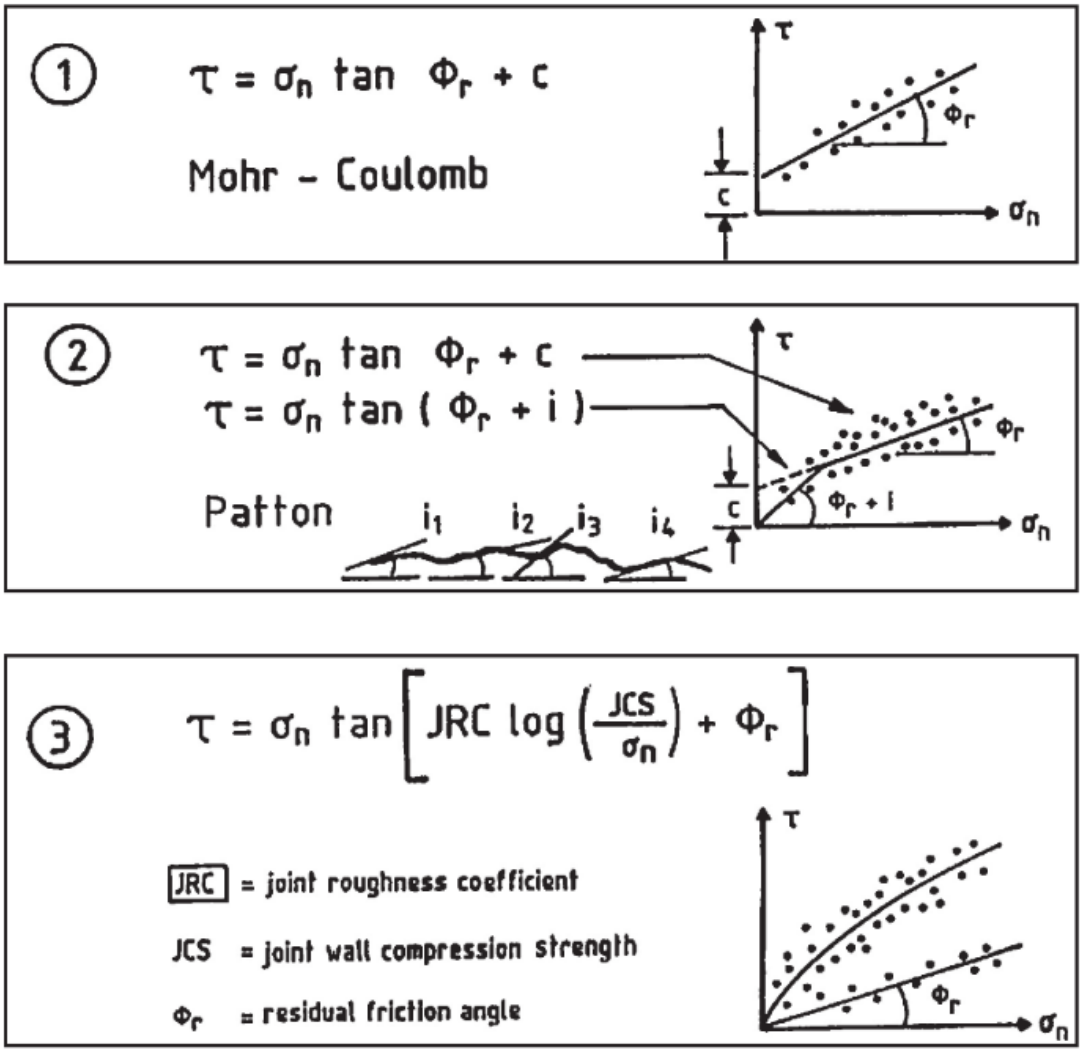

Figure 3-1: The commonly used rock joint shear strength criteria viz. Mohr-Coulomb, (Patton, 1966)*, and* (Barton & Choubey, 1977)*, are illustrated in figures with equations.*

3.1.6 Joint Dilation

When rocks undergo shear, it causes an expansion in the joint aperture. This expansion creates more room within the joint and changes its transmissivity, ultimately leading to a modification of the permeability of the rock mass (Zhou et al., 2018). Dilation is given in degrees and is given by Equation (3-21) (Barton & Choubey, 1977).

$$d = \frac{1}{2} \times JRC \times \log\left(\frac{JCS}{\sigma_n}\right) \qquad (3\text{-}21)$$

Where, σ_n is the normal stress acting in the joint.

3.1.7 Discontinuties and their properties

The rock mass is a matrix that consists of intact rock and discontinuties. Discontinuity, in general term, is the location having zero or low tensile strength. It is a collective terminology used for most of the types of joints, weak schistosity planes, weak bedding planes, weakness zones and faults (ISRM, 1978). For proper characterization of the rock mass, it is equally important to carefully describe the properties of discontinuties in addition to the intact rock mass as discontinuties largely determines the mechanical behavior of rock mass. The pressure transmission, fluid flow, displacement, and responsiveness of discontinuity due to pressure changes during transient are also largely affected by the properties of the joints.

The discontinuity is described by ten parameters (ISRM, 1978) viz, orientation, spacing, persistence, roughness, wall strength, aperture, filling, seepage, number of sets and block size. The schematic representation of discontinuties properties in a rock mass is shown in Figure 3-3. All these parameters affect how the rock mass behaves during transient in hydropower tunnel. The key attributes for characterization of rock discontinuity recommended by ISRM, (1978) and their relation to hydraulic behavior are listed below.

1. **Orientation**: Orientation of discontinuity in space expressed by dip direction and dip. The flow direction can be influenced by the orientation of a discontinuity with respect to the length axis of a tunnel (Panthi & Basnet, 2021). When a discontinuity is perpendicular to the fluid flow direction, it can obstruct fluid flow. Conversely, when it is parallel, it acts as conduit and can facilitate fluid flow. Inclined discontinuities can cause deviations from the original fluid path, which can alter the behavior of the flow.
2. **Spacing**: The distance measured at a right angle between two nearby discontinuities. Fluid pathways and their connectivity are affected by spacing of joints and discontinuities. Joints having narrow spacing can create a network of interconnected fractures which allows fluids to flow through the rock mass more easily. Conversely, wide spaced joints can act as barriers to flow of fluid which restrict the movement of fluid in rock mass.
3. **Persistence**: Persistence is the spatial extent of the discontinuity. A high persistence joint tends to be longer and relatively continuous which may create preferential pathways for flow of fluid within rock mass. In contrast, joints with low persistence are shorter and more isolated which may limit the fluid flow.
4. **Roughness**: Roughness is waviness or undulation related to the mean plane of discontinuity. Rough discontinuity surfaces can cause turbulence in the fluid flow,

increasing resistance to flow and reducing the overall flow rate. It is also an important parameter that governs the shear strength and stability of rock joints. To characterize the joint based on roughness, an empirical index called joint roughness coefficient (JRC) is usually used as shown in Figure 3-2.

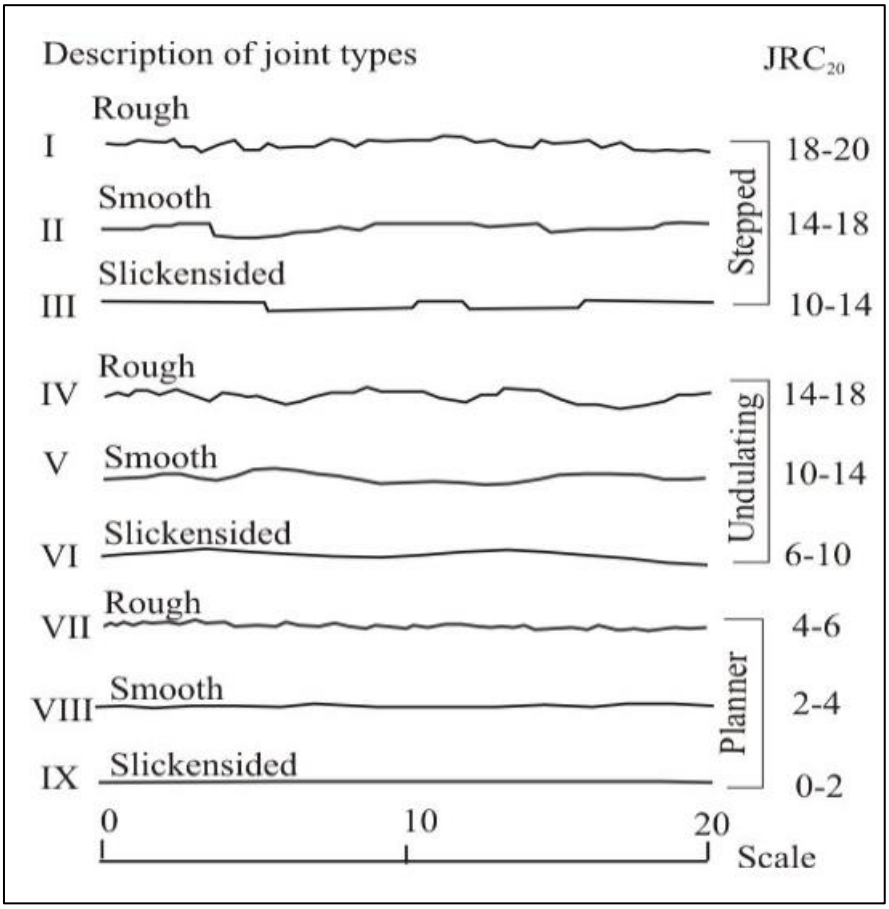

Figure 3-2: Joint roughness types modified by Panthi, (2006) *from* Barton & Bandis, (1990)

5. **Wall strength**: Wall strength is the compression strength of adjacent walls of discontinuity. It is an important variable that governs the shear strength of joint and is directly used in Barton-Bandis criteria.
6. **Aperture**: Aperture is the perpendicular distance between nearby rock walls of discontinuity. The aperture is the single most property of joint that affect significantly to the fluid flow. In fact, the flow is proportional to the aperture cubed, therefore, greatly defines joint responsiveness against transients. In this study, responsive joints are those that experience a significant change in their pore water pressure during transients, and conversely, non-responsive joints are those that show no or very little change in pore water pressure during transients.

7. **Filling**: The material infilled in the adjacent rock walls of discontinuity. Filling influences the fluid flow through the joint. If the filling is of clayey material with low permeability, the flow is minimum whereas the flow is higher due to higher permeability if the filling is of granular material.
8. **Seepage**: It indicates flow of water from joints. Seepage through joints indicates presence of water in the rock mass and connectivity to the source of water.
9. **Number of sets**: Number of joints in the joint system where they intersect each other. The flow of fluid increases as the number of sets increases as the interconnected and intersected joint allows fluid to flow freely through it.
10. **Block Size**: Dimensions of a rock block determined by the mutual orientation of intersecting sets of joints. When the block size is larger, it indicates a reduced presence of discontinuities in the rocks, resulting in less flow within the rock mass.

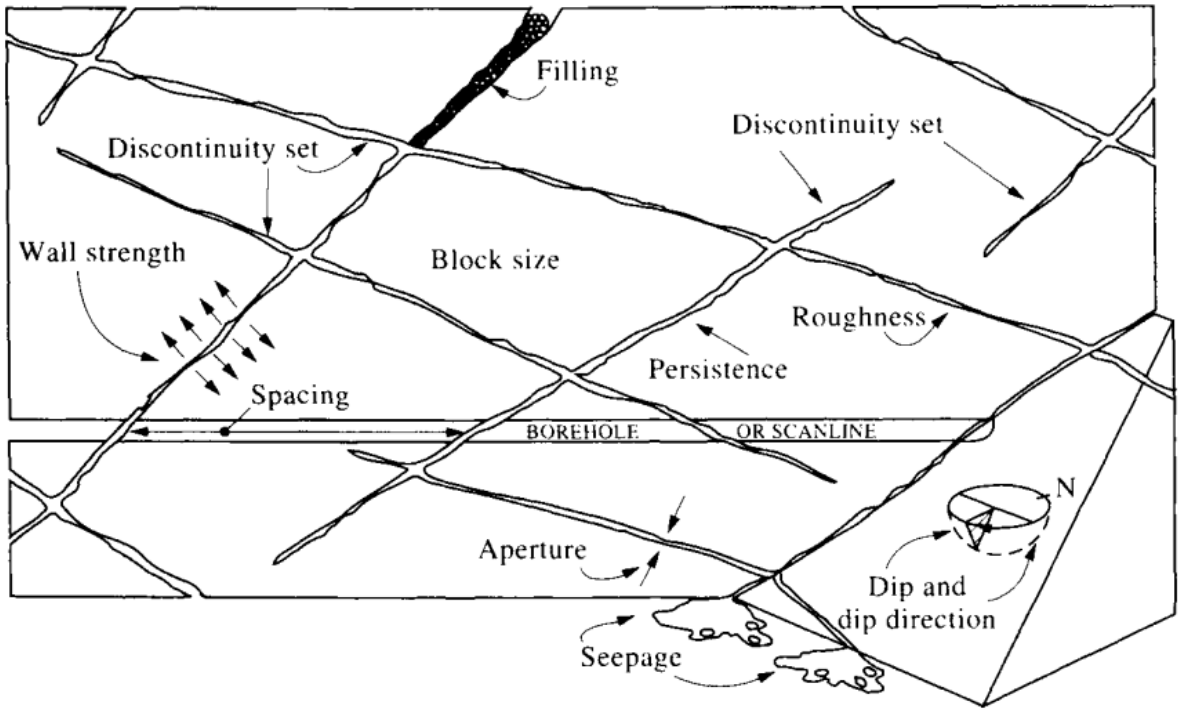

Figure 3-3: Schematic representation of discontinuties properties in a rock mass (Hudson & Harrison, 1997)

3.2 Modified cubical law:

Results from Witherspoon et al., (1980) suggest that the cubical law relating rate of flow of water through apertures to aperture cubed (Equation (3-22)) holds good with the apertures size varying from 250 μm to very small apertures of 4 μm. This applies to both radial and straight

flow geometries irrespective of open or closed fractures, rock type, load path and loading pattern. This indicates that permeability is primarily governed by fracture aperture.

$$q = \frac{a^3}{12\mu}\frac{\Delta p}{l} \qquad (3\text{-}22)$$

Where q is the flow rate, a is the aperture, Δp is the aperture and l is the length of the joint.

3.2.1 Joint character

Cubic law suggests that the water flow in joins is highly dependent on the aperture of the joints (Gudmundsson, 2000). The distance between two walls of joint that is measured perpendicular to the mean plane is regarded as aperture of joint. It depends upon many but not limited to mechanical properties of the rock. The hard and brittle rocks (for example granite) the joint opposes itself to become wide and open, and close least under normal stress. Hard rock also displays strong coupling between shearing and conductivity of joints (Barton et al., 1985). In the contrary, the joints in soft and deformable rocks get nearer easily. The connectivity of joints also governs the extent of flow of water in joints which depends upon joint length, spacing and its orientation (Odling, 1997). A continuous joint gives more flow in tunnel as compared to the discontinuous and staggered joints. In general, the volumetric flow rate is lower in horizontal joint/fracture as compared to the vertical ones (Gudmundsson et al., 2001). Joint roughness also affects the ability of joint to transport water. High roughness of joint can create numerous small channels for the water to move. Material coating also affect the conductivity by tightening the joints. When the compression strength of the joint wall is sufficiently high, even small shear movements can result in dilatancy, causing larger voids that allow water to flow more easily (Holmøy, 2008).

3.3 Numerical Modelling

Numerical modelling is an important aid in engineering geological planning and design. There are several methods and programs available and can be used to perform rock mechanics numerical modelling. They all have one thing in common, that they try to model the properties of the rock mass in a computer program, in order to simulate and study the behavior of the rock mass. Typical results from a rock mechanics numerical analysis are an overview of displacement, stresses, shape change, fluid flow etc. in the cross-section or space being modelled (Jing, 2003).

There are mainly two types of rock mechanics numerical modelling methods. These are continuous and discontinuous methods. In continuous method, the rock mass is viewed as a continuous medium that cannot be divided into smaller blocks. The continuous rock mass is discretized which means it is divided into a finite number of sub-areas called elements, in order to calculate results. It is a prerequisite that there is physical continuity between the elements. In discontinuous methods, the rock mass is seen as discontinuous medium. That is, the rock mass is modelled as a constituent of a finite number of individual blocks. Internally, these blocks are typically treated as continuous, but there is no continuity across the blocks. A key difference between continuous and discontinuous modelling methods is that continuous modelling methods simulate how the rock material is deformed overall, while discontinuous modelling methods simulate how components in the rock mass move separately. In continuous modelling programs, the input therefore typically describes the rock mass as a whole, while properties of joints and intact rock are defined separately in the discontinuous modelling programs.

When the rock mass is modelled as continuous, there are several instances of simplification or generalization in characteristics of rock mass as a whole or within individual blocks. A rock mass is not a continuous medium. It consists of larger and smaller blocks by the virtue of discontinuities. In some cases, it is appropriate to model the rock mass as a constituent of individual block with joints in between. Therefore, a continuous model may sometimes be appropriate to study a problem at hand. The fracturing and scale of the rock mass are important factors in determining the approach of modelling. A general rule may be that discontinuous modelling methods are used when the rock mass is moderately fractured and/or block stability issues are expected. If the rock mass has many joints, the discontinuous model may be very detail and cumbersome. In this case, the rock mass can instead be homogenized and modelled with a continuous modelling method. If the rock mass is intact or has few joints that are not expected to cause any problems, a continuous modelling method may be suitable.

Continuous and discontinuous models are simulated in different ways. The programs that make use of numerical modelling are for instance RS2 from Rocscience, (2023) and UDEC from Itasca Consulting Group (ITASCA, 2023b). These are 2D modelling tools. RS2 uses a continuous modelling method called Finite Element Method (FEM). UDEC uses a discontinuous modelling method called Distinct Element Method (DEM).

In FEM modelling, the behavior of the continuous rock mass can be expressed using partial differential equations. These partial differential equations are approximated to arrive at a

numerical solution to the model. This is done by discretizing the rock mass with triangular elements having nodes in the corners and on the sides of the elements. The material properties are assigned to the elements, and different elements can be given different material properties to simulate the heterogenous characteristic of rock. In addition, local sets of algebraic equations are obtained for various elements using interpolation functions. These are combined into one global set of algebraic equations that cover the whole rock mass. The algebraic equation describes the behavior of the rock mass such as nodal displacement as a function of loads and can be considered as substituting the partial differential equations at local and global level. The global equation set is solved iteratively through load steps with respect to initial and boundary condition to create a numerical solution to a problem (Jing, 2003). Here, finer discretization results in more nodes and smaller elements, which consequently contribute to a better representation of geometry and smaller deviations in the calculations. This will also extend the computation time for the model. Therefore, it is necessary to tradeoff between computational time and accuracy. Even though the rock mass is considered continuous in FEM, it is possible to model joints with this method. However, the requirement for continuity poses limits on letting the movement and deformation of modelled joints. Sliding, rotation and block failure cannot be simulated with FEM which limits its usage.

In DEM modelling, the rock mass is divided into blocks based on the joint system in the rock mass. The block can move with respect to each other, with no limit to how much movement is allowed. UDEC can model the blocks as rigid or deformable blocks. To handle deformation in deformable blocks, the blocks are discretized and modeled internally using continuous modelling method. The contact between the blocks is deformable and are designed with their own properties. Changes in stress field in the rock mass can cause block to move. The movement of the blocks is calculated with equations of motion at nodes in the blocks. The calculations are performed by iteration in time steps. In each time step, the displacement and stresses in the block system are updated. When blocks move relative to each other, the contact between them has to be detected and updated. The numerical solution of the model is obtained when a satisfactory state of equilibrium is achieved by the iteration (Jing, 2003).

The biggest limitation of DEM modelling is to achieve complete and actual representation rock mass with joint system. Therefore, it needs careful and detailed joint mapping which will contribute to describing and modelling the rock mass joint system with less uncertainty. It is also difficult to validate the extent of modeled joint system with reality.

In order to achieve results from numerical modelling to be close to reality, it is important that the model geometry and the material properties are representative. Numerical models do not have to be exact copies of reality to be useful. Simplification and generalization of the reality is generally necessary to some extent as it is difficult and often unnecessary to try to incorporate all the complexity of the rock mass in one model. In order for numerical models to be of good help, user must have the ability to assimilate all the information and know the limitations of the model. Acquiring representative input parameters for the rock mass is the biggest challenge for carrying out realistic numerical modelling.

3.4 Surge Tank

A surge tank is an expansion chamber which is located between pressure conduit (generally headrace tunnel) and sloping penstock. Surge tank is considered to mitigate or eliminate the potentially damaging effects of pressure surges resulting from water hammer, with the objective of intercepting or significantly reducing these surges thereby preventing the pressure tunnel from being subjected to excessive internal loads (Mosonyi, 1991). Surge tanks also improve regulation in various ways, firstly by reducing water hammer pressure fluctuations consequently increasing stability of system. Secondly, by reducing the distance between turbine and the next free water surface thus controlling the water acceleration time and network frequency.

The surge tank plays an important role in supplying water to the turbine during start-up and sudden increases in demand. When the turbine is started, the flow in the penstock undergoes rapid acceleration. In a steep penstock, water supply can meet the demand, but in a nearly horizontal pressure tunnel, the acceleration of the water mass is considerably lower. Without a surge tank, this can lead to discontinuous flow around the elbow, resulting in negative effects such as vacuum formation in the closed waterway and subsequent impact of water column. This interrupts the supply of water to turbines and interrupts power production. So, surge tank safeguards the waterway system in both start and stop of the turbines.

Two phenomena in transient flow

Every start and stop sequence of hydropower causes load change and pressure fluctuations in the waterway system. When those fluctuations are recorded by manometer or pressure transducers placed just downstream of the surge tank, it shows superposition of two pressure waves: (i) Short-cycled water hammer waves of few seconds. These are the oscillations of pressure that occur between the penstock and the surge shaft which have shot time

period/greater frequency close to the sound waves in water and air (ii) The slow-cycled surge wave of frequency significantly lower than the water hammer. So, Mass oscillation and water hammer are the two oscillations that occur during transient conditions thus creating a superposition of oscillations. Deceleration of the water masses moving in the penstock by closing of the valve causes sudden change in momentum of water mass and creates pressure wave (shock wave) through the penstock which is the primary cause of oscillating phenomena (Chaudhry, 2014). This pressure wave travels the total length of the closed conduit (penstock). This pressure wave doesn't affect the regime of the flow at first instant in the headrace tunnel. However, when this pressure wave reaches the surge tank, the steady flow regime gets disturbed in the tunnel and initiates the increase of water level at the surge tank as water is unable to enter the penstock. When the water level reaches the hydrostatic equilibrium level as shown in Figure 3-4, the momentum of water tends to surpass this level and reaches the highest upsurge level until its velocity becomes zero. This situation creates a difference in pressure between the reservoir and the surge tank. Consequently, the water level starts to decrease, reaches the hydrostatic equilibrium level, and again over travels this level due to its inertia. The amplitude of oscillation decreases gradually due to friction in the headrace tunnel and finally, oscillation dies out after a certain time. Figure 3-4 shows the simplified schematic profile of surge tank in a waterway system.

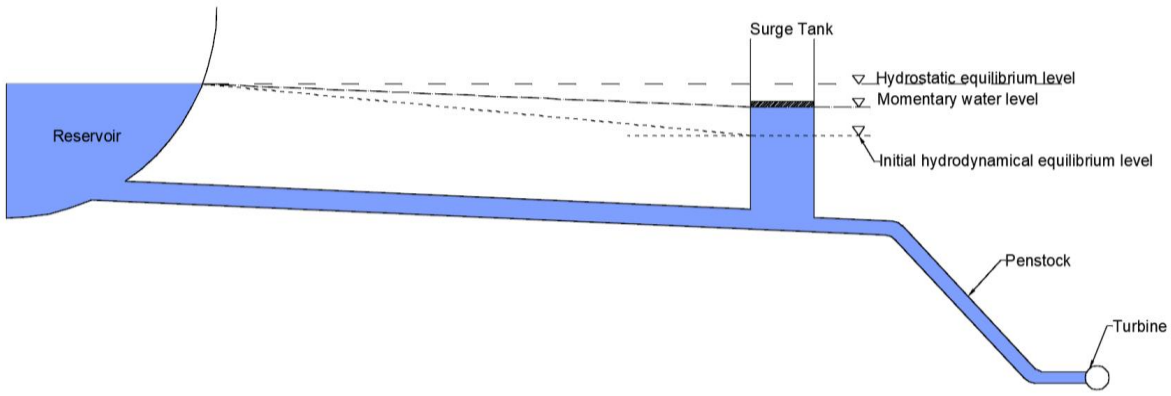

Figure 3-4: Schematic profile of surge tank along with waterway system. Level of hydrodynamic equilibrium is the level of water in surge tank when the water is flowing through the waterway system in a steady state.

Similarly, when the turbine is started or when there is demand increase in the system, the flow of water is suddenly initiated in penstock where water is delivered to the turbine from steeply inclined penstock. In horizontal tunnel, the acceleration of water is relatively low. In this case surge tank provides the necessary amount of water during fluctuations in operating conditions. This causes a decrease in the level of water in the surge tank which induces imbalance in

pressure between surge tank and reservoir. The water level tries to attain hydrostatic equilibrium level and again over travels that level due to its inertia. The oscillation due to this phenomenon also decreases due to friction loss and dies out after certain time.

Time period of mass oscillation

The time period of total cycle i.e., the period of the mass oscillation in frictionless pressure tunnel is given in Equation (3-23).

$$T = 2\pi \sqrt{\frac{LA_s}{gA_t}} \qquad (3\text{-}23)$$

Where, T is the time period of mass oscillation, L is the length of frictionless pressure tunnel, A_t is the cross-sectional area of tunnel, A_s is the cross-sectional area of surge tank, g is the acceleration due to gravity. It is clear from Equation (3-23) that the time period of mass oscillation depends only upon the geometric characteristics of pendulating system in case of frictionless pressure tunnel.

Velocity of water hammer waves

Halliwell, (1963) suggested the expression for wave velocity in rock tunnel which however consist of various rock characteristics and are not known with certainty. Therefore, a simplified expression for velocity of water hammer waves in rock tunnel from Parmakian, (1963) is generally adopted for calculating wave velocity and is given in Equation (3-24).

$$c = \sqrt{\frac{1}{\rho\left(\frac{1}{K} + \frac{1}{G}\right)}} \qquad (3\text{-}24)$$

Where, c is wave velocity, ρ is the density of water, K is bulk modulus of elasticity of water of water, G is the modulus of rigidity or shear modulus of rock.

3.5 Signal Processing

3.5.1 Nyquist criterion

The Nyquist criterion is generally used in data acquisition, data analysis and treatment of noise in data (Lévesque, 2014). According to the Nyquist sampling theorem, it is required to have a sampling frequency that is at least double the highest frequency component to be captured within the signal during data acquisition. This means, the sampling frequency should be at least

twice the frequency of the wave being sampled in order to properly reconstruct the original signal. If f_S is the sampling frequency and f is the frequency of the signal being sampled, then:

$$f_s \geq 2f \tag{3-25}$$

If the sampling frequency is lower than required, it results in under sampling known as aliasing. That means the recorder is unable to measure the wave fast enough to reconstruct an accurate waveform record.

3.5.2 Butterworth Filter

A butterworth filter (Butterworth, 1930) is a kind of an analog signal processing filter that produces output response with no ripple in the pass band i.e., frequency we want to get or the band we want to stop that results a maximally flat filter response at cost of a relatively wide transition band. Here, the analog signals are those signals which are continuous in both time and amplitude and represent physical phenomena like pressure in our case study. Analog signals are typically transmitted using electrical voltages or currents, and they can be susceptible to noise and interference. To reduce the impact of noise, the pressure signal is filtered and analyzed according to its use.

The general form of frequency response Butterworth low-pass filter is given in Equation (3-26).

$$H_{(j\omega)} = \frac{1}{\sqrt{1 + \varepsilon^2 \left(\frac{\omega}{\omega_c}\right)^{2n}}} \tag{3-26}$$

Where, n is the order of filter, ω is the operating frequency (passband frequency), ω_c is the cut-off frequency and ε is the maximum passband gain.

Phase shift in butterworth filter can be dealt in an offline setting i.e., when full signal is available. For this the filter is applied twice i.e. once forward and once backward which compensate the phase shift by the second run and the output signal is in phase with the given input signal (Lyons, 2011). There are three types of filters namely low-pass, high-pass and band filter. Low-pass and high-pass filters capture waves with frequency lower or higher than the cut off frequency respectively, and band filters capture waves between two cut-off frequencies. Figure 3-5 shows the three types of filter band that a filter can filter.

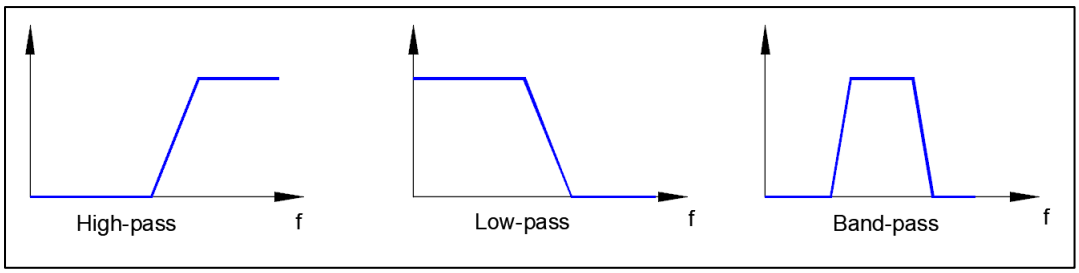

Figure 3-5: High, Low and Band pass filter , x axis being the frequency and y axis being the waves in or out.

3.5.3 Fast Fourier Transform (FFT)

The FFT is a mathematical algorithm that takes a signal, which is a sequence of numbers that represent pressure wave during transients and calculates the frequencies that make up that pressure waves. It does this by breaking down the signal into smaller pieces, or "sub-signals," and then combining those sub-signals to create a frequency spectrum. FFT is a powerful tool for analyzing signals in the frequency domain. It breaks down the pressure waves into its constituent natural frequencies, which can provide valuable insights into the behavior of the frequencies that generated the signal (Maklin, 2019). In this study, the FFT analysis is used to find the cutoff frequency and natural constituent frequency of water hammer and mass oscillation.

3.6 LSTM

LSTM stands for Long Short Term Memory. It is a neural network that was designed in order to deal with the long-term dependency problems faced by Recurrent Neural Networks (RNNs) (Dolphin, 2020). The feedback connection in LSTM allows it to process the entire sequence of data without treating each point in the data sequence independently. It retains the useful information from previous data to help with the processing of new data points. Basically, the output in a LSTM network is dependent on cell state which is the current long-term memory, hidden state which is the output at the previous point in time, and the input data at the current time step.

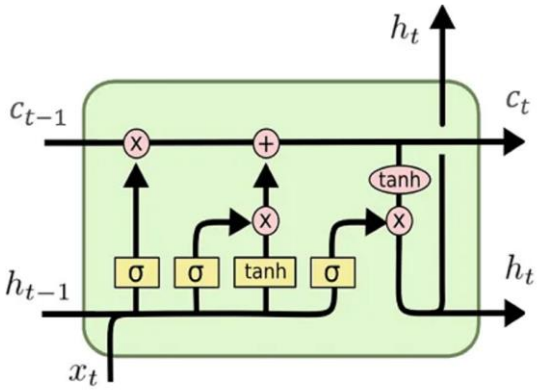

Figure 3-6: Schematic representation of Long Short Term Memory (Lees et al., 2022)

LSTM network consists of filters which are called gates namely forget gate, input gate and output gate. These gates control the information in the sequence of data that comes into, is stored in and that leaves the network. The first section in Figure 3-6 shows the input gate that controls the amount of new information added to the memory cell. The second/central section represents the forget gate that determines which information is discarded. The third section namely output gate regulates the amount of information retrieved from the memory cell and passed to the next time step. These gates enable LSTM network to selectively retain and forget information making it well suited for handling long term time dependency problems.

4 Fatigue in rock mass

The initial studies on cyclic loading were conducted for drilling in mining tunnels (Burdine, 1963). The concept of the cyclic loading and fatigue damage in rock has been studied in various context such as cyclic loading in rocks caused by hydraulic fracturing (Zang et al., 2013), seismic activity (Gischig et al., 2016; Hashash et al., 2001), emptying and filling of crude oil storage (Voznesenskii et al., 2015; Wang et al., 2015) etc. In relation to hydropower, fatigue has been envisaged in the area of hydraulic machines (Trivedi et al., 2013) which is believed to occur due to pressure transients caused by cyclic loads during changes in load and start and stop of turbines.

Failure of a rock material can occur when it is subjected to a monotonic stress exceeding its strength or when a cyclic stress applied to it exceeds its cyclic strength, which is lower than monotonic strength. The term “cyclic fatigue” is commonly used to describe such cyclic failure. Additionally, fatigue can also occur due to the prolonged action of a sustained load or residual stress over an extended period, which is known as stress corrosion. The cyclic load primarily leads to accumulation of plastic deformation and damage of the rock material cycle after cycle.

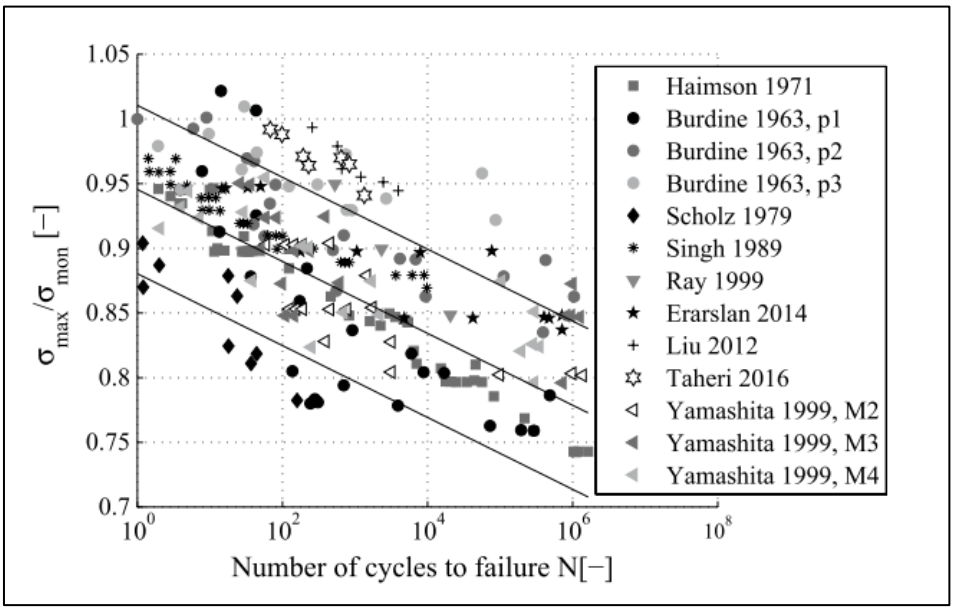

Figure 4-1: S-N material for different rock samples from different types of tests at constant amplitude (Cerfontaine & Collin, 2018), *σ_{max} is maximum cyclic stress and σ_{mon} is monotonic stress*

Fatigue limit along with the S-N curves are the general concepts used to describe fatigue behavior (Schijve, 2009). The fatigue limit, also known as fatigue strength, is the stress amplitude at which a specimen does not fail, resulting in an infinite fatigue life. Here, number

of cycles to failure (N) is related to the ratio of maximum cyclic stress to the monotonic strength to explain the fatigue behavior of a material. Literature suggests that, in case of unavailability of data for a specific rock material, the fatigue limit may be taken as 0.7 times the monotonic strength. Figure 4-1 shows summaries of results of S-N curves available from various literatures.

Figure 4-2: Brazilian disc specimens of Brisbane tuff after failure tested under (left) monotonic loading and (right) cyclic loading (Erarslan et al., 2014)

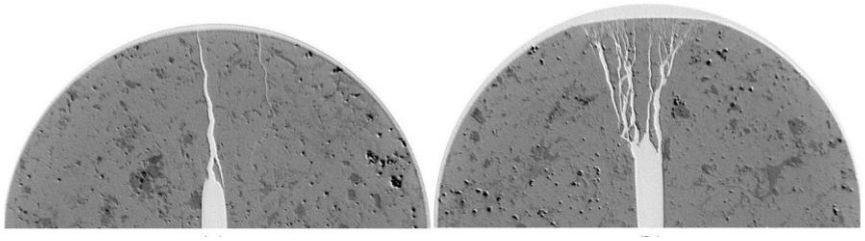

Figure 4-3: CT scan images of cracked chevron-notched Brazilian disc (CCNBD) specimen on Brisbane tuff under (left) monotonic loading (right) cyclic loading (Ghamgosar & Erarslan, 2016)

Based on conclusions of Cerfontaine & Collin, (2018), it is evident that fatigue mechanisms primarily occur when the stress amplitude is high and the mean stress is low. On the other hand, stress corrosion becomes dominant when the mean stress is high, and the stress amplitude is low. The primary reason for fracture during cyclic loading is the decohesion and loosening of the material, resulting from the propagation or initiation of microcracks within the rock before the formation of a larger crack.

There are distinct differences in the crack growth process between failure under monotonic and cyclic loading. Cyclic fatigue is characterized by the presence of dust and fragments whereas a clean and clear crack is seen in specimens failed under monotonic stress. The comparison of crack developed from monotonic stress and cyclic stress failure is shown in Figure 4-2.

Furthermore, cyclically loaded specimen exhibits an expanded fracture process zone as shown in Figure 4-3. Here the effect of monotonic and cyclic failure mechanisms becomes evident.

In monotonic loading, the failure mode of the rock is brittle, characterized by extensive cracking of the rock grain along the failure surface. The cyclic loading leads to wider fracture process zone and branching of the crack. Under cyclic loading, failure occurs along grain boundaries with inter-granular cracks as the main mechanism of failure. In addition, wear and shear between rock grains at the boundaries lead to the formation of intragranular cracks. The resulting failure is a result of the coalescence of multiple cracks rather than the propagation of a single macro crack. This results in plastic deformation measured at macroscale level (Cerfontaine & Collin, 2018; Ghamgosar & Erarslan, 2016).

Understanding the cyclic fatigue of rock joints is also important when accessing rock masses in general. The strength of rock joint decreases due to the shearing of asperities and degradation of the joint walls. Several constitutive model for have been presented by Belem et al., (2007; Nemcik et al., (2014) in regard to cyclic loading. Experimental studies show that factors such as frequency, number of cycles, stress amplitude, and loading rate can decrease the peak and residual shear strength of joint specimens under cyclic loading (Jafari et al., 2004; Liu et al., 2018; Tsubota et al., 2013).

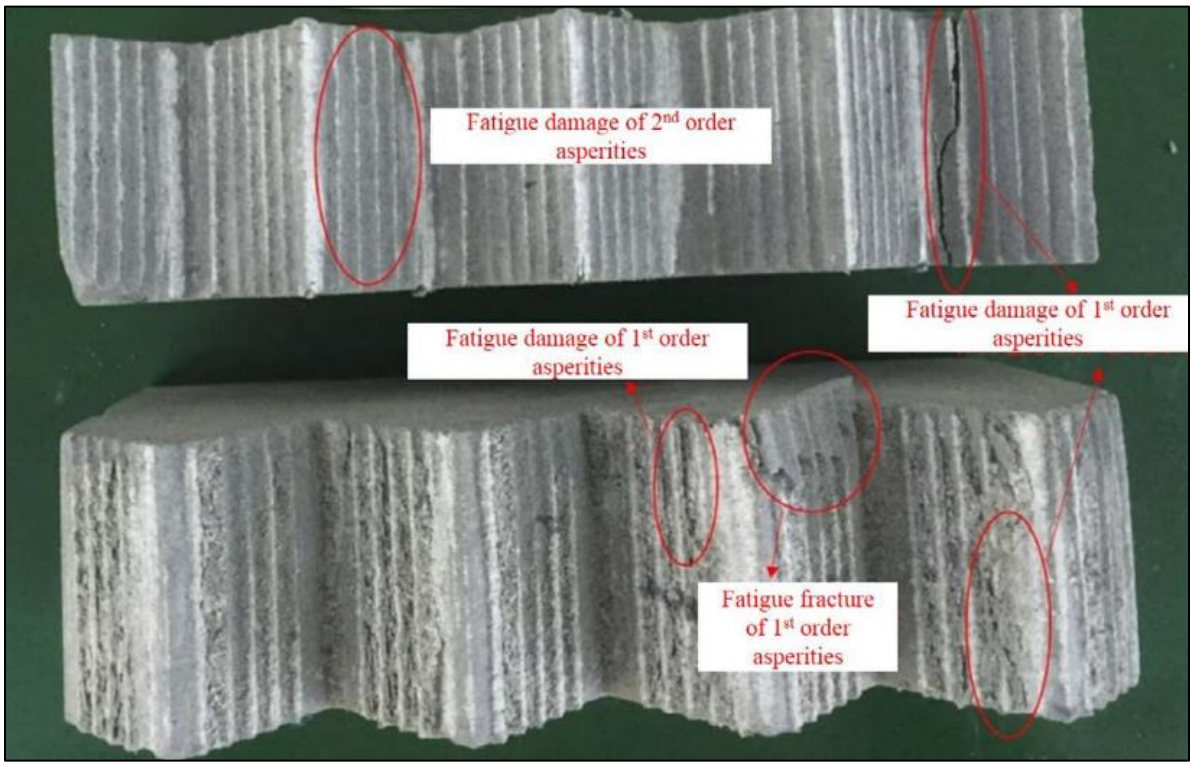

Figure 4-4: Fatigue failure in rock joint of sandstone samples consisting of triangular asperities at the end of cyclic loading (Liu et al., 2018)

The roughness of the surface consist of asperities which occur in different scales and basically categorized into first order (even with longer base and lower angle) and second order (uneven with higher angle and narrower base length) irregularities (Patton, 1966). Patton, (1966) stated that the characteristic of rock joint is at first controlled by second order asperity in small displacements and the shearing behavior of joints is controlled by primary asperity at large displacement. When the normal stress increases, shearing off of the secondary asperity takes place and the shear strength is governed basically by primary asperity (Yang et al., 2010). Figure 4-4 shows that the damage of first order and second order asperities after 500 cycles of shear loading from an experiment by Liu et al., (2018).

Experiments on rock joints conducted by Fathi et al., (2016) and Liu et al., (2018) subjected to cyclic loading have shown that initially under low cycles, the contact area between joint surfaces increases, leading to an increase in peak shear strength known as the "contraction effect." However, with high cyclic loading, the second-order asperities are damaged, resulting in degradation and a subsequent decrease in the peak shear strength of the rock joint.

The cyclic loads resulting from hydraulic transients during the start or stop of hydropower operations can potentially induce fatigue in the rock mass and rock joints. The cyclic fatigue induced by hydraulic transient is a relatively new topic and is investigated by Neupane, Panthi, et al., (2021) based on experiment and numerical simulations. The cyclic loading can lead to rupture of intact rock bridges, creating new joints that may introduce issues regarding stability of the tunnel. The pressure transients in the tunnel system can cause damage and degradation of the joint surfaces, resulting in reduced stiffness and frictional resistance, increased hydraulic aperture, and significant joint deformations. This was identified as a possible scenario caused by cyclic fatigue induced by transients.

5 Hydropower case project

5.1 Brief on Roskrepp HPP

Roskrepp Hydropower plant lies in Sirdal municipality in Vest-Agder in southern part of Norway and is run by Sira-Kvina Kraftselskap. The powerplant came into operation in 1979 having design discharge of 70 m^3/s and operating head between 52 and 109 m regulated by a reservoir, Rosskreppfjorden. The water from main intake is conveyed via 3513 m long, 7.5m wide and 6.5m high inverted D shaped headrace tunnel with an additional withdrawal from brook intake to an underground powerhouse generating rated power of 50 MW and annual energy of 105 GWh. The general project layout of the project is shown in Figure 5-1. The water is then released to Øyarvatn which is again used by 5 cascading hydropower projects downstream before it flows into the sea at Åna-Sira. The schematic interconnected system of hydropower plants is shown in Figure 5-2.

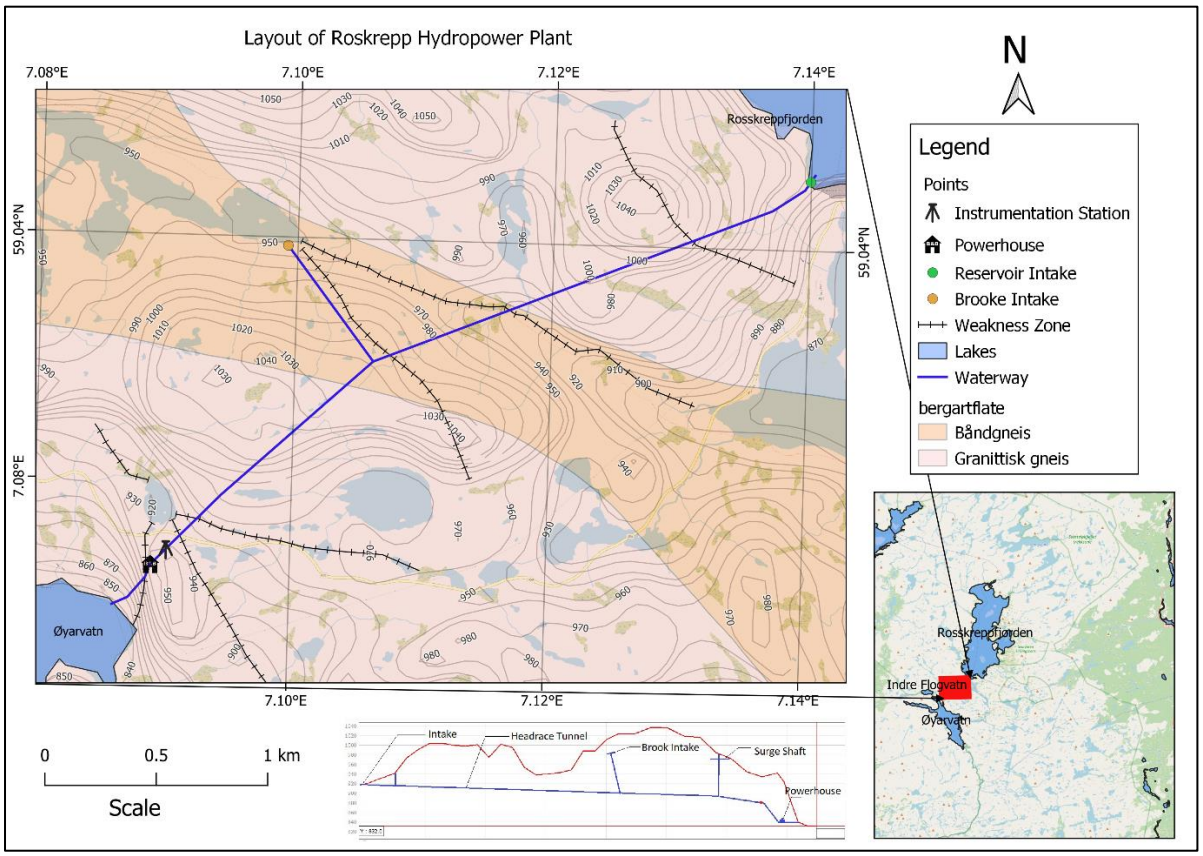

Figure 5-1: Location Map of Roskrepp Hydropower Plant along with geological setting

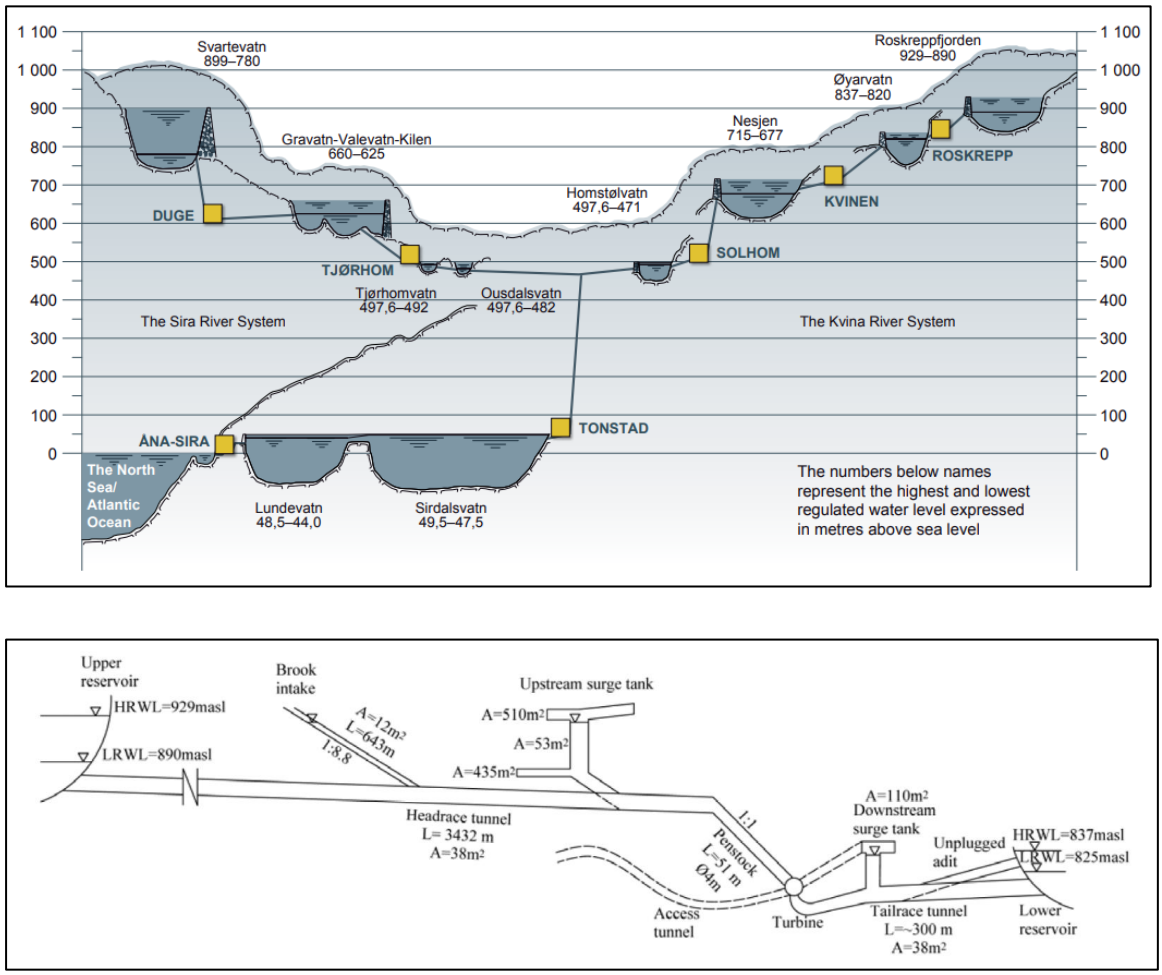

Figure 5-2: Series of interconnected hydropower system including Roskrepp hydropower which uses water from Roskreppfjorden at top right (top)(NFF, 2013), *Waterway system of Roskrepp hydropower (bottom)* (Pitorac et al., 2020)

The rock mass in the project area of Roskrepp Hydropower plant consists of course-grained banded gneiss and weakly schistose granitic gneiss. The headworks, powerhouse and most of the waterway area lies in Granitic gneiss whereas some portion of waterway (headrace tunnel) lies in banded gneiss. Surface mapping shows that the general orientation of the foliation joints range from N 135º -150º E/40º - 60º NE (Jf). In addition, two major cross-joint sets with strike/dip N 80º -100º E/70º -80º N (J1) and N 0º -20º E/ 40º -50º SE (J2) are present in the rock mass (Neupane et al., 2020). Table 5-1 shows the generalized joint orientation value of joint condition in the site area and Figure 5-4 (right) shows the stereo net plot of joint condition in the site area.

Table 5-1: Joint orientation at project location (based on (Neupane et al., 2020)*)*

Joint Type	Strike	Dip	Remarks
Foliation Joints	145º E	50º NE	Jf
Cross Joint	90º E	75 º E	J1
Cross Joint	10º E	45º SE	J2

5.2 Instrumentation Location

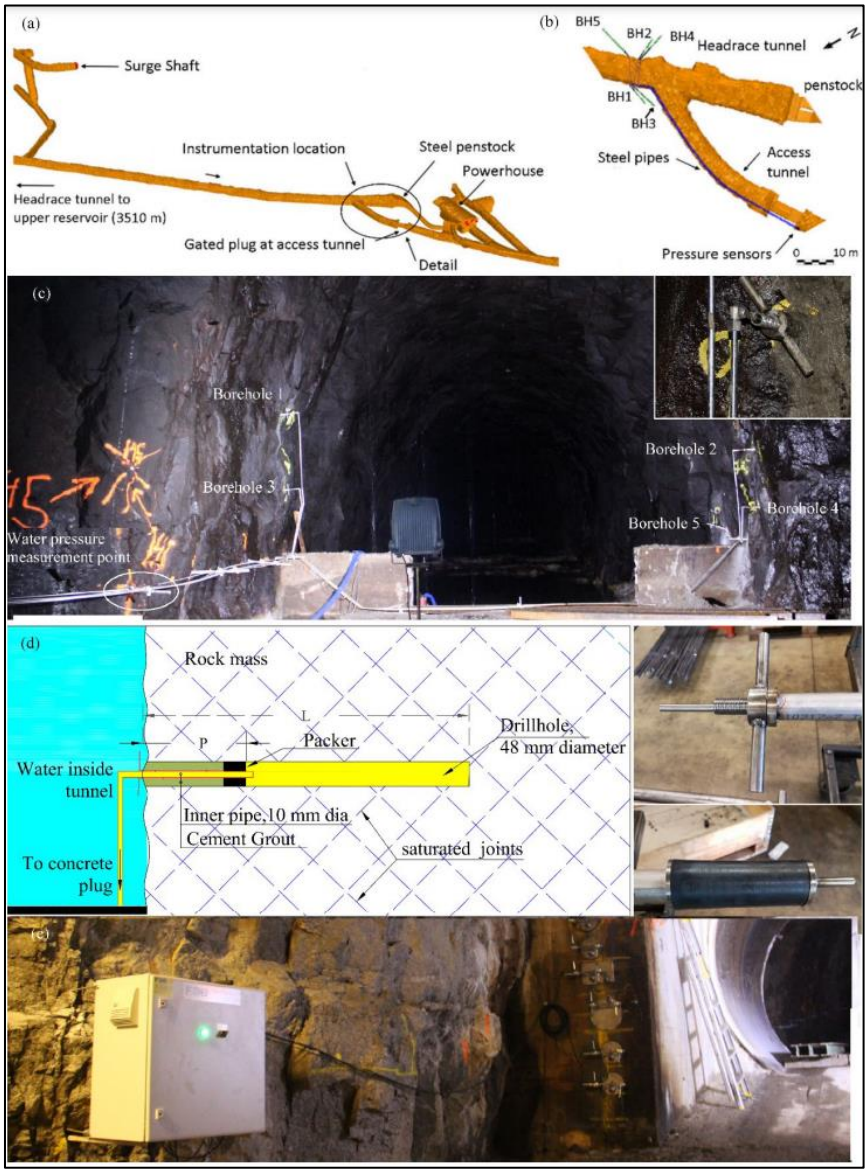

Figure 5-3: Details of instrumentation location (a) 3D view of instrumentation location b) Placement of boreholes with respect to access tunnel, head race tunnel and penstock c) Placement of borehole looking downstream d) Schematic diagram of borehole and packer arrangement e) Pressure sensor and data logger in access tunnel (Neupane, 2021).

The instrumentation location was selected nearby a construction adit which makes the area almost dry where the pressure transducers and data-loggers are placed safely (Figure 5-3 a,d).

A walkthrough survey carried out by Neupane et al., (2020) showed that the rock mass at the instrumentation location were distinct with proper hydraulic connection between different systems of joints and tunnel walls. The details of instrumentation location are shown in Figure 5-3.

During the survey, it was found that the rock mass inside the tunnel was of good quality with minimal rock support in place. The majority of the observed sections had tightly jointed rock walls. Results from comprehensive joint mapping done by Neupane et al., (2020) following ISRM, (1978) is shown in Table 5-2.

There was a weakness zone 150 m upstream of the instrumentation location (Figure 5-1) where the concrete lining was applied. The dipping flow was noticed further downstream of the weakness zone. Figure 5-4 (left) provides a detailed view of the instrumentation location and orientation of the boreholes relative to the major joint sets.

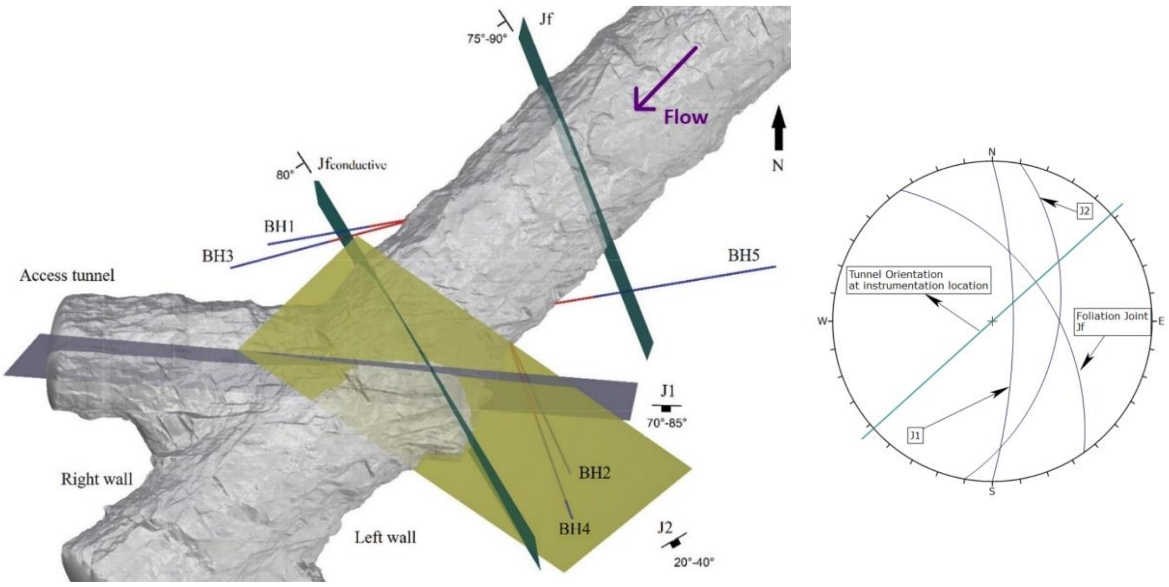

Figure 5-4: 3D laser scanned isometric view showing location of borehole with respect to joints at instrumentation location(left). Blue portion represents the segment of borehole between the packer and the end of borehole where the pore water pressure is registered. The red segment is grouted with cement to reduce leakage. J2 is a random joint occurring at instrumentation location. Modified from (Neupane et al., 2020)*. Equal area stereonet plot of joint sets at project location (right).*

The 3D laser scanned model of tunnel (Figure 5-4) shows the jointing conditions at the instrumentation location along with the boreholes and orientation of the joints. BH1 and BH3, located on the right wall of the tunnel, are positioned in such a way that they intersect with the foliation joint set (Jf) and are sub-parallel to the cross-joint set (J1). BH2 and BH4 on the tunnel's left wall are positioned in a way that they intersect with the cross-joint set (J1) and are

sub-parallel to the foliation joint set (Jf). BH5 intersects with the foliation joint set (Jf) on the left wall. The cross-joint set (J2) which was easily visible at instrumentation location at the top of the tunnel and is responsible for the majority of the water inflow into the tunnel.

Table 5-2: Joint characteristic at instrumentation location in the tunnel (Neupane et al., 2020)

Joint set	**Jf**	**$Jf_{conductive}$**	**J1**	**J2**
Strike	N 140º - 160º E	N 150º E	N 80º - 100º E	N 60º - 75º E
Dip	75º - 90º SW	80º SW	70º - 85º SW	20º - 40º SE
Persistence (m)	3-10	More than 10 m	3-10 m	3-10 m
Joint wall weathering	Fresh (W1)	Slightly weathered (W2)	Fresh (W1)	Slightly weathered (W2)
Joint roughness	Rough planar JRC 4-6	Rough undulating JRC 14-18	Rough planar JRC 4-6	Smooth undulating JRC 10-14
Joint aperture (mm)	Tight (0.1-0.25 mm)	Partly open (0.25-1 mm)	Tight (0.1-0.25 mm)	Partly open (0.25-1 mm)
Joint infilling condition	Clay	Washed out	Clay	Washed out
Seepage	Damp but no dripping or following water present	Continuous flow	Wet with occasional drops of water	Continuous flow
Typical spacing (m)	1-2 m	More than 10 m	1-2 m	More than 10 m

A single conductive joint with different properties than the regular joint-set sub parallel to the foliation joint Jf was also observed at instrumentation location named Jfconductive (Figure 5-4). This joint follows the same orientation as the foliation joint set (Jf) but has different aperture and filling conditions, especially near the top where it is close to the cross-joint (J2). On the right wall, both BH1 and BH3 boreholes intersect Jfconductive, as well as the foliation joints (Jf). It should be noted that in BH3, the packer is positioned 4 meters away from the tunnel wall, and the conductive single joint intersects this borehole in the grout-filled impermeable area behind the packer. Therefore, there is no direct hydraulic connection between the borehole and this single joint. BH4 intersects with the cross-joint (J2) on the left wall, whereas BH2 does not intersect J2. Therefore, only BH4 is hydraulically connected to cross-joint (J2) directly. It had been visible in walk through survey that the rock joints were relatively more exposed to the tunnel contour on the left wall near BH2 and BH4 compared to the right wall. The left wall had more prominent wedge formation due to unfavorable oriented joints in the tunnel during excavation, that exposed the joints on the left wall.

5.3 Instrumentation and Data acquisition

A total of five boreholes with diameter of 48 mm were drilled at selected locations, each varying in length and orientation (Figure 5-4). Inside each borehole, a stainless-steel pipe with a 10 mm internal diameter was securely fixed using rubber packers as shown in Figure 5-3 (d). The empty length of bore hole inside the rubber packer is used to collect water pressure information from the rock mass and convey it to the pressure transducers through the stainless-steel pipes. This arrangement allowed for the collection of water pressure data from the bore hole. It can be seen in Figure 5-3 (d) that the tightened packer secures the steel pipe firmly within the boreholes, creating a hydraulic barrier between the pore pressure in the rock mass and the water pressure in the tunnel. The packer is positioned at various distances from the tunnel wall inside the bore holes of varying length to study the variations bore hole pressure responses with respect to distance from tunnel wall (Table 5-3). In addition to the borehole pipes, a steel pipe was placed within the tunnel to monitor the water pressure. The open end of the pipe was located at the junction of the headrace tunnel and the construction adit, allowing for valuable observations of the water pressure inside the tunnel.

Table 5-3: Characteristics of boreholes

Borehole	**BH1**	**BH2**	**BH3**	**BH4**	**BH5**
Trend/Plunge	255º/10º	155º/10º	260º/10º	160º/10º	80º/10º
Location	Right wall	Left wall	Right wall	Left wall	Left wall
Borehole Length (L), m	7	7	9	9	11
Depth of packer from tunnel wall (P), m	2	2	4	4	2
Effective length	5	5	5	5	9

The instrumented data consists of the pore pressure from 5 boreholes and tunnel water pressure dated from 2018-06-20 to 2023-01-20. The pressure transducer measures the pore pressure with a temporal resolution of 0.1s (10 Hz). The computer saves the data in daily format in txt files. As there are 5 boreholes pressure data and 1 tunnel pressure data, there are 60 data in one second. So, extracting all the data together was not possible due to the severely large amount of dataset. Before drilling the boreholes some possible sources of errors were identified and measures were taken to improve the accuracy of measurements (Neupane et al., 2020) and are listed below:

1. Chocking of pipes: The boreholes were cleaned properly to avoid chocking. The boreholes were drilled at an angle 10º inclining downward to prevent interference of larger particles while measuring the pressure.
2. Water tightness of packer: After the packer was tightened, it was welded with the outer pipe. To prevent leakage, the borehole outside the packer was filled with non-shrinking cement grout mix. This ensures hydraulic connection of tunnel water only through joint system and not through the boreholes.
3. Leakage from pipes: The pipes were tested for leakage in connections applying 30 bars of pressure. Detected leakages were rectified by sealing and tested again.
4. Removal of entrapped air in pipes: To ensure the removal of entrapped air in the pipes, each pipe is fitted with a deaeration valve, allowing for the expulsion of any trapped air.
5. Pipe vibration while measurement: The pipe could vibrate while recording the pressure of flowing water. This was controlled by rigidly fixing the borehole pipes to the tunnel wall using grouted rock dowels and metal clamps.

The instrumentation program is unique in the following way:

1. The location of sampling is in an unlined section where there are effects of both water hammer and mass oscillation. Placement of pressure transducer any further upstream of the surge tank, it wouldn't be possible to record the water hammer waves as it is almost nullified by the free water surface in the surge tank.
2. Sampling frequency is relatively higher i.e., 10Hz. Even though the period of mass oscillation is about a few minutes, the wave speed of water hammer depends upon the length between the turbine and free water surface (surge tank). The time period of the water hammer is very low i.e., in seconds. So, the pressure transducer can record the water hammer waves with this high sampling frequency.
3. The bore holes are laid out in such a way that it can measure borehole water pressure of different joint systems, for instance, highly responsive, moderately responsive and non-responsive joints. Additionally, the measurement program aims to monitor the pressure changes at the vicinity of tunnel wall, with maximum distance of one tunnel diameter where most of the instability relating to block fall originates.
4. The instrumentation program measures pressure in tunnels and boreholes for long period of time. The pressure transducers have been measuring pressures since the start

of the sampling program. This is helpful to know any change in characteristics of borehole pressure in the long run.

6 Analysis and interpretation of acquired data

6.1 Analysis

6.1.1 Overview of Analysis

Processing the available raw data was the most important and challenging task throughout the thesis work. Due to the large amount of data, it posed many challenges on the way during the study period. Knowledge of digital signal processing and machine learning was also needed to carry out the analysis.

The data recorded by pressure transducers are stored in txt files that are created every day. To organize the data more effectively, a Python script was used to convert the daily data into monthly format. Since the dataset was extremely large, extracting all the data at once was not feasible. Therefore, the data was extracted and analyzed on a monthly basis.

To separate important information from severely huge dataset, it was necessary to isolate the pressure values of tunnel and bore holes when the transient occurs. The transient occurs when there is start and stop of the turbines. The start and stop sequences create abrupt respective rise and fall in pressure which is recorded by pressure transducers. These transducers also collect vibration signals from borehole pipes and structures which need filtering, especially when there is unwanted noise in the signal. The pressure peaks during transients were extracted using the peak finding algorithm.

Mass oscillation and water hammer are two superimposed oscillations in the raw signal of waveform. These waves have certain natural oscillating frequency, which can be determined using Fast Fourier Transformation (FFT). After the oscillating frequency of those waves were known, the cutoff frequency was determined. This cutoff frequency was hence used to filter out noise using Butterworth low pass filtering algorithm. The cutoff frequency was also used to separate the effect of water hammer and mass oscillation. The overall methodology of data extraction and analysis is shown in Figure 6-1. The detailed steps of data extraction and analysis are explained in the following sections.

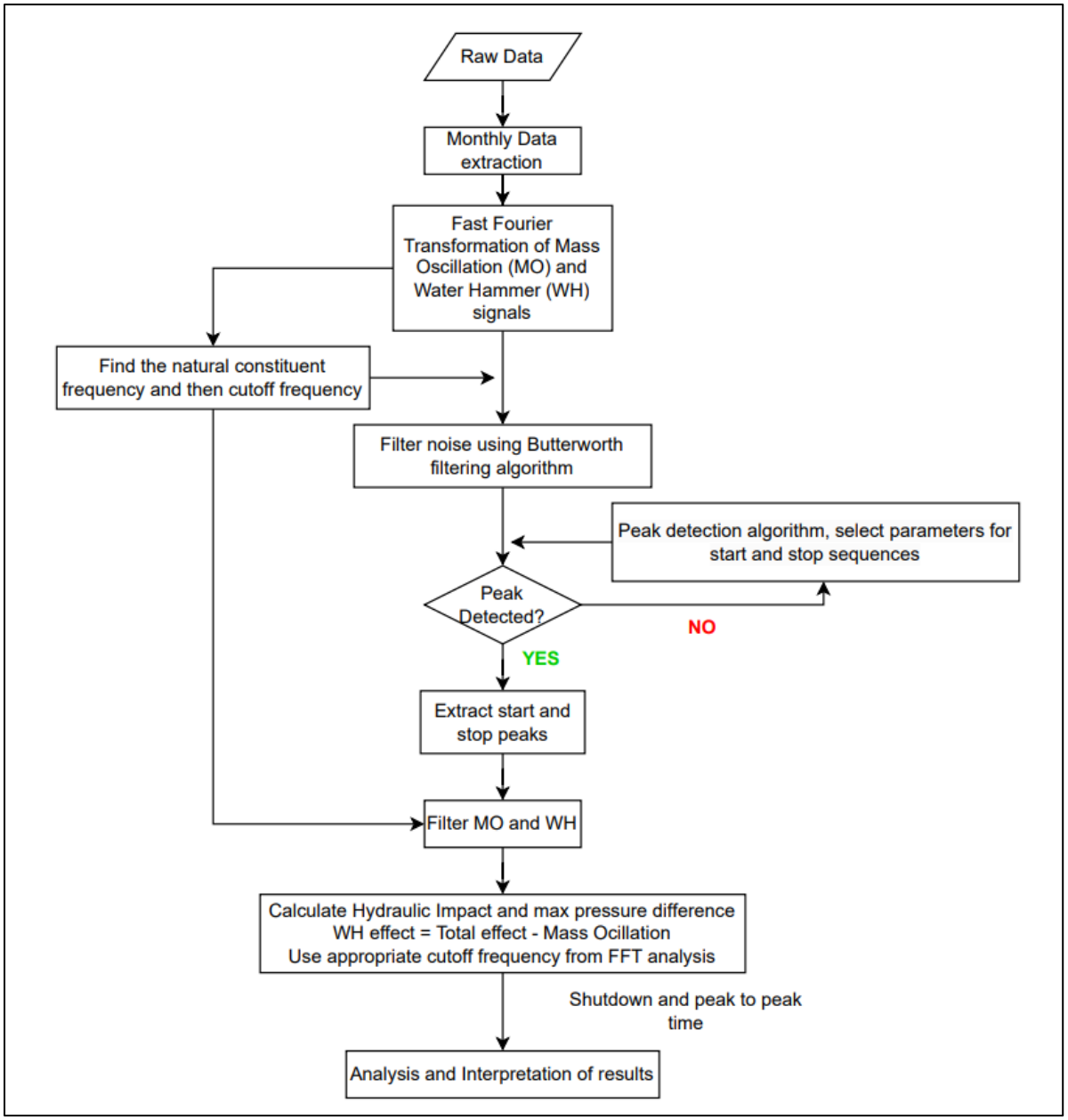

Figure 6-1: Formulated methodology flowchart for data extraction from raw pressure data from tunnel and boreholes to calculate impact of transient in unlined pressure tunnel.

6.1.2 Finding Peaks for data extraction

Pressure transducers measure water pressure in the tunnel and five bore holes, recording data at a frequency of 10Hz. This means there are 60 data points per second and millions of data points over the span of 5 years. Handling such a large dataset can be difficult and time-consuming, involving tasks like accessing, retrieving, saving, analyzing, and interpreting the data. The raw dataset for water pressure of the tunnel and boreholes in May 2021 is shown in Figure 6-2.

To make this process more manageable, it is necessary to extract the useful data series from this extensive dataset. The useful data series refers to the sections where start and stop sequences are present or where surge waves occur. These surge waves generate pressure peaks in both directions, namely upsurge and downsurge. However, these pressure peaks are not consistent and vary depending on factors like valve closure time, initial pressure, and load changes.

To efficiently analyze the data, it is essential to detect these pressure peaks and filter them in. However, this task presents challenges due to the presence of noise in the pressure signal. To overcome this, a peak finding algorithm called “scipy.signal.find_peaks” was implemented in a Python environment. While using the function itself was straightforward, finding suitable arguments for specific cases, such as transients, proved to be a challenging task.

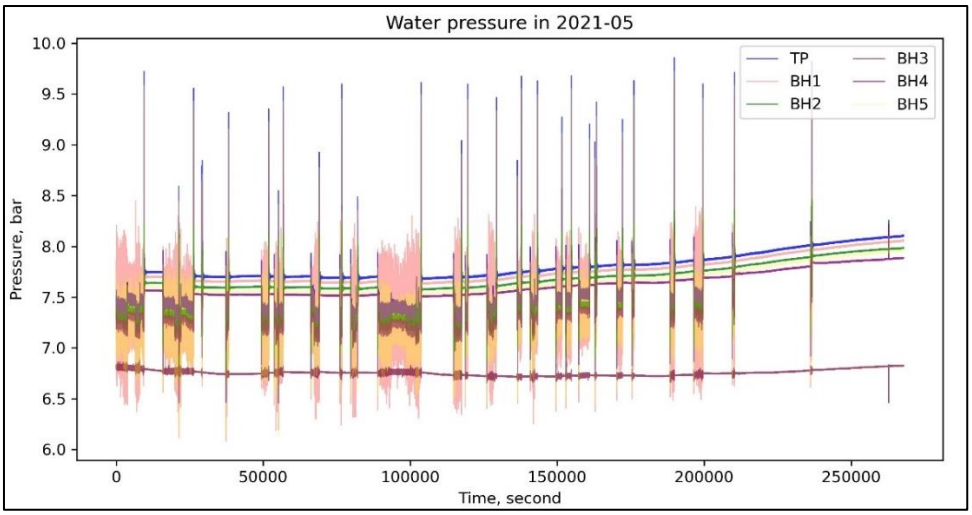

Figure 6-2: Dataset of 2021-05 without extracted peaks.

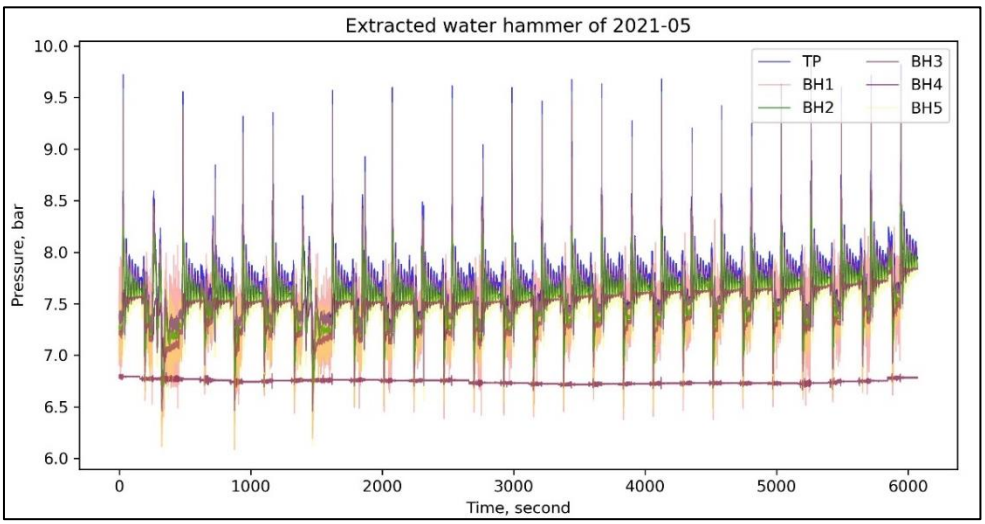

Figure 6-3: Dataset of 2021-05 after extraction. The time in x axis is the time period of extracted data and not to be confused with number of seconds in a month.

When the find_peaks function was directly used with raw data, it was unable to detect the peaks correctly due to the presence of noise. To address this, it's helpful to first smoothen the input before applying peak detection (Pröll, 2022). Continuous Wavelet Transformation (CWT) based peak detection algorithm was used but took longer computational time. However, the Butterworth filter offers a solution by creating smoother signals in a faster computational time, which simplifies peak detection (Pröll, 2022). Thus, the noise was filtered out using low pass Butterworth filter of 4^{th} order with a cutoff frequency of 0.005 Hz (time period of 200s). This resulted in data with a smooth signal.

The smooth signal was used again to find the peaks using find_peaks function. The function has multiple arguments, out of which prominence and width were used in the analysis. "Prominence" represents the minimum height of a peak relative to the lowest point in the waveform, while "width" indicates the minimum distance between two peaks. A hit and trial approach along with data visualization to determine the appropriate values for these parameters and ensure effective peak detection. Finally, the prominence of 0.7 bar and width of 200 s were optimal to detect the upsurge peaks.

When there is a start sequence, the water is intermittently supplied by surge tanks, consequently decreasing the water level up to the lowest downsurge level in the surgetank. The maximum drop in tunnel water pressure was identified by inversing the data in the find_peaks function.

To process the raw signal, Butterworth filter of 4^{th} order with cutoff frequency of 0.0055 Hz was applied followed by implementation of find_peaks function. By setting a prominance value of 0.8 Hz and a width of 160 seconds, it was able to identify nearly all the downsurge peaks throughout the entire study period.

The extracted tunnel and borehole pressure data for start and stop sequences is shown in Figure 6-3. In this way, the data containing start and stop sequences were extracted and further used in the analysis.

6.1.3 Natural frequency of oscillation

The instrumentation location is positioned just downstream of the surge tank, where significant pressure changes occur during transients. In this specific location, two different types of pressure wave can be observed when transient occurs. First, waves oscillating with relatively short time period of few seconds with high frequency, which are elastic shock waves. Second, waves oscillating with longer time period of few minutes that are synchronous with the water level change in the surge tank (Jaeger, 1953). This oscillation cannot be measured separately

because one wave superimposes with other as they occur simultaneously. So, it is necessary to differentiate these waves to interpret and analyze them separately.

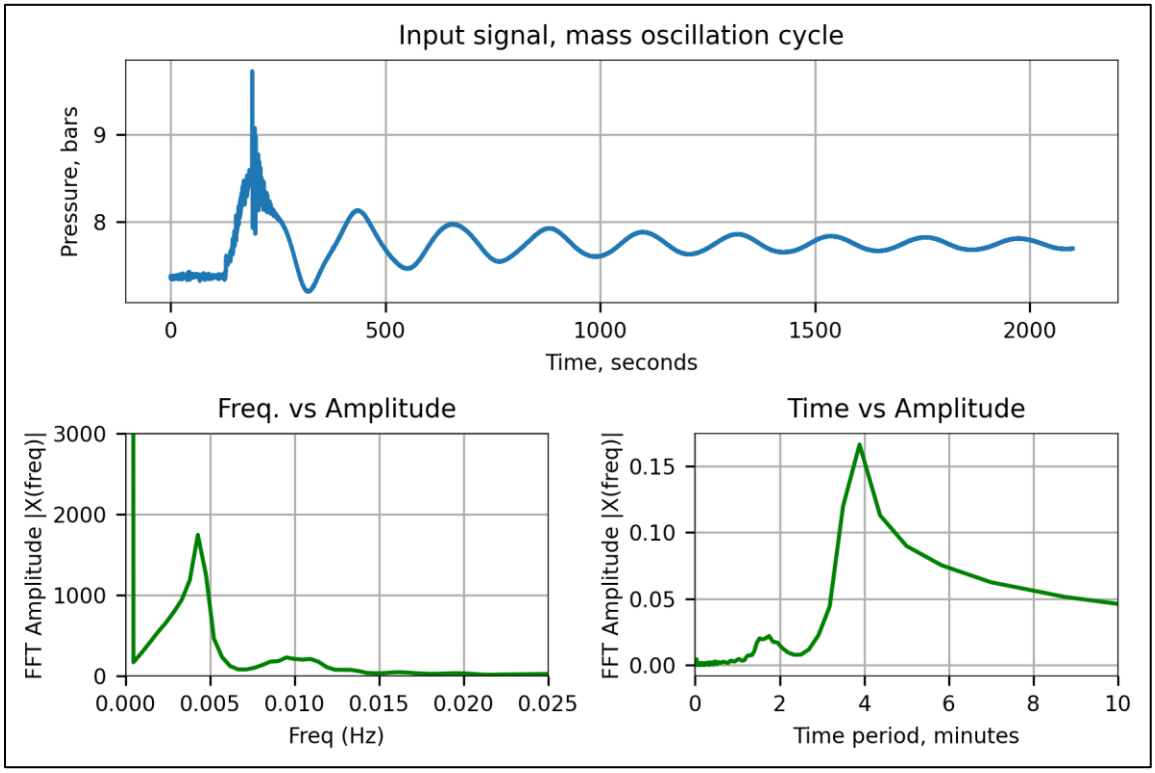

Figure 6-4: Results of FFT analysis applied in mass oscillation. Top figure shows the surge wave considered for analysis, here only the one half cycle of the osscilating wave is taken. Bottom left figure shows the results of FFT in frequency domain and bottom right figure shows the same result in time domain.

Fast Fourier Transformation (FFT) is an algorithm that converts a signal from time domain to frequency domain which can be used to find the natural or pure frequency of vibration. A fully developed waveform of tunnel water pressure in stop sequence was selected to find out the frequency of mass oscillation (Figure 6-4 top). When the signal is transformed from time domain to frequency domain, it shows the constituents frequencies that make up the signal. In Figure 6-4 (bottom left), it is evident that the there are two major constituent frequencies of 0.004 Hz and 0.01 Hz. These frequencies correspond to the time period of 3.75 minutes and 1.54 minutes, (Figure 6-4 bottom right). The wave with higher time period i.e., 3.75 min is the oscillation moving between reservoir and surge shaft and the second one with period 1.54 min is the wave oscillating between reservoir and brook intake. It is to be noted that the time period depends on the distance between the free water surfaces in the waterway system. If the distance between the free water surfaces is greater, the moving waves will have a longer time period, and vice versa.

The same analysis using FFT on all the start and stop sequences throughout the study was performed. The results consistently showed a natural frequency of oscillation corresponding to a time period of 3.75 minutes (Figure 6-5). For this analysis, the tunnel water pressure data is only considered because the borehole data does not provide information about the frequency of actual pressure surge waves occurring in the tunnel. This consistency in natural frequency shows that the time period of mass oscillation remains unchanged regardless of the discharge amount, reservoir head, start or stop sequences, and other parameters. It is solely the function of geometric characteristics of the pendulating system and frictional resistance of the headrace tunnel (Mosonyi, 1991).

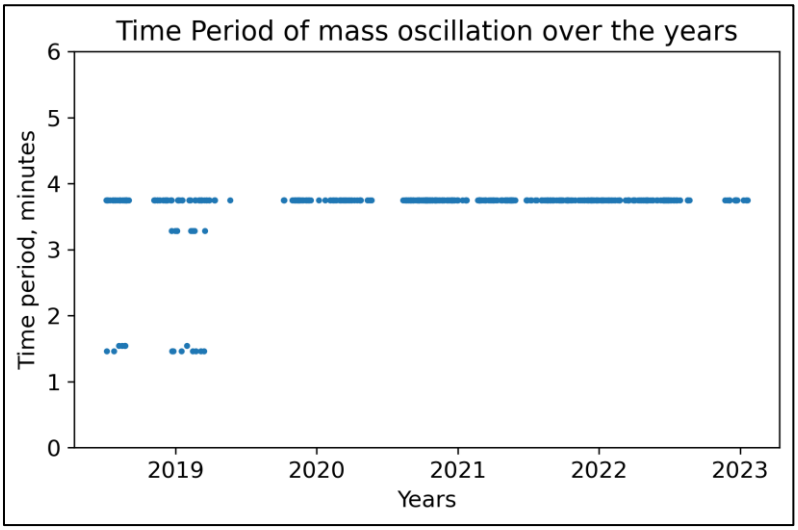

Figure 6-5: Time period of mass oscillation over the study period.

In the analysis done in preceding section, it was seen that the FFT was able decompose wave into the constituent frequency that make up the signal of mass oscillation. However, it couldn't reveal the frequency of water hammer. At first, a simple theoretical approach was carried out to find the frequency of water hammer waves. For this, a theoretical water hammer frequency was calculated using Equation (3-24) which depends upon the modulus of rigidity (shear modulus) of rock. The average shear modulus of 25 GPa was estimated on elasticity modulus obtained from experimental data from intact rock samples (Neupane & Panthi, 2021). With a distance of 87 meters between the free water surface (surge tank) and turbine, the wave velocity obtained from Equation (3-24) is 1391 m/s. This results in a water hammer frequency ($f = c/2L$) of 8 Hz. Frequencies higher than this are generated by other structures, such as the vibration of the penstock.

One major limitation of FFT is that it captures total or overall information about frequency. That means, FFT analyzes the frequency that exists over entire pressure signal. If we consider

the full wave that includes mass oscillation, the effect of water hammer is barely noticable because there are other superimposed waves which make the water hammer wave difficult to detect. Water hammer waves die out after 1-2 cycles of oscillating waves which are highly localized in time. Therefore, it is necessary to separate and isolate the oscillating wave associated with water hammer for FFT analysis in order to effectively detect water hammer. Figure 6-6 (top) shows the extracted water hammer wave considered for FFT analysis.

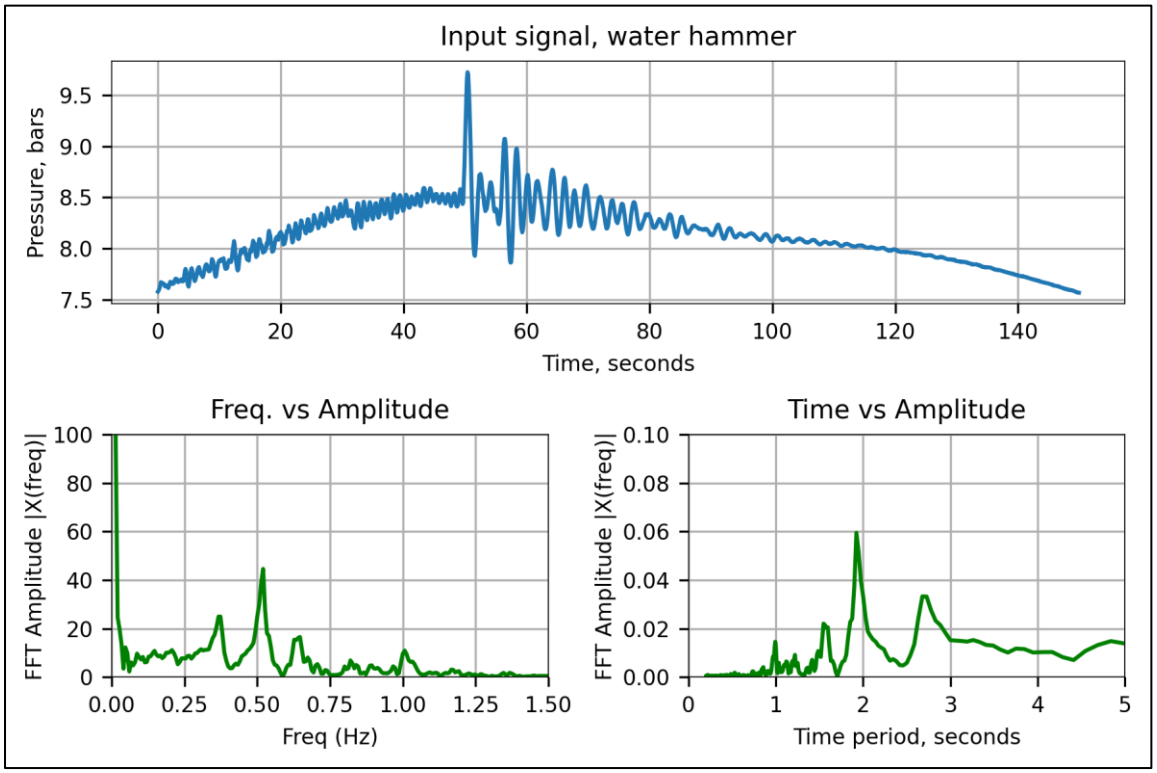

Figure 6-6: Results of FFT analysis applied only in water hammer surge wave. Top figure shows the surge wave considered for analysis, here only the one half cycle of the osscilating wave is taken. Bottom left figure shows the results of FFT in frequency domain and bottom right figure shows the same results in time domain.

It can be seen from the time-domain graph (Figure 6-6) that the highest amplitude is obtained at time period of 2s. This time period corresponds to the water hammer surges in the system. Other waves with small and large frequencies are also observed because of pipe vibration and different parts of water hammer reflected by various physical structures and transitions between sensor location and turbine. However, the waves generated by reflection from structures would only be recorded if the measurements were taken close to the turbine. So, the major source of these high-frequency signals in the measurements is predominantly due to pipe vibration. This argument is supported by the fact that when the MIV is completely closed, signals with frequencies higher than 1 Hz decrease significantly. Closing the MIV stops the water flow towards the turbines, resulting in minimal vibrations in the pipes.

It is evident that there are no significant waves of natural frequencies having time-period less than 1s (Figure 6-6 bottom right). The small amplitude rise at 1s in Time vs Amplitude graph indicates that the frequency corresponding to 1s i.e. (1 Hz) can be used to filter unnecessary noise for calculating total impact.

There is a notable discrepancy between the theoretical and FFT approaches when comparing the water hammer frequency. The FFT method, being a practical approach that yields results from real site conditions, is used for further analysis.

6.1.4 Shutdown

There are two methods for shutting down hydropower plants. The first method is an emergency shutdown, which involves rapidly closing a particular unit in the event of it being stopped by the protection systems or disconnected from the power grid during operation. This type of shutdown is occasional and produces significant pressure amplitudes and transients. The second method is a normal shutdown, where the plant operator gradually reduces the unit's load manually in stages. The aim of a regular shutdown is to execute a gradual shutdown in multiple stages, aiming to minimize stress on the electromechanical components.

Both emergency and regular shutdowns can be divided into two stages. In the first stage, the guide vanes are closed to reduce the flow through the turbines, while in the second stage, the MIV is fully closed to completely halt the flow. The closure of the MIV results in the generation of maximum pressure or pressure peaks in the pressure wave, as illustrated in Figure 6-7.

During a normal shutdown process, the operator of the power plant determines the appropriate number of steps to gradually reduce the power output before initiating the final shutdown. This can be done by decreasing the output in steps, such as 10 MW at a time, over a period of several minutes. Alternatively, the shutdown can be completed in a single operation, taking only a few minutes. Once the final shutdown signal is given, the guide vanes are fully closed, disconnecting the unit from the grid, and causing it to decelerate. To bring the unit to a complete stop, the brakes are engaged. Typically, the MIV starts closing after a specified time interval following the shutdown signal, which usually occurs between the unit's disconnection from the grid and its complete stoppage.

Determining the shutdown duration presents a challenge as the closure maneuver of the valve cannot be solely obtained from the pressure transient curve. To accurately ascertain the shutdown time, it is necessary to consider valve properties such as the coefficient of discharge, area, and discharge transient curve. Although there may exist certain uncertainties that hinder

the precision of obtaining the shutdown time (pers. com, Vereide, 2023), a relative measure of the shutdown speed is established in the analysis. This measure is derived from the time elapsed between the initiation of the shutdown event and the occurrence of the highest amplitude of mass oscillation after noise reduction, as depicted in (Figure 6-7). This relative measure is henceforth referred to as the "shutdown duration."

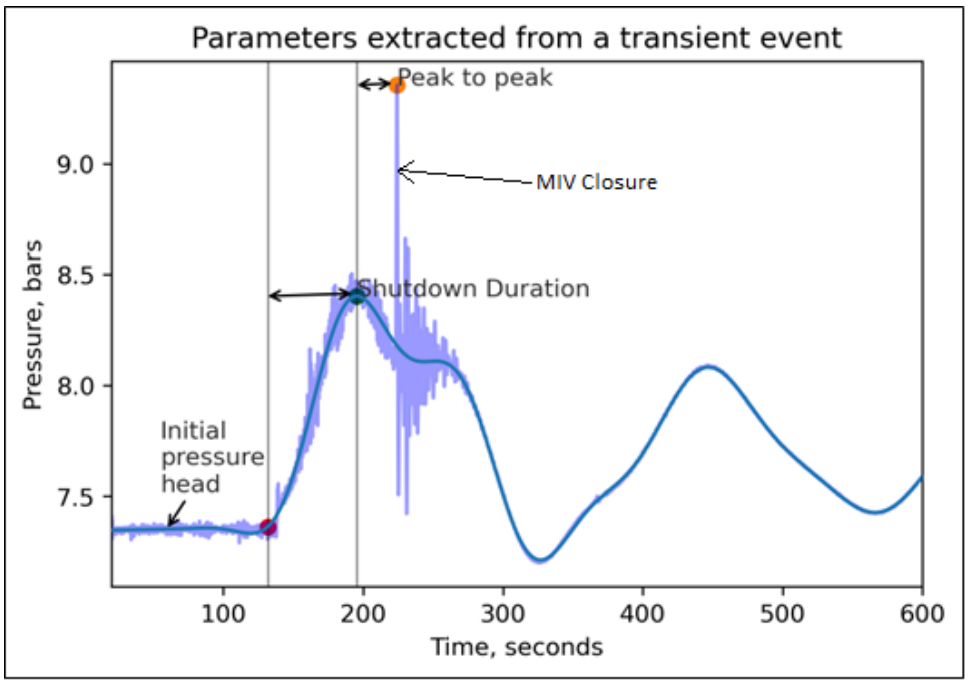

Figure 6-7: Shutdown duration and the initial pressure head (water head) in a stop transient event. Faint blue shows the raw data with noise and blue line shows filtered data with cutoff frequency of 0.0167 Hz.

Figure 6-8 illustrates the shutdown duration trends from the start of the instrumentation until January 2023. Notably, there was a significant reduction in shutdown duration, dropping from approximately 120 seconds to around 60 seconds in late 2019. This sharp decline is believed to have occurred due to a change in the operational manager of the power plant (pers. com. Vereide, 2023). However, this change has provided a unique opportunity to explore the relationship between shutdown duration and its impact on the surrounding rock mass during transients. For the purpose of this study, shutdown durations of less than 75 seconds are classified as fast shutdowns, while durations exceeding 100 seconds are classified as slow shutdowns.

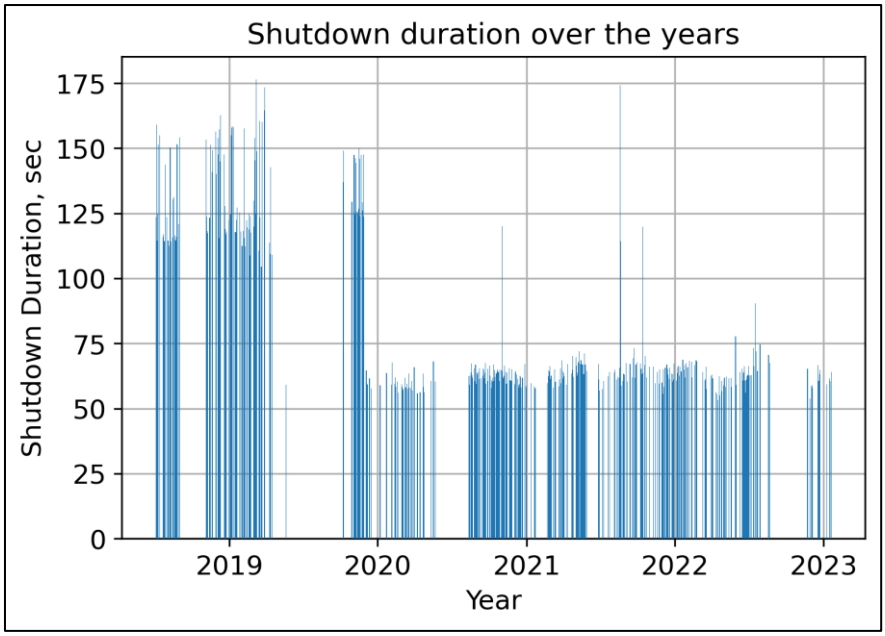

Figure 6-8: Shutdown duration over the years.

6.1.5 Quantifying the impact

When plotting a transient event in the waterway system, it becomes evident that there is a delay in the pore pressure response within the rock mass compared to the tunnel water pressure. The delay in joint pressure compared to tunnel pressure occurs because of a lag in the formation of pressure within the rock joints, which is influenced by factors such as their openness, location, length and pressure difference.

The presence of higher pore pressure in the rock mass compared to the tunnel water pressure poses an impact on the surrounding rock mass adjacent to the tunnel. This is primarily due to the stress exerted by the surrounding rock mass towards the tunnel, which is predominantly destabilizing in nature and unfavorable against the resistance capacity of rock joints. This unfavorable condition persists for a certain duration and occurs in two or three cycles following the closure or opening of valves, raising the possibility of block falls caused by the unbalanced force directed towards the tunnel. As the transient attenuates, the time lag between joint pressure and tunnel water pressure gradually diminishes, eventually reaching a state where both pressures nearly equalize or the pressure inside the tunnel becomes higher.

In order to assess the impact of transients on the surrounding rock mass of a tunnel and establish an objective measure, a quantification method is necessary. Given that a situation where joint pressure exceeds tunnel water pressure is considered undesirable, it becomes essential to express this condition in numerical terms. This additional stress condition, referred to as "hydraulic impact" (HI), was defined by Neupane, Vereide, et al., (2021) and is measured in

MPa.s. HI can be compared to dynamic viscosity or the force exerted on the joint surfaces per unit area over time. The mathematical expression for HI is provided in Equation (6-1). It is recognized as a destabilizing force and the primary factor contributing to rock block destabilization in the tunnel periphery during hydraulic transients, potentially leading to rock falls and tunnel collapse.

$$HI = \begin{cases} \int_{t_1}^{t_2} BHP - TWP\,, & TWP < BHP \\ 0, & TWP \geq BHP \end{cases} \qquad (6\text{-}1)$$

Where HI is hydraulic impact, BHP is bore hole pressure, TWP is tunnel water pressure, t_1 and t_2 are two time periods.

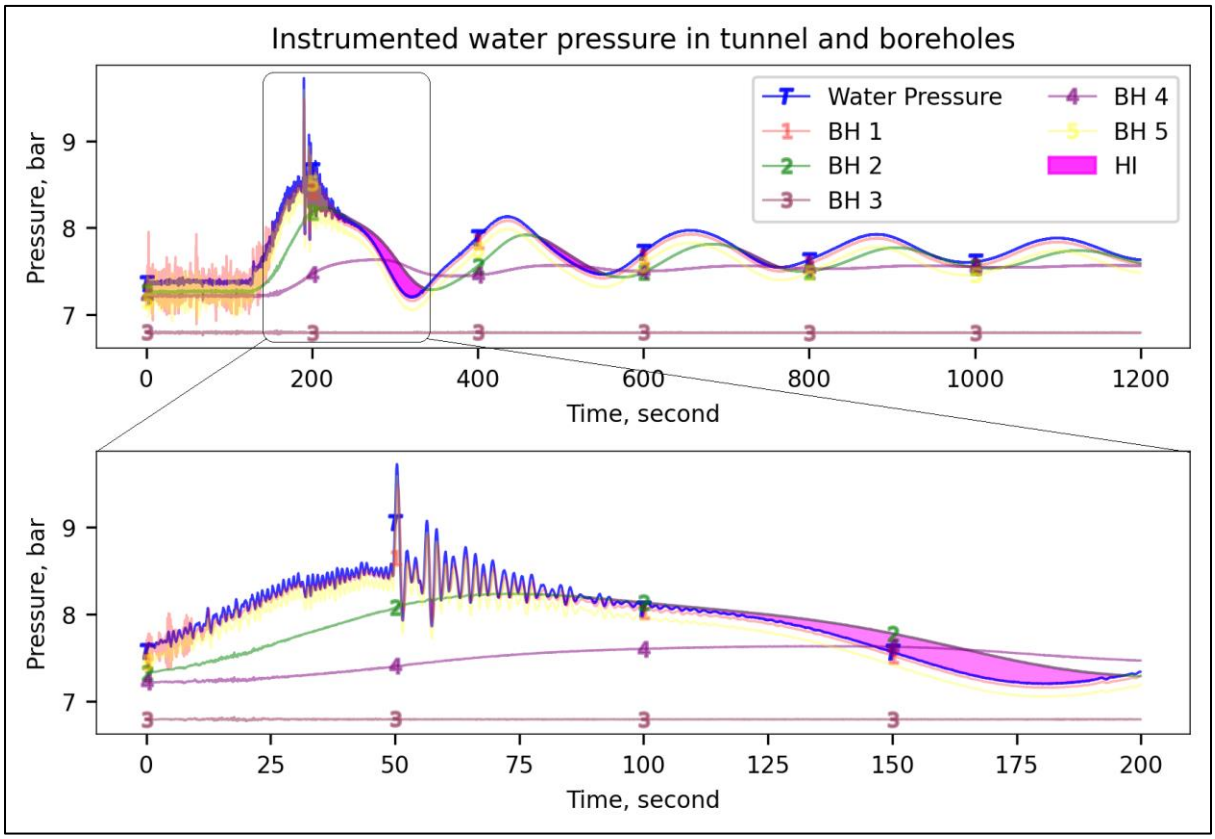

Figure 6-9: Response of pore pressure of all the boreholes and tunnel water pressure. The top figure shows a typical stop sequence, and the bottom figure shows the water hammer waves within the mass oscillation waves.

From a typical shutdown event of May 2021 (Figure 6-9), it is evident that boreholes 2 and 4 experience the hydraulic impact due to pressure-lag between tunnel and rock mass. At some instances after the valve closure, the pressure in borehole is larger than the tunnel water pressure, which is unfavorable for tunnel walls. This unfavorable situation persists until three

complete mass oscillation for borehole 2 and two complete mass oscillation for borehole 4 (Figure 6-9).

Observing a typical shutdown event that occurred in May 2021 (Figure 8 9), it becomes evident that BH2 and BH4 experience pressure lag between the tunnel and rock mass. Following the start of shutdown event, the pressure within these boreholes surpasses the tunnel water pressure, posing an unfavorable condition for the tunnel walls. This adverse situation persists until three complete mass oscillations for borehole 2 and two complete mass oscillations for borehole 4 (Figure 6-9).

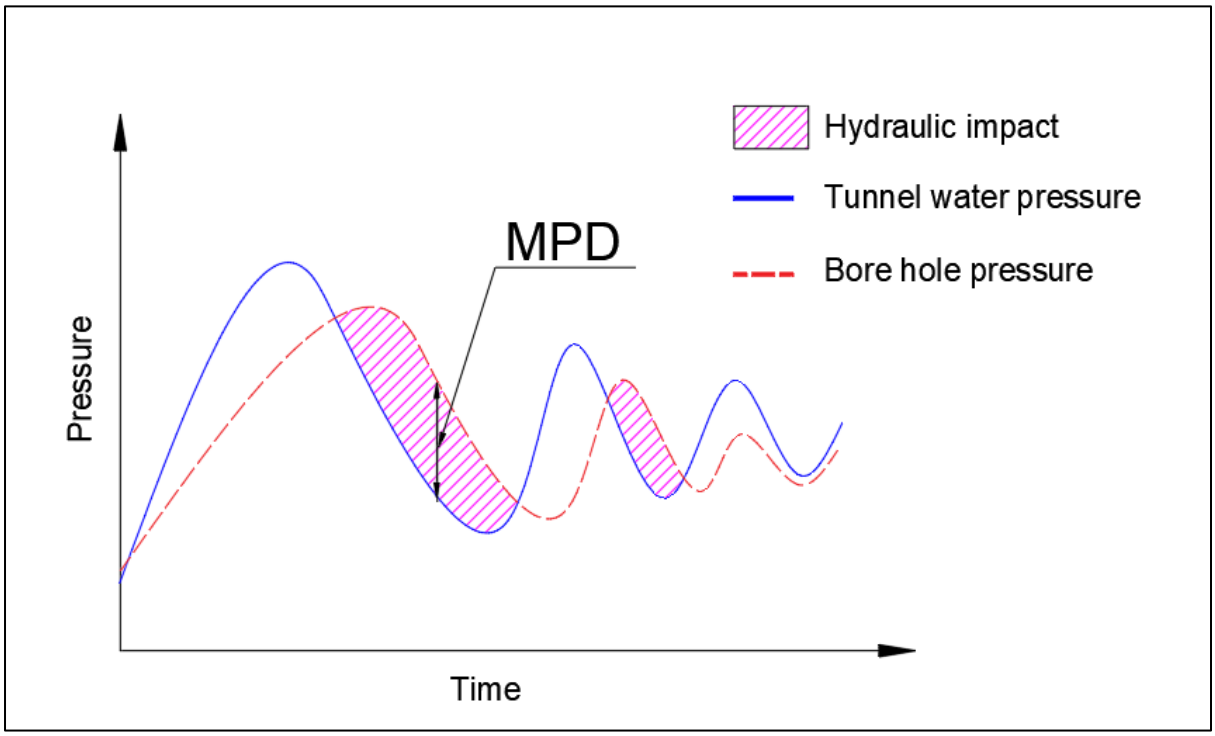

Figure 6-10: Schematic figure representing quantification parameters for impact of transients in rock mass.

In contrast, BH1 and BH5 exhibit no phase lag between tunnel pressure and borehole pressure, suggesting a lower risk to stability compared to the other three boreholes. This is due to the smaller pressure difference between the tunnel and bore holes. The pressure in BH3 is unaffected by transient and way below the tunnel water pressure. So, BH3 does not create any hydraulic impact on the tunnel walls.

This study introduces a new term called "maximum pressure difference" (MPD). It refers to the largest difference in pressure between tunnel water and bore hole during a transient event, when the bore hole pressure exceeds the tunnel water pressure. It is the force exerted per unit area on the joint surface and is measured in MPa or bars. It does not take account of the time

of action of stress but only accounts for the magnitude of stress induced due to hydraulic transients. So, for one transient event there is one value of MPD. The expression of MPD is given in Equation (6-2). The schematic representation of HI and MPD is shown in Figure 6-10.

$$MPD = \begin{cases} BHP - TWP, & TWP < BHP \\ 0, & TWP \geq BHP \end{cases} \quad (6\text{-}2)$$

6.1.6 Method of calculating HI and MPD

The raw data contains a significant amount of noise of higher frequencies. The first step involved removing these noises to ensure a noise-free signal. Subsequently, the waves generated by water hammer and mass oscillation were separated. It was necessary to separate them in order to assess the impact of each component individually. The natural frequency of vibration is already calculated using FFT as described in Section 6.1.3. With this knowledge, a Butterworth low-pass filter is used to filter out waves with frequencies lower than the cutoff frequency. Figure 6-6 provides information that the water hammer frequency with the largest amplitude in the frequency domain is 0.5 Hz, corresponding to 2 seconds. Another peak is observed at 1 second. As explained in Section 6.1.3, the frequency corresponding to 1 second is adopted as the cutoff frequency for noise filtration. After applying Equation (6-1) and (6-2), the noise-filtered signal enabled the calculation of the total hydraulic impact and maximum pressure difference.

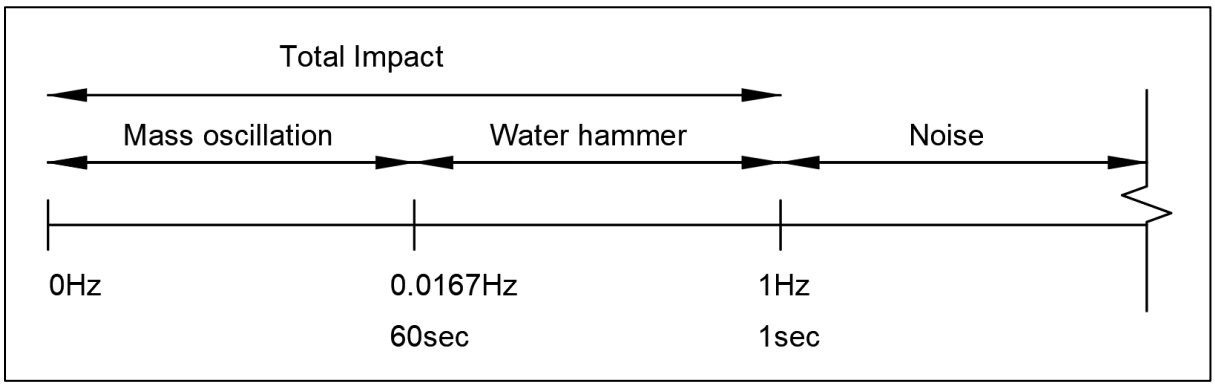

Figure 6-11: Cutoff frequencies used for quantifying impact.

To determine the hydraulic impact (HI) and maximum pressure difference (MPD) specifically due to mass oscillation, it is necessary to remove the water hammer waves from the signal as well. The frequency domain analysis revealed that the maximum amplitude of mass oscillation waves is 0.004 Hz, corresponding to 3.75 minutes, as depicted in Figure 6-4. Additionally, smaller amplitudes up to 0.015 Hz are also present. Hence, a cutoff frequency of 0.0167 Hz, corresponding to a time period of 1 minute, was selected to filter out the water hammer waves

from the overall signal. The subsequent calculation involved determining the area and magnitude between pressure pulses after applying this filter, which provided the HI and MPD values for mass oscillation, respectively. Finally, by subtracting the HI and MPD values obtained for mass oscillation from the total HI and MPD, the corresponding values for water hammer were calculated. The cutoff frequencies for obtaining impacts due to various components of waveform is shown in Figure 6-11.

6.2 Results

6.2.1 Pore pressure response

This section provides an overview of the intersection of boreholes in relation to different joint systems. It describes their expected response to transients and observes their behavior throughout the study period. It also explains how the behavior of the boreholes can be understood by using HI and MPD.

BH1: BH1 intersects through approximately five Jf. It also passes through Jfconductive having washed out filling and larger aperture with continuous flow. The intersection point between Jfconductive and BH1 is located approximately 1.5 m along the joint from the tunnel contour. Due to these characteristics, it is expected that BH1 acts as a responsive borehole and is responsive to transient events.

Initially, BH1 exhibited responsiveness, particularly during shutdowns. However, from August 2018 until mid-November 2018, it stopped being responsive. After that period, it resumed being responsive. During shutdowns, BH1 has more water hammer pulses compared to other boreholes, resulting in the highest MPD, as depicted in Figure 6-14. This is explained further in Section 8.10. The phase lag of BH1 is minimum as compared to the other responsive boreholes. It can also be observed from Figure 6-12 that BH1 is almost in phase with the tunnel water pressure.

BH2: BH2 intersects with J1, running subparallel to Jf. There is no hydraulic connection between BH2 and J2, which has a partially open joint with washed out filling. J1, on the other hand, is a tight joint filled with impermeable clay. Therefore, it can be anticipated that BH2 would not exhibit significant response to the transients.

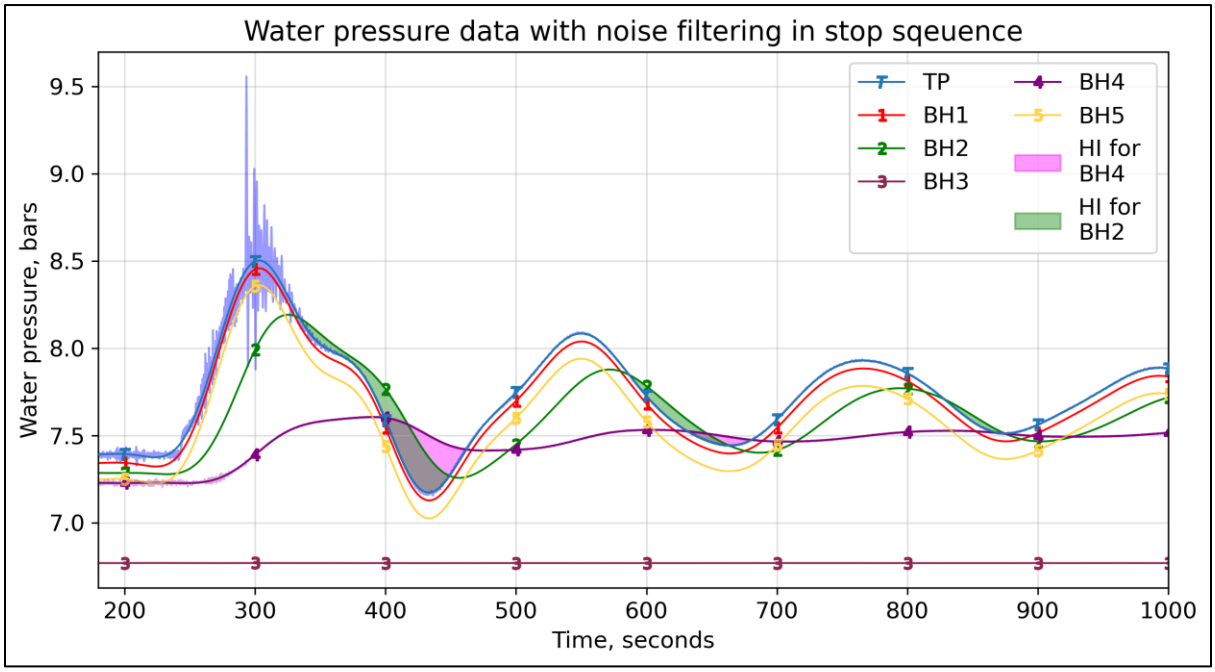

Figure 6-12: Water pressure data of tunnel and boreholes in a typical stop sequence (normal shutdown) and the hydraulic impact caused by it. The noise is filtered using butterworth filter with cutoff frequency of 0.0167 Hz (60s) for tunnel water pressure and boreholes. Typical filtering is shown only for tunnel and borehole 4. Other boreholes data are filtered in the same way.

BH2 initially did not show a response when the instrumentation program began. However, it gradually became moderately responsive starting in December 2018. Following the dewatering of the tunnel in May 2019 and its subsequent filling in September 2019, the behavior of BH2 changed, and it transformed into a moderately responsive joint. Over time, its responsiveness increased. By the end of August 2020, BH2 became more responsive compared to BH4, particularly during the start sequence (Figure 6-13). A typical response of BH2 during stop sequence with its HI along with other boreholes is shown in Figure 6-12.

During the inspection carried out one year after setting up the instrumentation station, it was discovered that the pipe connected to BH2 was broken. Efforts were made to fix the pipe and minimize its vibration by grouting (pers. com. Neupane, 2023). However, the pipe could not be fully repaired as it continued to induce HI even after maintenance. The broken pipe acted as a dummy or artificial joint since it was not fully connected to the tunnel water pressure, yet it still caused HI. Despite the broken pipe connecting BH2, it can potentially be utilized to investigate the effects of variables like shutdown duration and static head on HI and MPD (pers. com. Vereide,2003).

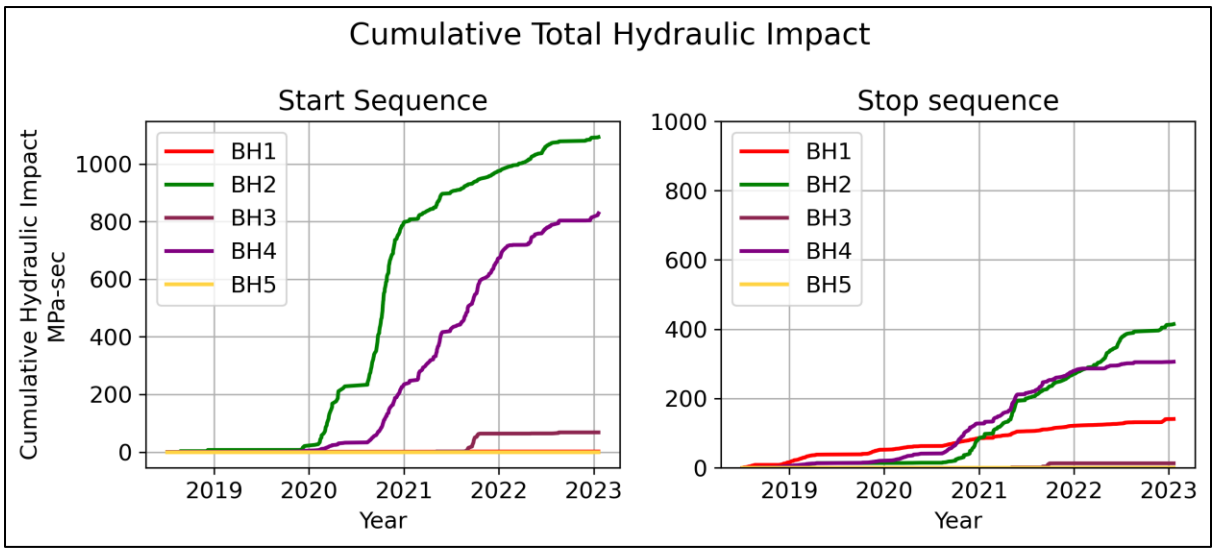

Figure 6-13: Cumulative hydraulic impact for boreholes and tunnel pressure. The cumulation of pressure difference shows start sequence is severe in all boreholes except for BH1. It indicates that moderately responsive boreholes possess more impact in start sequence than in stop sequence.

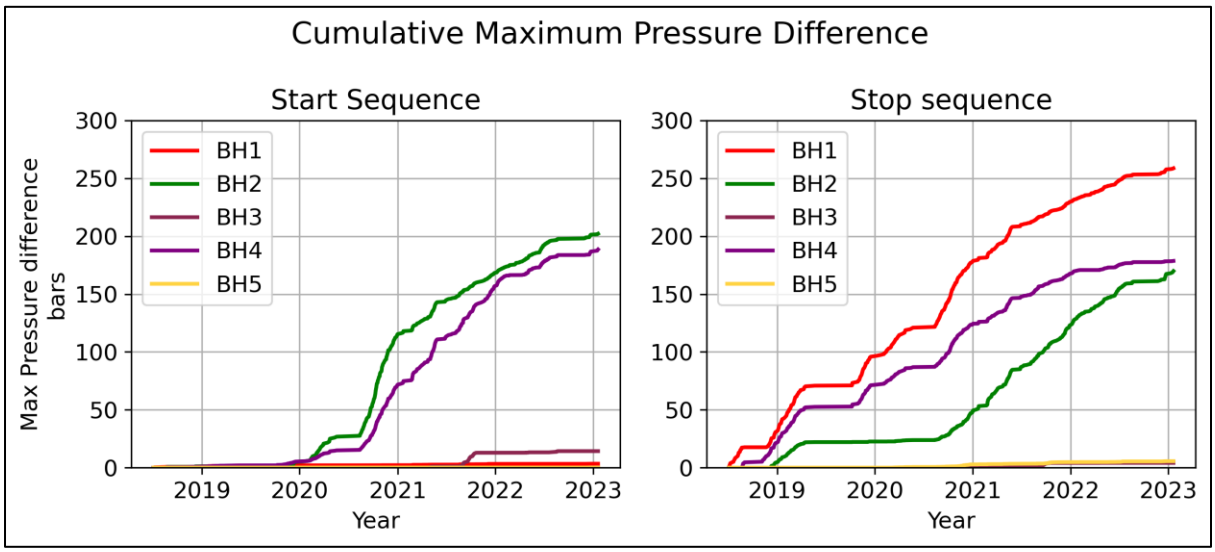

Figure 6-14: Cumulative maximum pressure difference for boreholes and tunnel pressure. The cumulation of pressure difference shows start sequence is severe in all boreholes except for BH1.

BH3: BH3 intersects with approximately 4 to 5 foliation joint, Jf, which is also a tight joint filled with clay. There is no hydraulic connection between BH3 and Jfconductive. Additionally, BH3 runs subparallel to J1. Therefore, it is expected that BH3 would not exhibit any response to the transients.

BH3 has been a non-responsive joint from the beginning of the instrumentation program. It shows little to no response to the transients and does not induce any HI and MPD (Figure 6-12). However, the pressure of BH3 went higher than tunnel water at some instances following the

start sequence in Sept and Oct-2019. The reservoir operation level started decreasing but the BH3 being a non-responsive joint didn't respond quickly to the reservoir and tunnel water level. Following the start sequence, tunnel water level decreased steeply below the pressure of BH3 which induced HI and MPD in such situation. The HI and MPD resulting from this situation can be observed in start sequence depicted in Figure 6-13 and Figure 6-14.

BH4: BH4 intersects with approximately 4 to 5 J1 which is a tight joint filled with clay. It passes also through J2 which partly open joint with washed out infilling. The intersection point between J2 and BH4 is located approximately 8 m along the joint from the tunnel contour. So, this borehole is expected to be responsive to transients.

BH4 is a moderately responsive joint. The responsiveness of this joint started decreasing from late Dec-2020 and again became normal from late Jan-2021. It induces more hydraulic impact in start sequence than in stop sequence. Figure 6-15 shows the HI caused by BH4 in start sequence enclosed by large area between BH4 and tunnel water pressure. On some occasions, it causes HI even after 20 minutes of start event as shown in Figure 6-16. From Feb-2022, the characteristics of BH4 changed making it unable to induce hydraulic impact significantly especially in stop sequence as indicated in Figure 6-13.

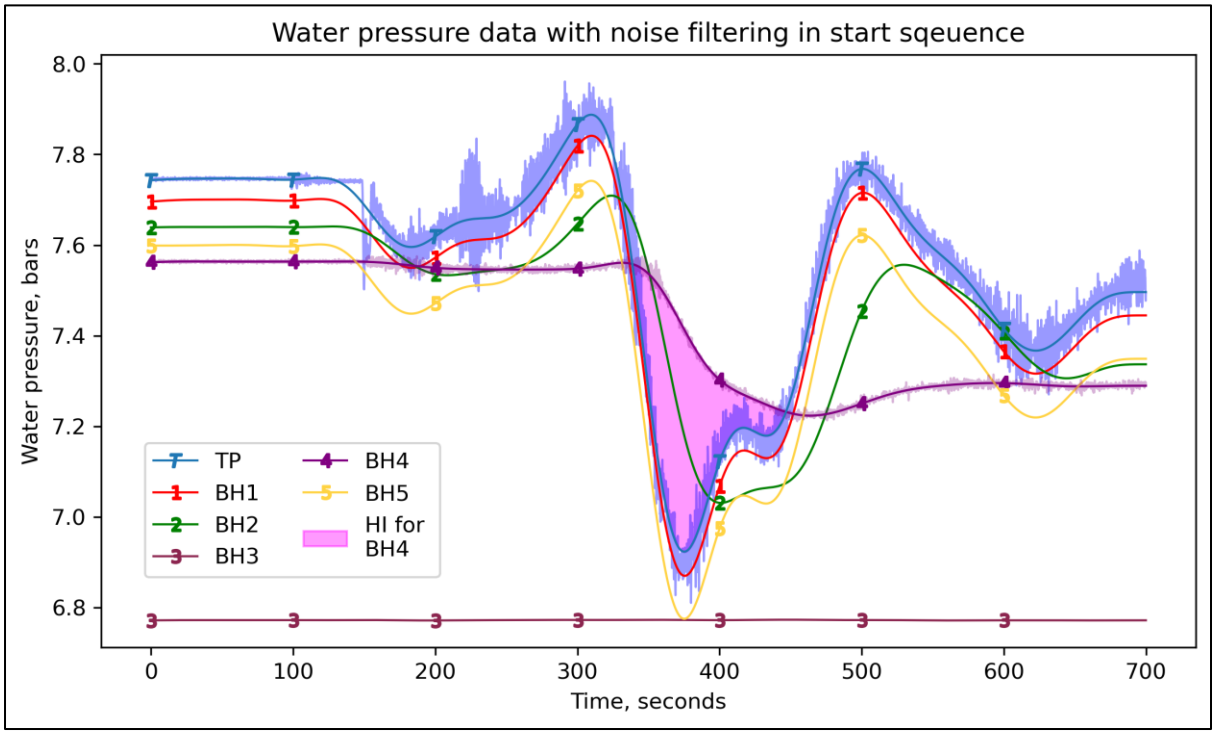

Figure 6-15: Water pressure data of tunnel and boreholes in a typical start sequence and the hydraulic impact caused by it. The noise is filtered using butterworth filter with cutoff frequency of 0.0167 Hz (60s) for tunnel water pressure and boreholes. Typical filtering is shown only for tunnel and borehole 4. Other boreholes data are filtered in the same way.

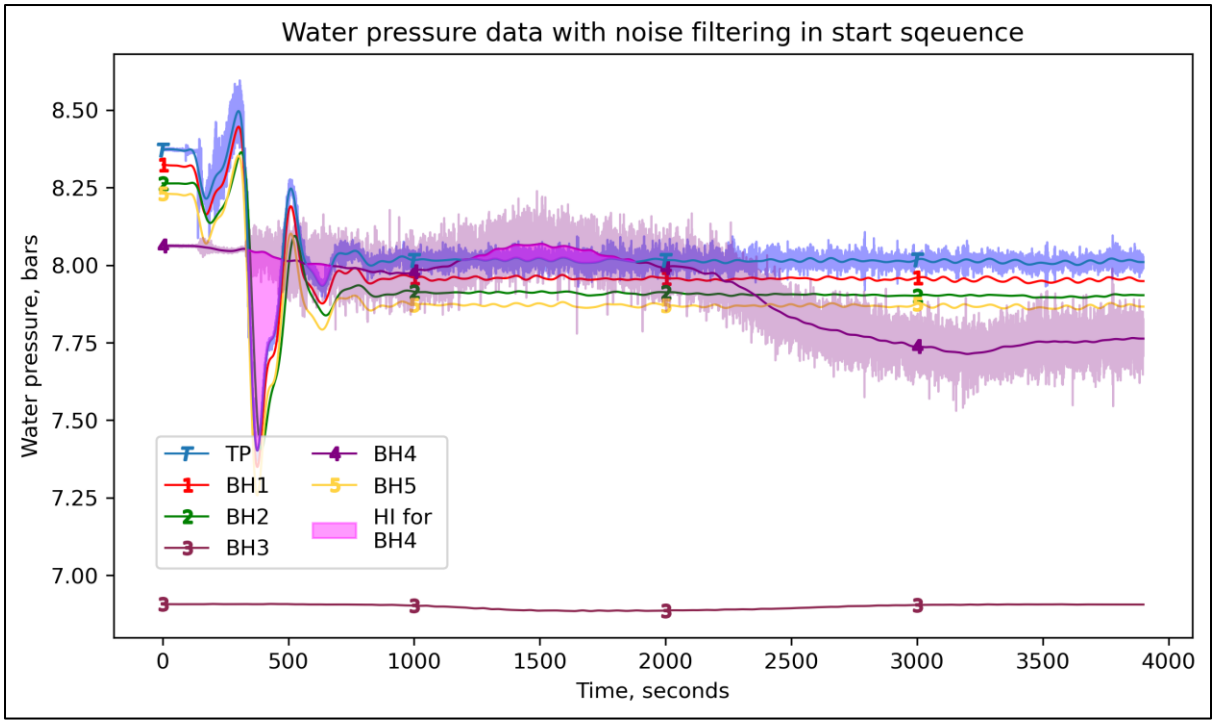

Figure 6-16: Water pressure data of tunnel and boreholes in a typical start sequence and the hydraulic impact caused by it. The noise is filtered using butterworth filter with cutoff frequency of 0.0167 Hz (60s) for tunnel water pressure and boreholes. Typical filtering is shown only for tunnel and borehole 4. Other boreholes are filtered in the same way. Borehole pressure causes hydraulic impact even after 20 minutes of hydropower starts.

BH5: BH5 is on the left side of the tunnel wall and passes only through Jf which is a tight joint. So, it is expected to be a non-responsive borehole. However, the effective length of this borehole is 8m so could be bit responsive than BH3 having effective length of 5m.

BH5 was non-responsive and started becoming a highly responsive borehole from March-2020. This point onward, BH5 became the responsive borehole but did not induce HI or MPD because it follows the tunnel water pressure without phase lag. The characteristics of BH5 lately can be classified as highly responsive joint that follows tunnel water pressure without generating HI and MPD. However, there might be leakage from BH5 due to broken pipes.

6.2.2 Start and stop sequence

The previous study did not analyze the start sequence, even though there are significant pressure fluctuations in the tunnel water during turbine startup. This omission was due to presence of a considerable amount of noise in the measurement data of the start sequence, making it challenging to analyze (pers. com. Neupane, 2023). Figure 6-15 also shows that when the water starts flowing, it induces vibrations in the borehole pipes after the tunnel startup. Hence, the start sequence was not considered in the previous study (Neupane, 2021).

It was observed that the oscillation time period remains constant, regardless of other variables, except for the geometry of the pendulating system and the friction of the headrace tunnel. This means that the time period does not depend on whether it is a start or a stop sequence. Therefore, the start sequence was analyzed in the same manner as the stop sequence. However, obtaining the start duration solely from the waveform information is challenging (according to Vereide, 2023).

The analysis of hydraulic impact (HI) indicates that, on average, the HI induced during start sequences is three times as much as that during stop sequences over the entire study period, which includes 1008 start and stop sequences. The cumulative values of HI and MPD, shown in Figure 6-13 and Figure 6-14 respectively, demonstrate that BH2 and BH4 exhibit greater HI during start sequences compared to stop sequences. On the other hand, BH1 exhibits higher MPD during stop sequences because the impact induced by water hammer is relatively greater than that by mass oscillation. In average, the start sequence produces three times as much HI as compared to the stop sequence.

The start and stop sequences are two different events that occur one after the other. During the stop sequence, water cannot enter the penstock and instead moves towards the surge shaft, causing an increase in water level and pressure in the tunnel. The borehole pressure follows the tunnel water pressure but with a slight delay and a reduced peak. As the water level drops in the surge tank after reaching its maximum, the borehole pressure still follows the tunnel water pressure but with a lag, and the pressure in the borehole becomes higher than the tunnel water pressure, resulting in hydraulic impact (Figure 6-12).

On the other hand, during the start sequence, water is intermittently supplied to the turbine from the surge shaft, leading to a sudden decrease in water level and tunnel water pressure. So, naturally the first series of oscillation is down surge. The boreholes also follow the tunnel water pressure but with a delay, and their pressure becomes higher than the tunnel water pressure. This creates an unfavorable situation because of a destabilizing force acting towards the tunnel. The decrease in water level during the stop sequence after reaching the peak is not as significant as the fall in water level during the start sequence. In certain cases, during the stop sequences, the pressure in the borehole remains higher than the tunnel pressure even after the water level in the tunnel stabilizes. This can be observed in Figure 6-16, which illustrates BH4 induces HI even after 20 minutes of start of turbines. Therefore, the HI induced during the start sequence is observed higher as compared to the stop sequence. The HI for all start and stop events over the study period is shown in Figure 6-17.

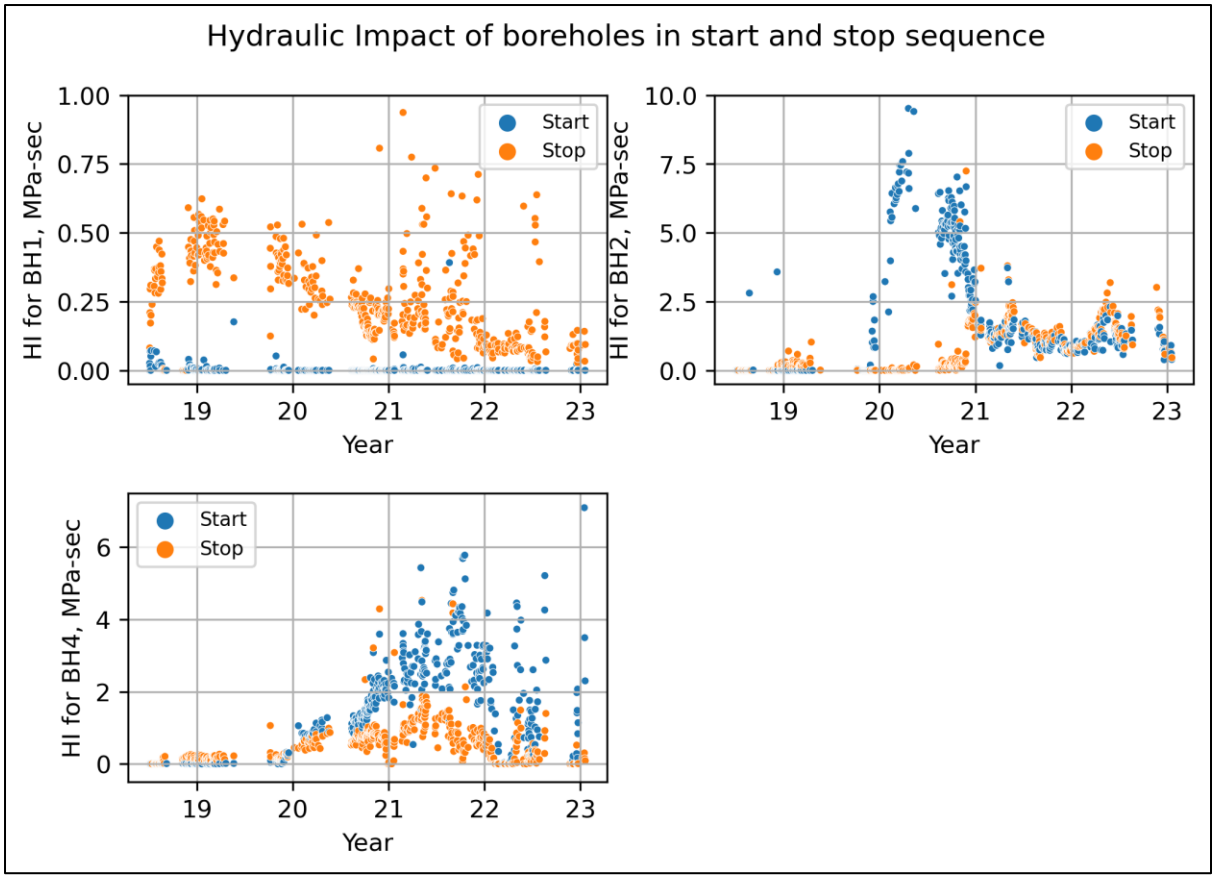

Figure 6-17: Hydraulic Impact of boreholes in start and stop sequences for BH1, BH2 and BH4.

6.2.3 Effect of Shutdown duration

Shutdown duration can have influential effect on the transients in the waterway system of hydropower (Bhattarai et al., 2019). The shutdown duration can also have effect on rock mass surrounding the tunnel (Neupane, Vereide, et al., 2021). So, it is necessary to understand the effect of shutdown duration in transients and the impact on the rock mass surrounding the tunnel.

The minimum and maximum shutdown duration in Roskrepp Hydropower Project is 53s and 177s respectively whereas the average shutdown duration is 80s. Due to the shutdown procedures as explained in Section 6.1.4, normal shutdowns area rarely similar with each other because shutdowns are manual operations which depends on the powerplant operator. Figure 6-18 demonstrates the impact of these variations by comparing pressure signals from two distinct shutdown events. Although both events have a similar duration until the closure of the Main Inlet Valve (MIV), they result in different pressure signals.

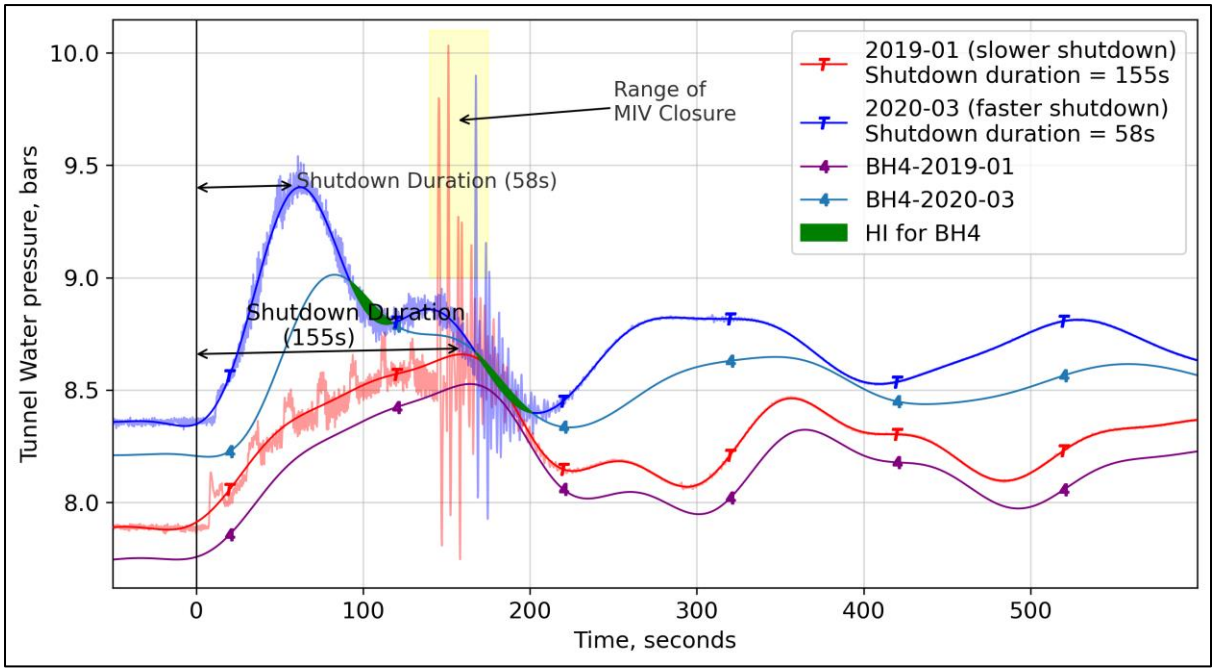

Figure 6-18: Typical stop sequence before late 2019 and after late 2019. Note that in faster shutdown duration of 2020, BH4 is exerting Hydraulic Impact. Tunnel water pressure for both 2019 and 2020 is filtered with cutoff frequency of 0.01167Hz. Note the pulsating wave in 2019 shutdown before MIV closure.

The comparison depicted in Figure 6-18 clearly illustrates the distinct characteristics between the 2019 and 2020 transients. In the 2019 transient, a gradual de-loading and shutdown process is observed, while the 2020 transient exhibits a faster shutdown prior to MIV closure. Despite having a similar range for MIV closure, the 2020 transient generates larger water-hammer pulses, indicating a more rapid shutdown. Furthermore, the amplitude of mass oscillation is greater in the 2020 transient compared to the 2019 transient, with the peak being reached much more quickly. This faster shutdown results in a steeper curve for mass oscillation, leading to a larger time-lag between the tunnel water pressure and the bore hole pressure in the rock mass, as shown in Figure 6-18. This shorter shutdown duration in the 2020 transient allows less time for the rock mass pore pressure to increase, leading to the generation of Hydraulic Impact (HI). The shutdown durations for the 2019 and 2020 transients are 58 seconds and 155 seconds respectively, while the MIV closure time is 145 seconds for both transients. The combination of a larger time lag and a greater amplitude during the shorter duration results in a larger HI.

Figure 6-19 shows the HI of 504 shutdown events recorded over the study period. It can be seen from the Figure 6-19 (top left) that the HI for BH1 is primarily due to water hammer for both longer and shorter shutdown duration. The effect due to mass oscillation is almost

negligible for BH1. In fact, the mean value of HI for slower shutdown is higher than the faster shutdown.

When shutdown is faster, there is more phase lag between tunnel water and bore hole pressure for BH2 and BH4. This creates a situation when bore hole pressure is greater than tunnel water pressure for longer duration. As HI is the pressure difference times time, HI becomes larger for mass oscillation due to larger area of pressure difference. In case of slower shutdown, the pressure amplitudes and steepness of surges are less as compared to faster shutdown. This provides time for the borehole pressure to adjust with the tunnel water pressure as evident from the typical transient sample from 2019 in Figure 6-18. Thus, slower shutdown does not induce considerable HI due to mass oscillation which is also evident from Figure 6-19 (top right and bottom left).

In both faster and slower shutdown, the water hammer component is still present in the waves that have higher frequency. This induces HI in BH2 and BH4 even during slower shutdown but is not as strong as mass oscillation. In moderately responsive joints, HI is primarily caused by water hammer for longer shutdown duration.

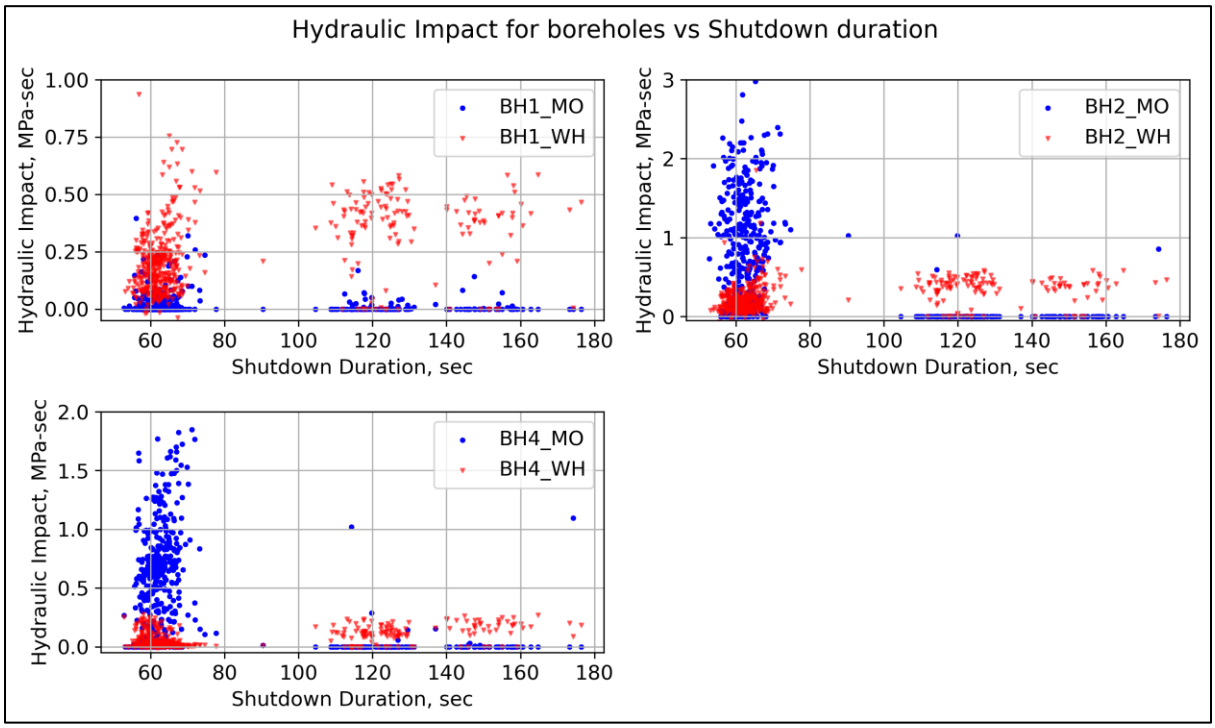

Figure 6-19: Hydraulic impact by mass oscillation and water hammer of stop sequences over the years for borehole 1,2 and 4.

If we consider MPD with respect to shutdown duration to quantify the impact of transient, the scenario is different as compared to HI. It is seen that the effect water hammer is larger than

mass oscillation in all bore holes irrespective of the shutdown duration as shown in Figure 6-20. MPD measures only the water pressure difference between boreholes and tunnel and doesn't consider the area of pressure with time like in HI. MPD has two clusters for slow and fast shutdown duration. It ranges from 0.2 to 0.8 bars for faster shutdown and 0.6 to 1 bar for slower shutdown.

Results from relation of HI and MPD with shutdown duration suggest that the impact of transients due to water-hammer increases with longer shutdown duration because longer shutdown duration allows more pulsating waves before MIV closure. After MIV closure, the water hammer waves also create some time lag which induces more pressure difference. The response of a responsive BH1 to transient is different from moderately responsive BH2 and BH4. This shows that the rock mass can respond differently for same joint conditions.

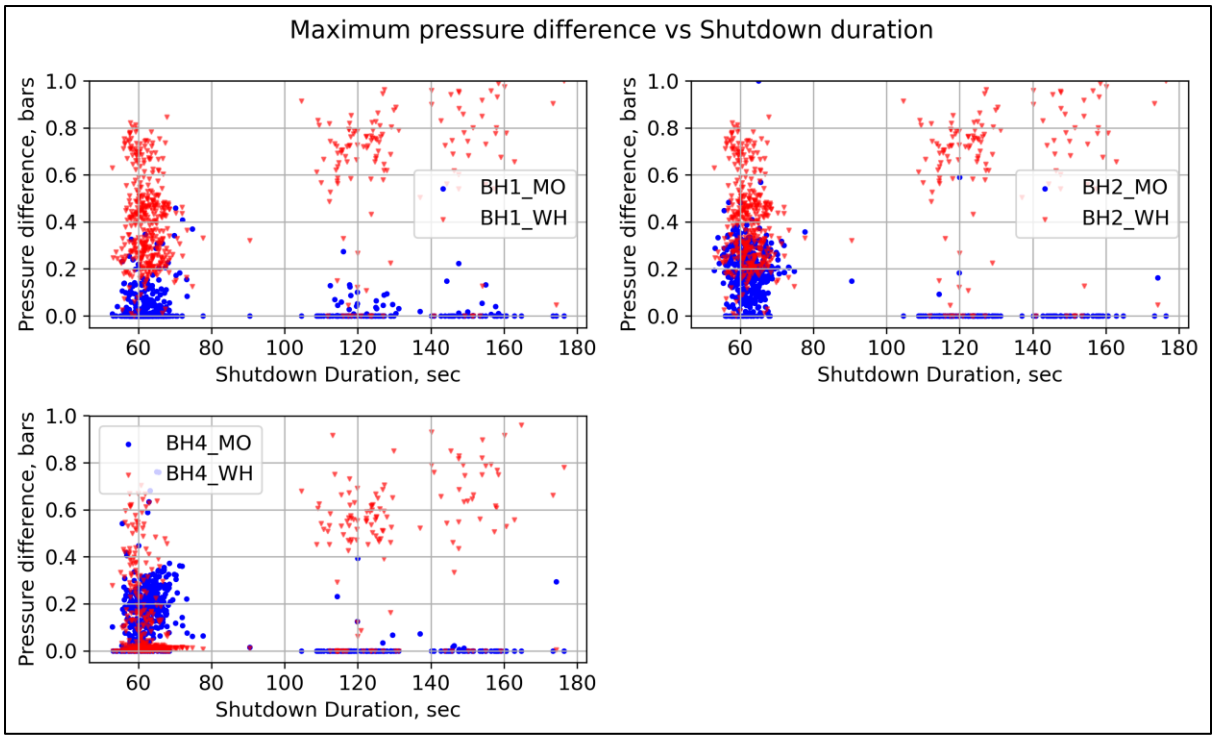

Figure 6-20: Maximum pressure difference by mass oscillation and water hammer of stop sequences over the years for borehole 1,2 and 4.

The average of HI for shutdown durations shows that when the shutdown duration is decreased by half the HI can be as high as 5 times. This is valid for BH 2 (5.02 times) and BH4 (4.65 times) whereas the variation in shutdown has opposite relationship for BH1 (0.7 times).

6.2.4 Effect of initial water head

Initial water head or the static water head upstream of the turbine as illustrated in Figure 6-7. The shape of the mass oscillation curve can be influenced by the static pressure prior to the transient due to two factors. Firstly, it determines the starting level of water in the surge tank and brook intake from which the oscillation initiates. Secondly, varying static heads means different water levels in the reservoir, potentially affecting the HI and MPD caused by mass oscillation to some degree. However, when impact of transient in surrounding rock mass of tunnel is considered, the increase in static pressure does not have any impact on the HI and MPD values. Figure 6-21 and Figure 6-22 shows that HI and MPD remain unaffected by variation in initial water head. Larger values HI and MPD are from the events with shorter shutdown duration.

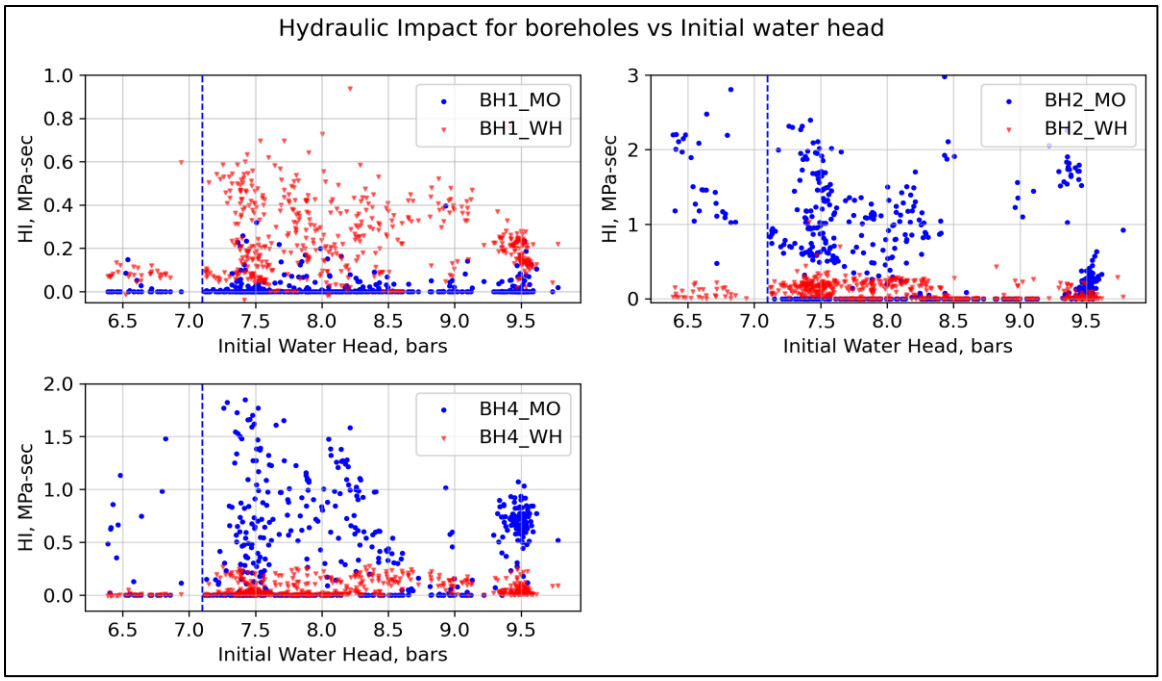

Figure 6-21: Hydraulic Impact for boreholes vs initial water head. Note that 71m is the minimum drawdown level of reservoir.

Figure 6-22 shows the MPD for boreholes with respect to initial water head. It can be seen from MPD that water hammer dominates the mass oscillation in entire ranges of operating head in all boreholes (Figure 6-21 and Figure 6-22). It can be concluded that variation in static head only changes the maximum upsurge and downsurge level. However, relative effect due to phase lag of water pressure in boreholes and tunnel remains the same.

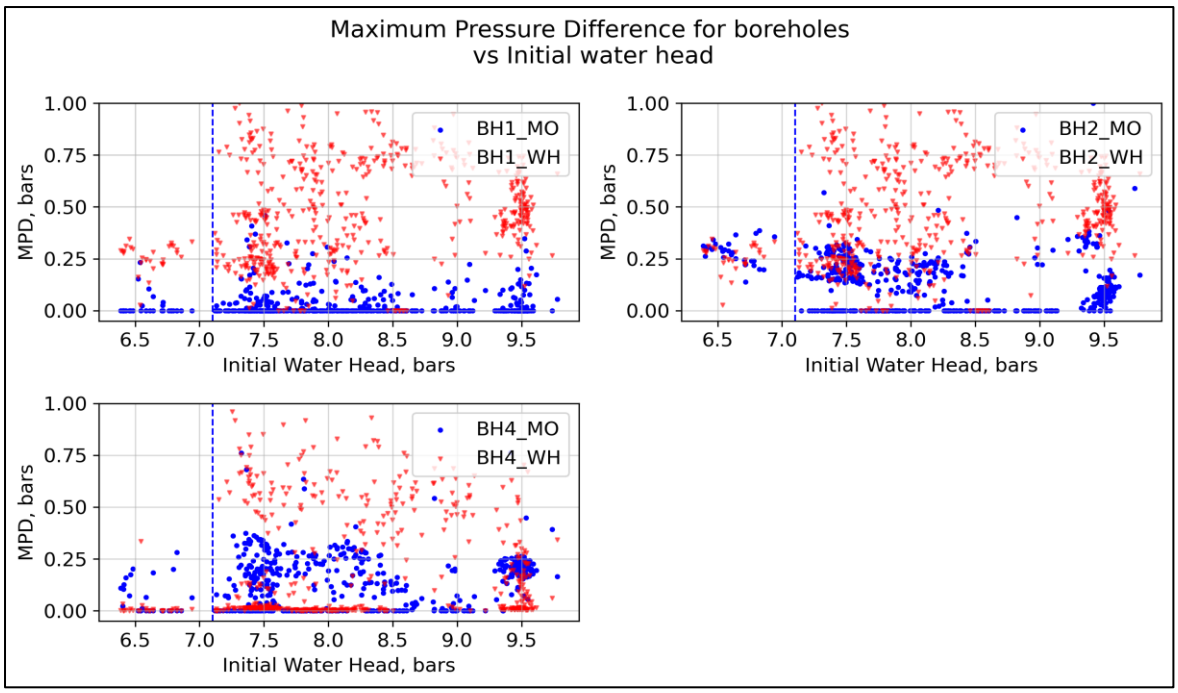

Figure 6-22: Maximum pressure difference for boreholes vs initial water head

The limited influence of static pressure on the results can be attributed to the fact that the effective stresses in the rock mass are substantially higher compared to the variations in static head and static pressure. As a result, these variations lack the capability to induce significant changes in the aperture of the joints. Furthermore, the joint surfaces of hard rocks exhibit high stiffness, effectively preventing any noticeable alterations in the joint aperture.

6.2.5 Correlation analysis

A correlation analysis was conducted using the Pearson correlation coefficient to examine the relationship of operational variables of power plant with HI and MPD. The correlation matrix in Figure 6-3 shows that there is generally a low correlation between dataset variables, with a few exceptions. In the field of geological and hydrogeological studies, correlation values ranging from 0.3 to 0.5 are generally considered to indicate medium to high correlations (Holmøy, 2008). The results from correlation analysis are:

- Shutdown duration has negative correlation with HI and MPD indicating increase in shutdown duration will reduce impact due to transients.
- Poor correlation is seen among other variables like initial water head and peak to peak distance.

This suggests that there is a lack of significant interdependency between the operational parameters and HI and MPD, except for the shutdown duration. The variations in HI and MPD

cannot be solely explained by these operational parameters alone. It is evident that joint properties play a significant role in fluid flow behavior. Therefore, in future studies with more data from different instrumentation station, it is important to incorporate joint properties as additional factors to better understand and predict the variations in HI and MPD.

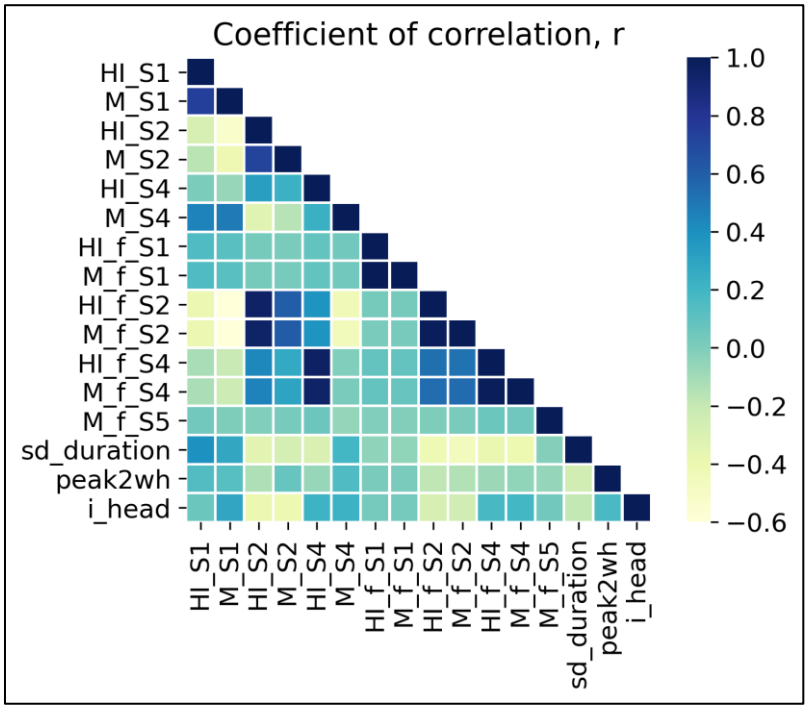

Figure 6-23: Correlation between different variables of transients. No significant relation is found indicating complex interdependency of parameters with joint properties. S represent sensor number, HI represent total hydraulic impact, M represent maximum pressure difference, f represents filtered data for mass oscillation, i_head represent initial head.

6.3 Machine Learning for predicting borehole pressure

The relationship between variables obtained from pressure wave analysis of tunnel and bore holes shows that the parameters and intertwined in a complex way. No concrete relationship could be found to conduct parametric analysis so that the bore hole pressure be predicted from tunnel water pressure. The delay and attenuation of peak is believed to be greatly governed by the shortest distance between tunnel and bore hole, joint properties, and aperture. Since there are only five boreholes, the relationship of tunnel pressure and boreholes pressure cannot be obtained by such few boreholes sample. So, an attempt is made to predict the borehole pressure considering tunnel water pressure alone using machine learning technique.

Firstly, a linear regression method was used which couldn't address the time lag between tunnel water and bore hole pressure. After consultation (pers. com. Alfredsen, 2023), LSTM method was opted, which is generally used machine learning technique for time series data.

The model simulation period was selected so that there is no significant change in properties of borehole pressure and only stop sequence is considered. May-2021 was chosen as calibration and validation period where there are a greater number of start sequences. The data used for calibration and validation is illustrated in Figure 6-24.

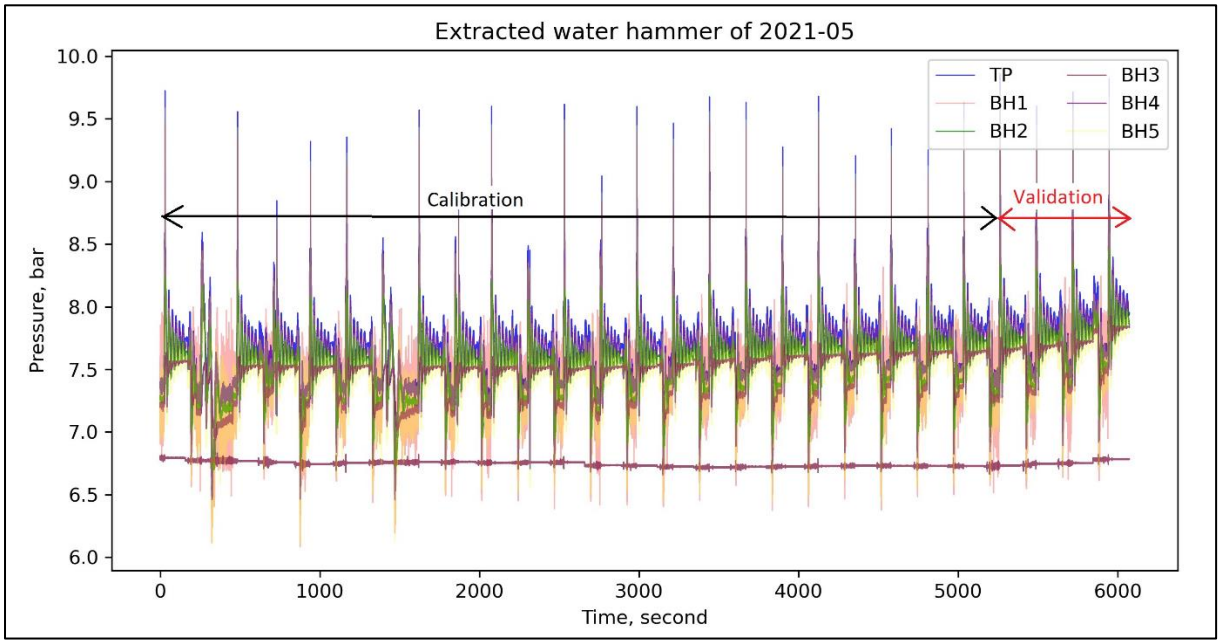

Figure 6-24: Period used for calibration and validation used in LSTM method.

Borehole 2 exhibits a phase lag that resembles the shape of tunnel water pressure, making it suitable for modeling purposes in machine learning (pers. com. Alfredsen, 2023). In order to

simulate only the mass oscillation, the input data was initially filtered with a cutoff frequency of 0.0167 Hz.

A simple LSTM network was implemented to predict the borehole pressure using water pressure data. It makes use of the TensorFlow and Keras libraries. The model was compiled with the Adam optimizer and mean squared error loss function. The used dataset was split into training and testing sets, with 70% of the data used for training and the remaining 30% for testing as shown in Figure 6-24. The number of epochs used in this model was 32.

To assess the accuracy of the predictions, the Mean Squared Error (MSE) and Nash Sutcliffe Efficiency (NSE) metric was employed. The hydroeval library was used to calculate the MSE and NSE value by comparing the predicted borehole pressure values with the corresponding actual values from the testing set. The MSE provides an indication of the relative error in the prediction.

The result obtained from a simple LSTM model is shown in Figure 6-25.

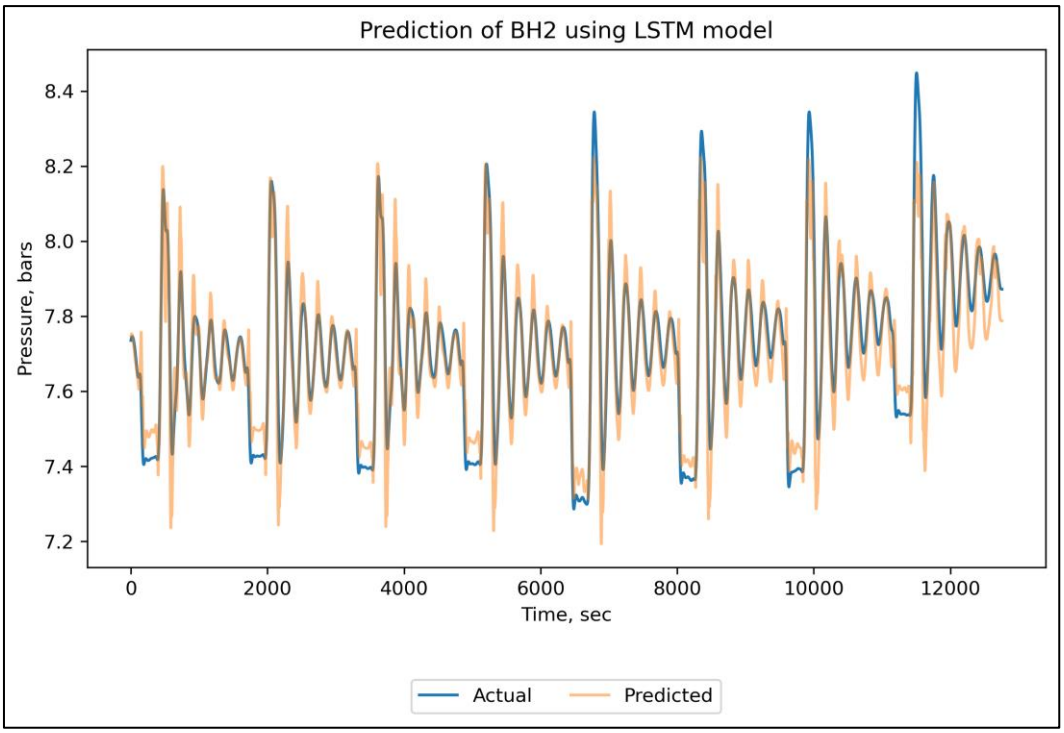

Figure 6-25: Prediction of BH2 pressure using LSTM model

The result shows satisfactory statistical parameters in calibration. The MSE value was found to be 0.0055, R2 was found to be 0.82 and NSE was found to be 87%.

7 Numerical analysis by UDEC simulation

It has been seen from experimental and numerical analysis that degradation of surface of joint due to pressure transients could be characterized by the reduction in frictional resistance of the joint (Neupane, Panthi, et al., 2021). In this regard, the aim of using numerical modelling is to see the movement of blocks by varying joint characteristics which gives an indirect impression of the effect of cyclic fatigue due to transients on the surrounding rock joint system. For this purpose, numerical modelling program, UDEC of version 5.00.228 is used. UDEC is a two-dimension distinct element numerical program which has capability of simulating quasi-static or dynamic response to loading of a media consisting of several intersecting joint structures. Through its explicit solution scheme, it is capable of modeling complex and nonlinear behaviors of discontinuous media. In this modeling approach, the medium is represented as a collection of discrete blocks with the discontinuities serving as boundary conditions between them. The system allows for large displacements along discontinuities and rotations of blocks.

At the instrumentation location of Roskrepp hydropower, there are distinct joint sets present in the rock mass and is colloquially termed as jointed rock mass. In this type of case, the stability of tunnel could be governed more by joint behavior rather than by the physical properties of rock mass itself (Choi et al., 2004). Distinct element simulation code such as UDEC can provide realistic results on the jointed rock mass situations. The UDEC numerical modelling program is used in this study based on comprehensive review of different numerical models (Jing, 2003), license availability (UDEC 5.0.228), dataset requirement, realistic representation of site condition in model with moderately fractured rocks (explained in Section 3.3), reproducibility of model and capability of model to simulate displacement of blocks.

7.1 Model set-up

7.1.1 Choice of cross-section and model design

The cross-section modeled in UDEC is a tunnel cross-section that cuts normally on the tunnel axis. When choosing a cross-section for the modelling, the focus has been on finding a cross-section where all joint sets are visible, so that they can be modelled. The most interesting cross-section to study with UDEC is the cross-section where J1, J2, Jf and $Jf_{conductive}$ pass each other. Figure 5-4 shows the orientation of joints with respect to the tunnel. At the junction of access tunnel and main tunnel, the joints J1, J2 and J_f are present where these joints will be visible in the cross-section. In consultation with the supervising professor, this location was chosen as the cross-section to study with UDEC where 3 joint sets are visible (pers. com. Panthi,2023).

The dip angle in the model is adapted from the field measurements at the instrumentation location conducted by Neupane et al., (2020). The three joint sets J1, J2 and J_f cross the longitudinal alignment of tunnel in acute and obtuse angles. J2 has a spacing larger than 10m, so it crosses the vicinity of the tunnel only for one instance. Joint J1 and Jf have spacing of 1 to 2 m. For conservative analysis, the spacing for these joints is set to 1 m and apparent dip is calculated with respect to the tunnel axis with the help of obliquity angle. The apparent dip for J1 and Jf is taken as 70º and 80º whereas apparent spacing in the cross section is taken as 1.5m and 2.8 respectively. J2 is dipping apparently at an angle of 39º. The apparent spacing and dip for modelled joint sets is shown in Table 7-1. Since, the cross-section is modelled viewing the tunnel towards the direction of flow, J1 is dipping towards right and (J2 and Jf) are dipping towards left in the geometry of the model as shown in Figure 7-1.

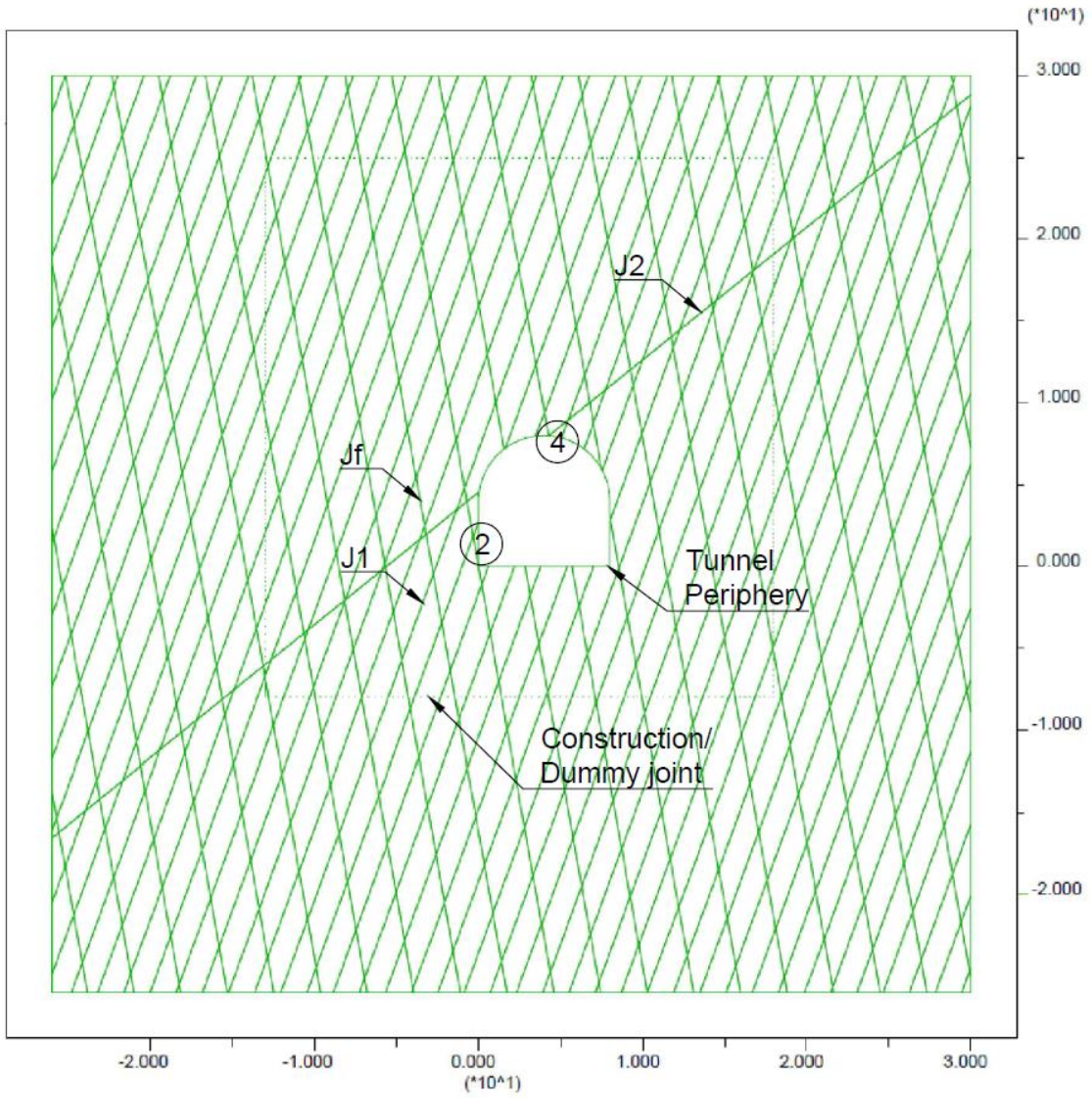

Figure 7-1: Geometry creation in UDEC. Location 2 and 4 are interesting points where displacements in y direction are calculated.

A construction/dummy joint was used to define an external boundary of the tunnel periphery. A construction joint was also created at a distance equal to dimension of the tunnel to separate the assignment of edge length to make the blocks deformable. The edge length was set to 0.5 m for the zone inside the construction joint and 3m outside of it. This separation reduces the computation time without greatly influencing the behavior of the model (Bøe, 2020).

In UDEC modelling, boundary conditions are based on velocity. The lower boundary in the model restricts movement in vertical direction and the sideways boundary prevents movement in horizontal direction. In situ stresses causes clamping/confining forces acting on the wedges and have positive influence in stability of blocks thus restricting their movement. This is because normal stress increases thus increasing the shear strength of the joint. It is generally assumed that the in situ forces are diminished for some reason in wedge analysis (Hoek, 2006). Thus, in consultation with supervising professor, in situ stress was not considered for boundary condition for UDEC modelling (pers. com. Panthi, 2023).

Table 7-1: Apparent spacing and dip of J1 and Jf used in UDEC modelling.

Joint Name	**Obliquity Angle**	**True Dip**	**Apparent Dip**	**Deviation angle**	**Actual Spacing**	**Model Spacing**
J1 (min)	42	70	63.9	48	1	1.5
J1 (max)	42	85	83.3			
J2 (min)	13	20	19.5			
J2 (max)	13	40	39.3			
Jf (min)	21	75	74.0	69	1	2.8
Jf (max)	21	90	90.0			
$Jf_{conductive}$	11	80	79.8			

7.2 Material Properties and Parametric Assessment

It is believed that block removability is one of the major contributing factor leading to fatigue and gravity induced instability caused by pressure transients (Neupane, Panthi, et al., 2021). UDEC mainly focuses on the joint properties, so a simple elastic material model is chosen for the intact rock. An overview of the properties of intact rock used in UDEC model is given in Table 7-2.

The results from numerical analysis can greatly vary with different constitutive models. So, it is necessary to select an appropriate constitutive equation for accurate analysis of a geological problem. Mohr-Coulomb model is largely used model in soil and rock problem which however

couldn't precisely describe several behaviors of rock joints such as sliding, separation, dilation etc. Moreover, this model cannot express the behavior or rock block, for instance, rotation and movement of rock block. Mohr-Coulomb model is a linear model where the dilation angle is constant and is independent of the shear behavior of rock. In contrast, Barton-Bandis model produces realistic results in jointed rock mass because it allows the non-linear behavior of the dilation angle with the shear displacement of rock blocks (Choi et al., 2004). So, Barton-Bandis failure criterion is chosen to describe the behavior of the joints. Each joint set in the model has been given its distinctive joint properties. The properties of various joint sets, as well as their parametric value used in the model are shown in Table 7-3.

Table 7-2: Properties of intact rock in UDEC

Properties	**Units**	**Value**	**Reference**
Density	kg/m^3	2741	(1)
Poisson's ratio	-	0.29	(1)
Young's Modulus	GPa	65	(1)
Bulk modulus	GPa	52	Eq. (3-12)
Shear modulus	GPa	25	Eq. (3-11)
(1) The values are mean values from lab test results conducted by Neupane & Panthi, (2021).			

Table 7-3: Overview of joint properties used in UDEC modelling. Properties in italics are varied in parametric study.

Properties	**Notation**	**Units**	**Joint sets**			**Reference**
			J1	**J2**	**Jf**	
Dip	-	degree	70	39	80	Table 5-2
Model	Constitutive model	-	BB model	BB model	BB model	-
Joint aperture	a	mm	0.175	0.625	0.175	Table 5-2
Maximum dilation	bbdmax, d	degree	5	5	5	Eq. (3-21) (1)
JCS	jcso, JCS	MPa	50	50	50	Eq. (3-5) (2)
Shear stiffness	jks, k_s	MPa/m	48000	14400	48000	Eq. (3-13)

Normal stiffness	jkn, k_n	MPa/m	138000	40000	138000	Eq. (3-14)
JRC	jrco, JRC	-	*6,2,1*	*14,2,1*	*6,2,1*	(3)
Residual frictional angle	phir, ϕ_r	degree	*40,32,25*	*40,32,25*	*40,32,25*	(4)
Compressive strength	sigmac, σ_c	MPa	148	148	148	

(1) Assuming 2x1x1 m^3 block size, σ_n = 2 MPa from Eq. (3-21), d = ½ JRC log(JCS/σ_n) = ½ . 6. log (50/2) = 4.2 ~ 5º.

(2) JCS is taken as rock mass strength from Eq. (3-5) (pers. com. Panthi, 2023).

(3) JRC is varied based on personal communication with supervising professor (pers. com. Panthi, 2023).

(4) Residual frictional angles is fixed based on personal communication with supervising professor (pers. com. Panthi, 2023) and reference from Neupane & Panthi, (2021)

7.3 Modelling

The UDEC modeling focuses on examining the influence of joint properties on the movement of the block within the surrounding rock mass of the tunnel. A parametric study is conducted to investigate how changes in joint characteristics; φ_r and JRC, impact the displacement of the block. This study simulates rough, smooth, and slickensided joints.

Experimental and numerical study shows that the shear strength of the rock joint decreases due to the rate of loading, number of cycles, level of frequency and stress amplitudes (Jafari et al., 2004). It has already been explained in Section 4 that the transient results in cyclic loading which leads to cyclic fatigue of intact rock as well as rock joints. This cyclic loading increases stress in the surrounding rock mass of the tunnel periphery which can contribute to fatigue (Neupane, Panthi, et al., 2021). The cyclic loading can also cause loosening of the rock joints combined with reduction in friction angle causing larger joint deformation (Neupane & Panthi, 2021). This can contribute to block falls and tunnel collapse in the long run. This phenomenon was seen in a failure caused by transients in an unlined pressure shaft at Svandalsflona Hydropower project where the joint infilling material was eroded leading to opening of joints and collapse of structure (Neupane & Panthi, 2018). Since, in the jointed rock mass, the characteristics of joints can be governing factor for stability than the physical properties of rock mass itself, it is justifiable to see how does the displacement of block changes with respect to the joint properties viz. JRC and φ_r.

The parameters of joint characteristics are assigned in the model based on site observation made by supervising professor. The joint type is primarily described as planar with rough, smooth and slickensided category (pers. com. Panthi,2023) and the values are given in Table 7-3. Rough and smooth joints are likely to occur in the site, however, slickenside joints are formed by frictional movement between the rocks along a fault. In the worst case, if two block moves frequently due to cyclic loading, may cause smoothening of joints and further result in slickensided joint (pers. com. Panthi, 2023).

Table 7-4: Values of joint roughness used in parametric study (pers. com. Panthi, 2023). R, Sm and Sl denotes Rough, Smooth and Slickensided joints respectively

Property	**Notation**	**Unit**	**J1**			**J2**			**Jf**		
			R	Sm	Sl	R	Sm	Sl	R	Sm	Sl
JRC	jrco, JRC	-	6	2	1	14	2	1	6	2	1
Residual frictional angle	phir, ϕ_r	degree	40	32	25	40	32	25	40	32	25

The normal and shear stiffness of joint depends upon spacing of joints (ITASCA, 2023a). When an average value of stiffness was used, an error was encountered stating that the joint stiffness value is low. This is caused when the block penetrates too far into each other (ITASCA, 2011). When the joint spacing is high the value of stiffnesses are low (Equation (3-13) and (3-14)). So, the joint spacing for J2 was kept at 5m while calculating joint stiffnesses to avoid this error (pers. com. Panthi, 2023). A variable overlap tolerance, "ovtol" was also increased to 0.5 in order to eliminate the error (pers. com. Bøe, 2023).

The modelling in UDEC is carried out as follows:

1. Model geometry is drawn, and the model is discretized. Material properties and boundary conditions are determined.
2. The model is consolidated i.e., calculations are run until mechanical equilibrium is reached. This was verified by plotting unbalanced force with calculation cycle. Here, the maximum unbalanced force approached zero which means the equilibrium stated is reached.
3. The tunnel is excavated and interesting points (Figure 7-1) in the tunnel periphery are marked for monitoring movement during calculation of model.
4. The model is further simulated for several thousand cycles.
5. Joint characteristics parameters are altered, and the model is run again.
6. The model is calculated until the equilibrium state is achieved (solved).

7. Steps 5 and 6 are repeated for changed parameters.

7.4 Results

As mentioned in earlier section, three sets of joint properties are used in parametric study to study the effect of degradation of joint roughness induced by transients. The vector plot for total displacement for three cases are shown in Figure 7-2. The maximum total displacement for rough, smooth and slickenside joints are 6.1mm, 8.51mm and 9.64mm respectively.

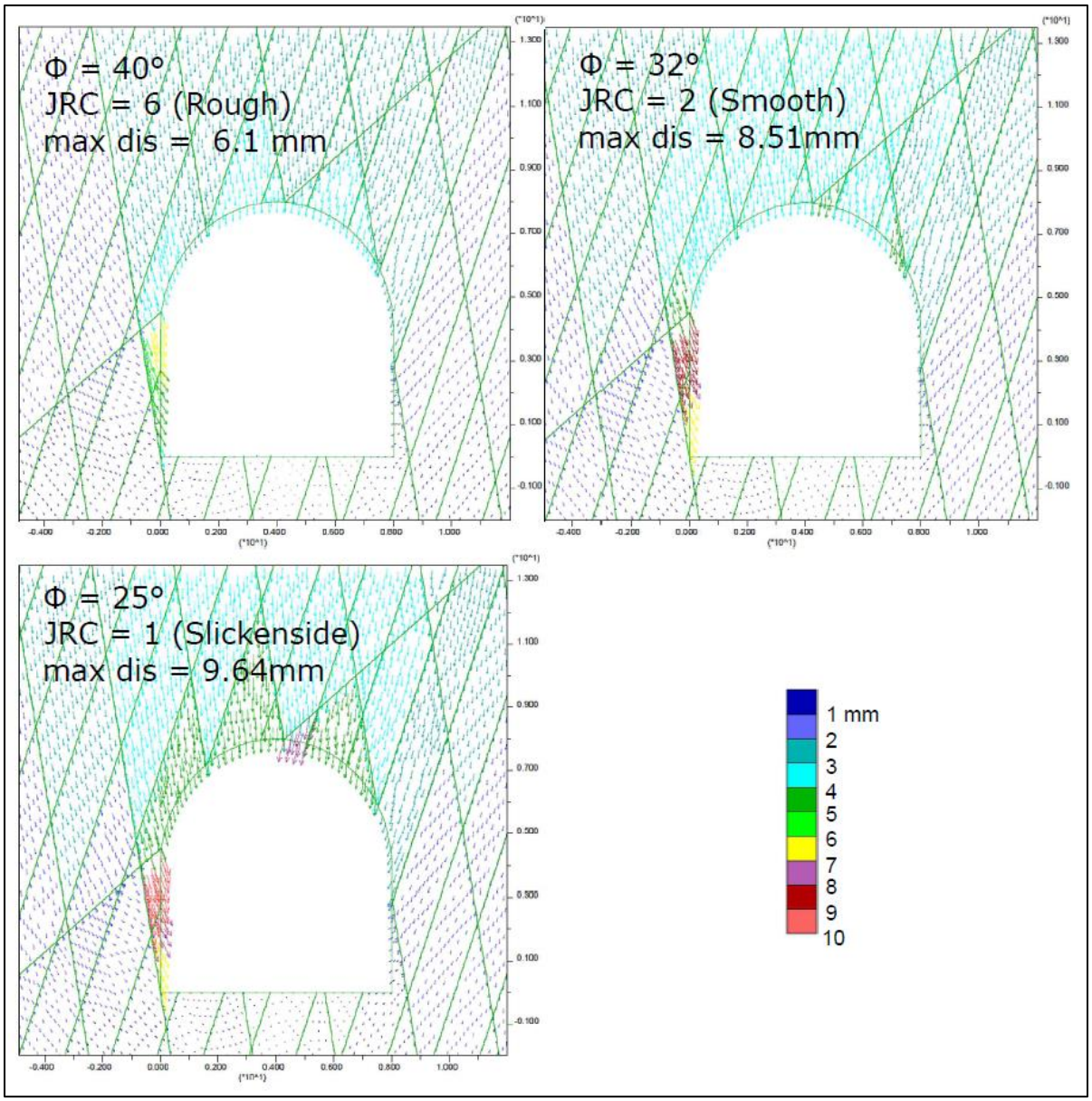

Figure 7-2: Vector plot showing displacements in the UDEC model with rough, smooth and slickensided joints.

Figure 7-2 shows that the blocks on left wall of tunnel experience greatest movement. Here it is clear that the reduced roughness parameters due to transient induced erosion and

smoothening of joint filling has led to larger displacement even after 15,000 cycles. No blocks have fallen freely into the cross-section in any of the scenarios when the calculation stops, and they are almost at rest condition. The movements of blocks increase little by little with time. The blocks that experience the greatest displacement are the blocks that slide with the greatest speed. It indicates that the blocks are stable even after the joint has degraded to slickensided from rough at the instrumentation location.

Two interesting blocks are noticed while running the model viz. 2 and 4. One is the block from the left wall, and one is the block from the crown of the tunnel (Figure 7-1). Those blocks have larger displacement than other blocks. Block 2 has the largest displacement in all cases. Figure 7-3 shows the displacement in vertical direction and the number of cycles in the model. Both block at location 2 and 4 stabilizes after 25000 cycles, 62000 cycles and 47000 cycles for rough, smooth and slickensided joints respectively.

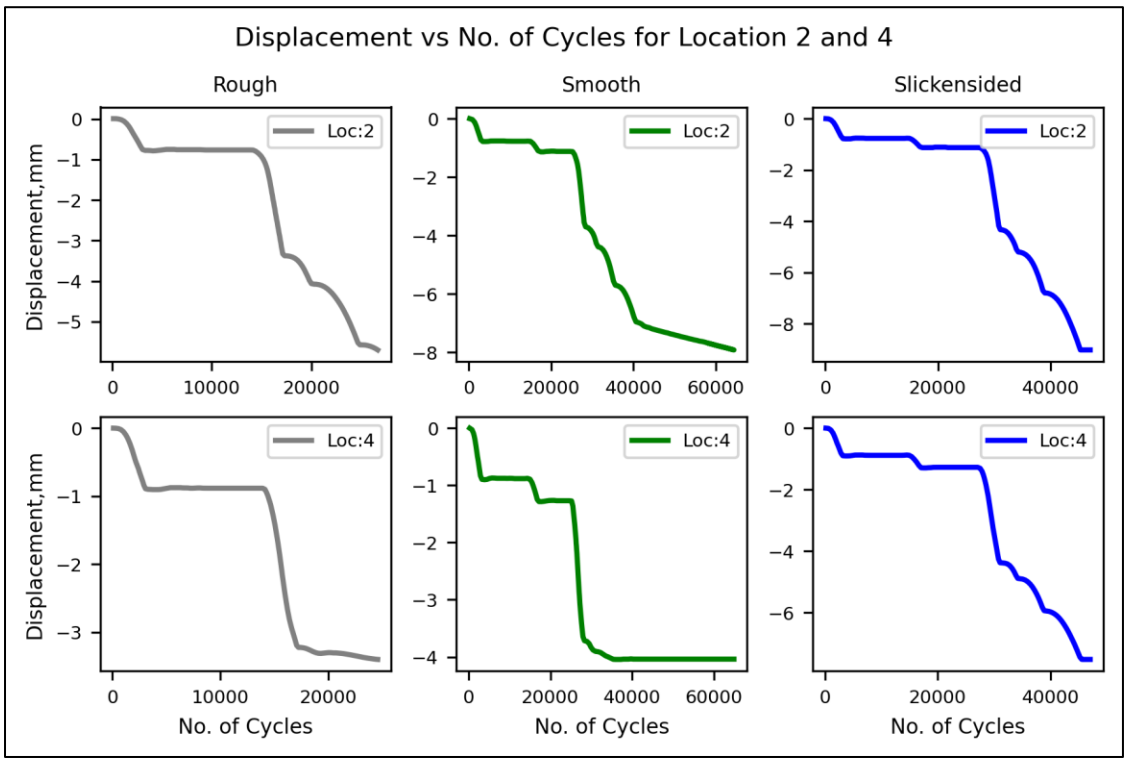

Figure 7-3: Displacement in vertical direction vs Number of Cycles at location 2 and 4 at the tunnel periphery. Locations are illustrated in Figure 7-1.

Results	**Unit**	**Rough**	**Smooth**	**Slickensided**
Maximum displacement	mm	6.10	8.51	9.64
Maximum shear displacement	mm	5.00	7.00	8.00

Shear displacement in excess of 0.5mm for three cases of joint properties is shown in Figure 7-4. The maximum shear displacement for rough, smooth and slickenside joints are 5 mm, 7mm and 8 mm respectively. The increase in block displacement indicates reduction of stability of tunnel. Results from shear displacements also show that there is larger displacement in joints of blocks to the left wall of the tunnel. This clearly shows that degradation of roughness of joints increases displacement of blocks. The degradation occurs due to cyclic fatigue of rock joints caused by transient induced cyclic loading in waterway system of hydropower.

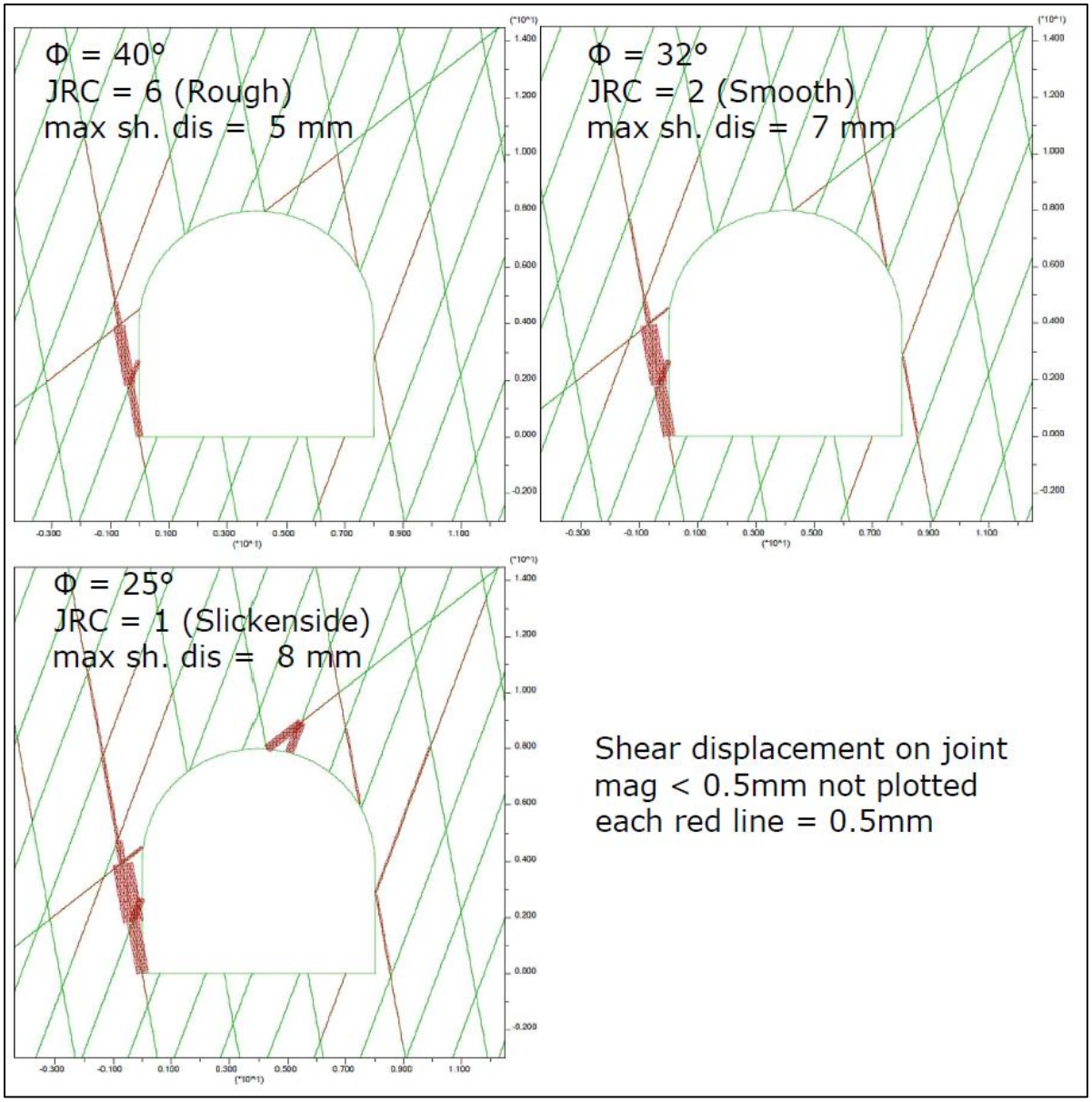

Figure 7-4: Plot indicating shear displacement in joints in the UDEC model with rough, planar and slickensided joints. Plots have the same scale, and the thickness of red lines indicates shear displacement equivalent to 0.5mm. Shear displacement <0.5mm not plotted in the figure.

8 Discussion

8.1 Behavior of boreholes

Pore water response of boreholes behaves differently throughout the study period. BH1, BH3, and BH4 remained relatively stable throughout the study period, while BH2 and BH5 exhibited changes in their behavior after they were installed. Initially, both boreholes showed little to no response, but over time, they became moderately responsive and highly responsive respectively. Based on their later behavior after 2021, the borehole responses are classified into four types: highly responsive, responsive, moderately responsive, and non-responsive. Schematic representation of response of different types of boreholes during transients is shown in Figure 8-1. Information about the borehole type is listed in Table 8-1. Highly responsive boreholes are in phase with tunnel water pressure during transients and do not induce any HI or MPD. Responsive borehole; BH1, exhibit HI and MPD during water hammer but is in phase lag most of the time. Moderately responsive boreholes, such as BH2 and BH4, induce HI and MPD during both water hammer and mass oscillation. Non-responsive boreholes show little to no response during transients and do not induce any HI and MPD. Based on the characterization of the type of boreholes, the type of impact caused by it can be quickly known from newer boreholes from any instrumentation location.

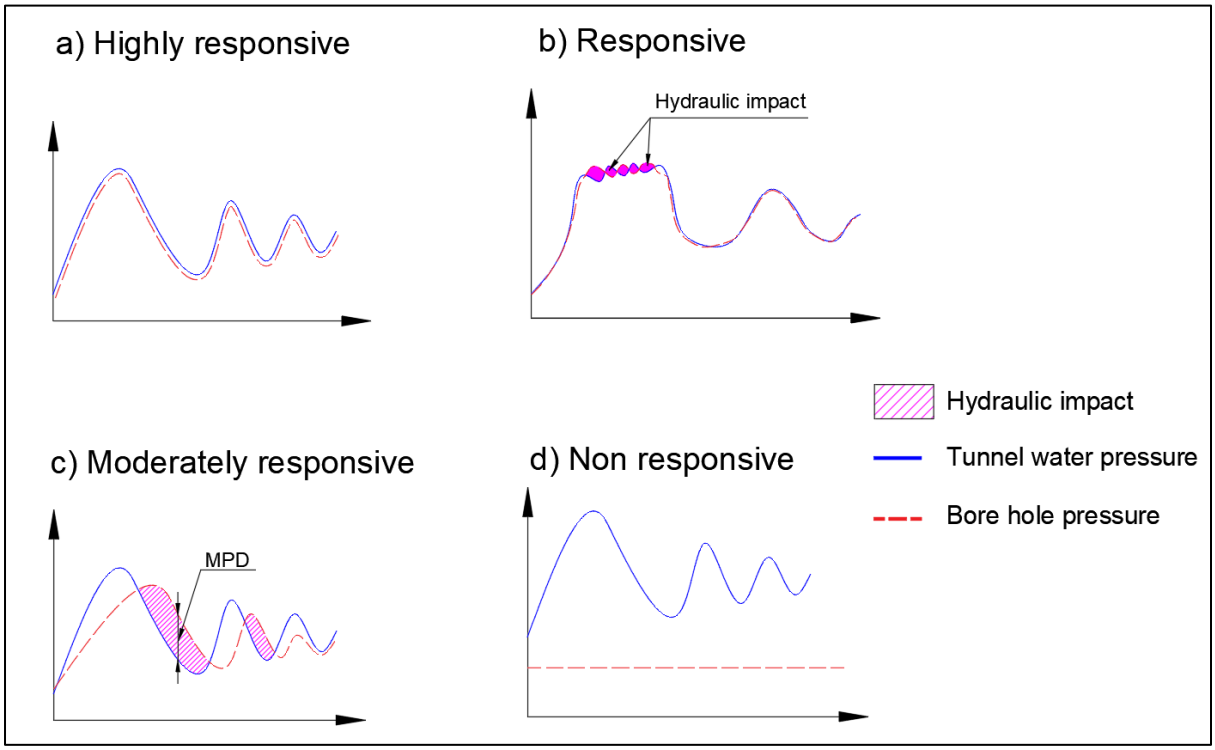

Figure 8-1: Schematic representation of 4 types of boreholes based on responsiveness with respect to tunnel water pressure during transient (shutdown event).

Table 8-1: Bore hole type and there response due to MO and WH . (Mass Oscillation and Water Hammer)

Borehole type	**Bore hole**	**Remarks**
Highly responsive	BH5 (after March 2020)	No HI and MPD due to MO and WH
Responsive	BH1	HI and MPD only due to WH but less HI due to MO
Moderately Responsive	BH2 (after Sept 2019) and BH4	HI and MPD due to both WH and MO
Non responsive	BH2 (before Sept 2019), BH3, BH5 (before March 2020)	No HI due to both WH and MO

8.2 Joint Characteristics

Based on the analysis, it was observed that initially BH1 and BH4 showed a responsive behavior, while BH2, BH3, and BH5 were nonresponsive. The nonresponsive boreholes intersected joints Jf or J1, which have a narrow aperture with clay filling and a spacing of 1m. On the other hand, BH1 intersected the conductive joint Jfconductive, while BH4 intersected J2. Jfconductive and J2 were found to have partially open joints with washed-out filling. It can be concluded that the responsive nature of the boreholes is influenced by Jfconductive and J2. Therefore, the joints can be categorized based on their responsiveness, with conductive joints referring to those with large apertures (such as J2 and Jfconductive) that have a direct hydraulic connection to tunnel water pressure, and nonconductive joints referring to those with tight joints (such as J1 and Jf2).

Additionally, it is important to note that the boreholes passing through these conductive joints induce HI and MPD. This suggests that the effect of mass oscillation and water hammer can reach deep into the rock mass as well through the network of joints. This also highlights that the pore pressure response of the rock mass is primarily controlled by the conductive joint system, which allows for direct hydraulic connections to tunnel water pressure through larger apertures. It seems logical as the discharge through joints is cube of the aperture as stated by cubical law.

8.3 Natural, Cutoff and Sampling frequency

In analysis done in Neupane, Vereide, et al., (2021), three distinct frequencies of mass oscillation: 3.4, 1.6, and 1.1 minutes were observed, representing the flow of water between

the reservoir and the surge shaft, between the reservoir and the brook intake, and between the brook intake and the surge shaft, respectively. This study has identified natural frequency of 3.7 and 1.54 minutes which are close to the values obtained in previous study. However, the current analysis using FFT analysis was unable to capture the natural frequency of mass oscillation between the brook intake and surge shaft. The limited impact of the small-sized brook intake on the mass oscillation process may explain why the transducers couldn't record that specific wave. The slight discrepancies in time periods between the two studies may be due to order of filter used in the analysis.

Calculating the cutoff frequency for water hammer based on theoretical approaches considering wave velocity and the length of the free water surface and turbine can lead to discrepancies. In this study, a cutoff frequency of 8 Hz was obtained, while a previous study by Neupane et al. Neupane, Vereide, et al., (2021) reported a cutoff frequency of 3 Hz. However, these frequencies cannot be used to calculate the impacts of water hammer. FFT analysis provides detailed information on the natural frequency of pressure waves, and it is a practical approach to determine the cutoff frequency and separate signals based on frequency. The waveform containing water hammer, when analyzed using FFT, revealed that a cutoff frequency of 1Hz can effectively filter out noise and capture the total hydraulic impact.

The sampling frequency before the instrumentation period was fixed at 10 Hz. It was decided on the basis of the time required by the wave to reflect from instrumentation location and the turbine back to the instrumentation location (pers. com. Neupane, 2023).

The current high sampling frequency from the pressure transducer generates a large amount of data, making data handling and processing challenging If long-term data storage is necessary, the sampling frequency can be reduced to 2 Hz (0.5 seconds) based on the Nyquist theorem. This frequency is obtained by doubling the maximum frequency of water hammer i.e. 1 Hz. However, due to presence of noise it is recommended to keep it at 5 Hz. This ensures quality of data and at the same time increases the storage duration of pressure data.

8.4 Effect of Water hammer and mass oscillation

There are two clusters of shutdown duration around 60s and 120s which can be visualized in Figure 6-19 and Figure 6-20. The average of HI around those two shutdown durations shows that when the shutdown duration is decreased by half the HI can be as high as 5 times. This is valid for BH 2 (5.02 times) and BH4 (4.65 times) whereas the variation in shutdown has opposite relationship for BH1 (0.7 times).

Previous study predominantly focused on analyzing stop sequence while giving less attention to start sequence (Neupane, 2021). However, upon analyzing the HI and MPD for the boreholes it was observed that the start sequence imposes higher stress on rock joints compared to the stop sequence. Specifically, the average HI values for all start-stop sequences during the study period were approximately 2.97 times higher for BH2 and 3.05 times higher for BH3. These findings suggest that the start sequence generates approximately three times more HI than the stop sequence, indicating its significance in terms of stress induction.

8.5 Predicting borehole pressure

The results obtained from the LSTM model indicate that it simulated the borehole pressure during the validation period. The statistical analysis showed good performance, with an NSE (Nash-Sutcliffe Efficiency) of 87% and MSE (Mean Squared Error) of 0.005. However, it was observed that the model was unable to accurately capture the peak pressure during the initial 3 to 4 upsurges. During transients, HI and MPD are induced in the first few oscillations. Therefore, based on the current phase of analysis, the LSTM model cannot be directly employed for predicting HI and MPD. Nevertheless, there is a prospect for future research work and further improvements can be done in predicting HI and MPD using LSTM or similar methods.

There are only 5 boreholes and hence 5 characteristics of responsiveness. The joint properties like aperture, persistence, filling, and the shortest distance of intersection of borehole and joint to the tunnel etc. are 5 in numbers. There are 3 moderately responsive, 2 responsive and 1 nonresponsive joint which are less when we need quantifiable results. So, the LSTM couldn't use the relevant properties of the joint properties and boreholes to predict the bore hole pressure when tunnel water pressure alone is given. In order to accurately predict the response of boreholes when the pressure in the tunnel fluctuates, it would be beneficial to have a larger dataset of instrumentation programs in various hydropower and geological conditions. This would enable the use of regression or machine learning techniques to predict the borehole reaction by considering both the borehole and joint properties.

8.6 UDEC modelling

The results from the modelling in this study should not be interpreted as a conclusion on how the rock mass deforms from the cyclic loading. This study only provides an impression on how the joint deformation takes place induced by cyclic loading during transients. In the model, simplifications and assumptions have been made during the modelling which might have

significant impact on the results. In geometry creation, joints are created by assigning spacing and angle for each joint. As a discontinues model, joint geometry and properties highly determine the result of the UDEC model (Bøe, 2020). The shape and size of block size changes deformation of blocks and stress distribution around the tunnel (Solak & Schubert, 2004). So, it is advisable to draw the joint manually in UDEC (pers. com. Bøe,2023). Since the study focused on examining the relative deformation of joints caused by cyclic fatigue and there were only two main joint sets along with an additional single joint in the cross-section, the joint creation tool was adequate.

Based on the author's experience, UDEC is considered to be an inefficient and less user-friendly software. However, it is possible that the latest versions have improved with the inclusion of a more intuitive graphical user interface. The modeling process in UDEC primarily involves using buttons, menus, and dialog boxes. It is important for new users to familiarize themselves with the program, read the user manual, and understand the UDEC's code language in order to efficiently use the software.

The Barton-Bandis model was chosen as the constitutive model for shear strength in the UDEC modeling, considering the significant influence of joint properties. This model is preferred due to its ability to accurately represent the nonlinear stress-strain behavior and properly capture the shear strength of rock. Moreover, the extended form of the Barton-Bandis model has been successfully used for cyclic loading and has shown good validation results (Fei & Choo, 2023).. Given that the stability and deformation of blocks are primarily governed by joints, selecting the Barton-Bandis criteria as the constitutive model is a favorable choice.

The high cycle loading of hydropower (Lee & Barr, 2004) where mean cyclic stress is lower than strength of rock mass. In this situation, fatigue behavior is dominant. During high cyclic loading primary and secondary asperities undergo fatigue damage degrading the joint roughness (Liu et al., 2018). In this context, the large-scale deformation causes joint fatigue which is logical to be represented by decrease in roughness characteristics of joint.

In this study, the transient induced damage and degradation of joint is simulated by changing frictional resistance parameters, JRC and φ_r. However, the impact of transients on joint surfaces goes beyond just reducing frictional resistance. It also includes a decrease in stiffness and an increase in hydraulic aperture, indicating a change of other parameters of joint surfaces (Neupane & Panthi, 2021). So, it should be noted that there are other variables relating to joint characteristics also changes due to joint fatigue induced by cyclic loading.

One of the important information from Numerical modelling is that the block displacement results in the model are consider reasonable (pers. com. Panthi,2023). Displacement is considered a very important indicator of stability and an increase in total and shear displacement is seen as the characteristics of joint degrades due to long term operation fatigue.

8.7 Fatigue Process

Erarslan & Williams, (2012) suggests that the extent of fatigue in rock mass is likely to be influenced by the stress magnitude. MPD, a term introduced in this study, is a quantification parameter that directly links with stress magnitude. In this context, MPD can be a potential parameter for quantifying the impact of transients on the surrounding rock mass caused by cyclic loading. While HI represents the average pressure difference over time between borehole pressure and tunnel water pressure, it does not account for stress amplitude. Numerically, HI can be high for small amplitude of stress subjected to longer period than high amplitude stress subjected to shorter period. On the other hand, MPD considers the highest stress amplitude during an event. Furthermore, the pressure difference captured by MPD can be used to investigate the fatigue behavior associated with the maximum stress applied and the number of cycles required for failure through SN curve. Based on the MPD magnitudes obtained for slow and fast shutdown scenarios (Figure 6-20), water hammer could potentially act as a triggering factor for cyclic fatigue due to the multiple changes in loading direction caused by the high-frequency characteristics of water hammer.

In the author's viewpoint, HI is useful for wholesome quantification of impact of transient in the rock mass when dealing with total or cumulative impacts and comparing with other variables, whereas MPD is useful for studying cyclic fatigue or finding out number of cycles of loading in specific time periods.

From different literature it is clear that there exist a fatigue limit for rock materials (Cerfontaine & Collin, 2018). In our specific case, the Maximum Pressure Difference (MPD) reaches a maximum magnitude of approximately 1 bar/0.1 MPa, which is a low stress, while the Joint Compressive Strength (JCS) measures 50 MPa. Consequently, the probability of any breakage occurring in the intact rock bridge at the instrumentation location is minimal. However, it is important to note that in the presence of weak rock masses, such as phyllite and schist, the strength of the rock mass is lower compared to the rock mass found at the instrumentation station. In such instances, failure may occur as a result of the long-term accumulation of

hydraulic impact or cyclic fatigue induced by frequent changes in loading conditions over a long run.

Through an experimental setup, it is possible to determine the maximum cyclic stress and monotonic stress, which enables us to establish the fatigue limit of the material. Additionally, the S-N curve of the rock material can be constructed using rock samples obtained from the site or relevant literature. By utilizing the S-N curve, the number of cycles to failure can be estimated, providing valuable information on the expected durability of the material. This approach would allow a rough estimation of the number of load changes that a tunnel can sustain critical locations before it experiences block failure due to cyclic fatigue.

The repeated loading experienced by hydropower tunnels at relatively low stress levels throughout many years of operation can be described as high cycle loading (Lee & Barr, 2004). Results from MPD suggest that the mean stress of loading is relatively lower than the strength of rock mass. Additionally, fatigue mechanisms are dominant at high-cycle amplitude and low mean stress (Costin & Holcomb, 1981). If we consider a transient event where the pressure change due to mass oscillation is for two to three cycles, the number of cycles wouldn't be high. However, if water hammer is considered, the number of cycles is high because the frequency of water hammer is higher. In this case, the number of cyclic loadings could be higher. Brattset hydropower experiences approximately 2000 load change events per year, while Ulset hydropower experiences around 1500 load change events annually (Neupane, Vereide, et al., 2021). Additionally, there are many small load changes due to water hammer pulsations which may increase the figure of load change. So, it is evident that there is high cycle loading at low stress in the tunnels due to transients where cyclic fatigue phenomena is dominant.

The transient in the waterway can lead to both failures related to cyclic fatigue and gravity included structurally controlled block falls. Based on the previous failure events and field visit experience, a new joint set can be formed which propagates due to cyclic loading and finally collapses as cyclic fatigue failure (pers. com. Neupane,2023). It is a valid assumption that the consistent variation in pressure during transient could result in the infilling material in joint to erode along with small scale sliding of joints leading to its dilation and decrease in its roughness. This will make the key block unstable and result in either sliding or falling of the block. Newer cracks in addition to naturally occurring joints may be formed by the action of transients leading to cyclic fatigue. If these newer cracks form a potentially unstable wedge

along with the naturally occurring joints around the periphery of tunnel, it may induce wedge failure.

By examining laboratory tests and analyzing failed rock samples from the site, it is possible to determine whether the failure resulted from monotonic loading, such as gravity-induced block falls, or from cyclic fatigue. This allows for the study of crack propagation and identification of the underlying mechanisms leading to failure.

8.8 Design Practice

The current state-of-art confinement criteria for design of unlined pressure tunnel basically proposes design considerations against hydraulic jacking. Some modifications have been made by introducing a multiplication factor to address the two-valley effect (Panthi & Basnet, 2018). However, this criterion does not consider design for load changes due to frequent transient events. Previously, it was assumed that short-duration transients do not propagate deep into the tunnel and only affect the shallow zone around it (Rancourt, 2010). This may explain why transient pressure was not taken into account in the design process. Benson, (1989) recommended a factor of safety (FoS) of 1.1 during pressure surges, assuming that hydraulic pressure is always lower than rock stress or that the duration of hydraulic stress during transients is too short to be significant and confined to the shallow zone.

This indicates that the existing principles only address protection against hydraulic jacking, while the possibility of block falls due to operational factors has not been considered in the design criteria. There could be instances of unnoticed intact rock bridges during tunnel construction that may weaken over time due to cyclic loading and cumulative HI and MPD (Neupane, Panthi, et al., 2021). This can exceed the fatigue strength of the intact rock bridge, leading to its rupture and subsequent block falls in tunnel. In a similar study conducted by Preisig et al., (2016) the investigation focused on the hydromechanical fatigue of intact rock bridges in deep-seated landslides. The primary cause of this fatigue was identified as the seasonal changes in pore water pressure. Neupane, Panthi, et al., (2021) also demonstrated the formation and failure of intact rock bridges in surrounding rock mass of tunnel, resulting in condition of block removability and potential block falls. These lessons are important in tunnels excavated through schistose rock formations such as phyllite and schist, especially in areas where there is a risk of future block falls due to damage in the intact rock bridge and the presence of partially open and conductive joints.

This emphasizes the significance of considering the long-term stability of pressure tunnels against instabilities caused by pressure transients, taking into account the start sequence and shutdown duration. The start sequence induces more HI and MPD, while the shutdown duration is a key parameter that affects HI and MPD. Therefore, new design guidelines need to address these aspects to ensure the long-term stability of unlined pressure tunnels.

8.9 Operational requirements

Hydropeaking refers to the rapid changes in hydropower production that occur in response to fluctuations in electricity generation and demand on the electricity market (Bakken et al., 2021). Hydropeaking is related to start and stop sequence in hydropower operations. To safeguard the environment, certain restrictions are imposed on the change in amplitude of discharge, rate of change of water level, and frequency of discharge and water level changes during hydropeaking. In some hydropower, there are also regulations for hydropeaking due to electromechanical constraints (Neupane, Panthi, et al., 2021). Coordinating factors with the start and stop sequence and shutdown duration can help minimize the hydraulic impact on tunnels, safeguard electromechanical equipment and protect environment simultaneously. This approach creates a win-win situation for all factors considered.

9 Conclusions and recommendations

9.1 Conclusions

This study analyzed pore water pressure data from Roskrepp hydropower, available for the period from 2018 to 2023, for understanding the effect of frequent start and stop sequences of hydropower in unlined pressure tunnels. A framework was developed to analyze data and quantify the impact caused by transients in rock mass of unlined pressure tunnels. Additionally, UDEC modelling was also used to simulate the long-term operational fatigue of joints. Based on the results of this study, the following conclusions can be derived:

- The impact of start sequence on the rock mass due to transient induced cyclic loading is greater than the impact of the stop sequence. Numerical analysis shows that the stop sequence produces three times as much high intensity (HI) as the start sequence over the study period.
- The analysis of pore pressure data reveals that the duration of shutdown is the key factor influencing HI. Specifically, when the shutdown duration is reduced by half, the HI increases by five times.
- The effect of pressure transients in rock mass is greatly influenced by the condition and properties of joint, its geometry and wall properties.
- HI and MPD can be used as complementary values to quantify the impact of hydraulic transient in unlined pressure tunnel.
- The response of pore pressure in boreholes is greatly influenced by the condition and properties of joint, its geometry and wall properties.
- LSTM method was able to predict the borehole pressure with tunnel water pressure in stop sequence. The MSE and R2 for calibration was 0.0055 and 0.82 respectively. However, it cannot be employed to predict the boreholes that change its characteristics for now and is prospect for future research.
- Numerical modelling shows that there is increased in total and shear displacement in blocks in the tunnel. The maximum total displacement for rough, smooth and slickensided joint is 6.1, 8.51 and 9.64 mm respectively. The maximum shear displacement is 5, 7 and 8 mm respectively. This shows that the cyclic fatigue induce joint degradation causes increased block displacement which provides impression of reduced stability of tunnel.

9.2 Limitations

The study is based on the analysis of the available long-term instrumentation data of tunnel water and bore hole pressure. Analysis begins with raw and non-interpolated data which may sometimes be affected by pipe blockages or leaks. The quality and representativeness of data may vary over time.

Site visit is a comprehensive approach for gaining firsthand understanding and visualization of actual conditions of rock mass around the instrumentation location. However, due to various constraints, a site visit was not possible during this study, limiting the direct observation and assessment of the site.

The time duration between the start of the shutdown and when the tunnel water pressure reaches its peak value was considered as the shutdown duration in this study. However, the computation of shutdown duration depends on the valve closure time data, which was not available for every shutdown event. Therefore, it is important to note that the absence of this data could potentially impact the results of this study.

The lack of power plant log data during the study made it difficult to determine whether a transient event was a complete shutdown/startup or a load change event. Therefore, in this study, a stop sequence was treated as a complete shutdown event and a start sequence as a complete start event. As a result, the effect of transient solely due to load changes on the rock mass could not be investigated.

In the UDEC modeling, the focus was on studying the block displacements caused by changes in roughness parameters. However, the actual impact of cyclic loading resulting from hydraulic transients on the joint system and its roughness parameters were not known. Therefore, an approximation was used to assess the scenario when the roughness deteriorated due to transients. It is important to mention that these displacement values were relative and could not be validated based on the site conditions.

Concepts of digital signal processing have played a significant role in analysis of pore pressure data. As a civil engineer, the exposure and familiarity with digital signal processing was limited, which may have constrained the depth and extent of the study in this particular field.

The results presented in this study are from the analysis from bore hole readings of a hydropower project at specified location and generalization cannot be made based only on this study.

Finally, the research and engineering work which is carried out in this study is for an educational purpose. Some assumptions have also been made, particularly in UDEC modelling, which may sometimes be considered inappropriate in a professional engineering context or design.

9.3 Recommendations

This study recommends minimizing the shutdown duration so that the impact caused by start and stop of hydropower in rock joints of unlined tunnels and shaft could be minimized, enhancing their lifetime. Based on results from instrumentation, shutdown durations longer than 100s seem to deliver lowest impact on rock mass due to transients. Similar analysis are necessary to quantify the recommended shutdown duration in other power plants.

It is also recommended to increase the number of instrumentation programs in other projects particularly where block falls are expected to better improve the understanding of transient induced instabilities in unlined pressure tunnels. The instrumentation has been done for recording pressure in the bore holes and not the deformation of joints. When the difference in pressure between tunnel and inside the joint changes, stresses acting on it vary too and may cause micro displacement. The permeability increases and the strength and stiffness decrease with these displacements (Hakami, 1995). The information on deformation of joints would help to validate the numerical model. Similarly, the model that incorporates stress-displacement-dilation-conductivity coupling of joints would be more helpful for representing the complex relationship between joint and tunnel water pressure during transients.

The cyclic loading or fatigue test of the specimen is necessary to characterize the strength and failure mechanisms of a material in fatigue. There should be differentiation of failure due to cycling loading induced by transients or gravity induced block falls that helps to further investigate and mitigate the challenges posed by transients in long-term functionality of unlined pressure tunnel. So, laboratory test of the rock specimen from failure sites with regard to crack propagation is necessary for this differentiation. Fatigue test of rock from the site would also help in better characterization of the failure process of the rock in cyclic loading.

It is recommended that the state-of-the-art design guidelines for unlined pressure tunnels be updated to address stability issues arising from pressure transients. Special attention should be given to the start sequence to ensure long-term serviceability of unlined pressure tunnels. This study also recommends implementing a more conservative design approach, particularly in tunnels with weak rock masses and projects that involve frequent load changes.

During the next site visit, it is advisable to inspect the functionality of BH2 and BH5 to determine if they are in proper working condition.

References

Bakken, T. H., Harby, A., Forseth, T., Ugedal, O., Sauterleute, J. F., Halleraker, J. H., & Alfredsen, K. (2021). Classification of hydropeaking impacts on Atlantic salmon populations in regulated rivers. *River Research and Applications*. https://doi.org/10.1002/RRA.3917

Barton, N. (2002). Some new Q-value correlations to assist in site characterisation and tunnel design. *International Journal of Rock Mechanics and Mining Sciences*, *39*(2), 185–216. https://doi.org/10.1016/S1365-1609(02)00011-4

Barton, N. (2013). Shear strength criteria for rock, rock joints, rockfill and rock masses: Problems and some solutions. *Journal of Rock Mechanics and Geotechnical Engineering*, *5*(4), 249–261. https://doi.org/10.1016/J.JRMGE.2013.05.008

Barton, N., & Bandis, S. (1990). Review of predictive capabilities of JRC-JCS model in engineering practice. *Proceedings: International Conference on Rock Joints*, *Balkema*, *Rotterdam*.

Barton, N., Bandis, S., & Bakhtar, K. (1985). Strength, deformation and conductivity coupling of rock joints. *International Journal of Rock Mechanics and Mining Sciences & Geomechanics Abstracts*, *22*(3), 121–140. https://doi.org/10.1016/0148-9062(85)93227-9

Barton, N., & Choubey, V. (1977). The shear strength of rock joints in theory and practice. *Rock Mechanics Felsmechanik Mécanique Des Roches*, *10*(1–2), 1–54. https://doi.org/10.1007/BF01261801/METRICS

Basnet, C. B., & Panthi, K. K. (2018). Analysis of unlined pressure shafts and tunnels of selected Norwegian hydropower projects. *Journal of Rock Mechanics and Geotechnical Engineering*, *10*(3), 486–512. https://doi.org/10.1016/J.JRMGE.2017.12.002

Belem, T., Mountaka, S., & Homand, F. (2007). Modeling surface roughness degradation of rock joint wall during monotonic and cyclic shearing. *Acta Geotechnica*, *2*(4). https://doi.org/10.1007/s11440-007-0039-7

Benson, R. P. (1989). Design of unlined and lined pressure tunnels. *Tunnelling and Underground Space Technology Incorporating Trenchless*, *4*(2), 155–170. https://doi.org/10.1016/0886-7798(89)90049-7

Bergh-Christensen, J., & Dannevig, N. (1971). Engineering geological evaluations of the

unlined pressure shaft at the Mauranger hydropower plant (in Norwegian). *Unpublished Report, Geoteam A/S, Oslo, Norway*.

Bhattarai, K. P., Zhou, J., Palikhe, S., Pandey, K. P., & Suwal, N. (2019). Numerical Modeling and Hydraulic Optimization of a Surge Tank Using Particle Swarm Optimization. *Water 2019, Vol. 11, Page 715*, *11*(4), 715. https://doi.org/10.3390/W11040715

Bieniawski, Z. T. (1993). Classification of Rock Masses for Engineering: The RMR System and Future Trends. *Comprehensive Rock Engineering. Vol. 3*, 553–573. https://doi.org/10.1016/B978-0-08-042066-0.50028-8

Bøe, S. (2020). *Ingeniørgeologisk kartlegging og numerisk modellering i UDEC og RS2, med parameterstudier, for Fornebubanen (in Norwegian)*. Norges teknisk-naturvitenskapelige universitet.

Bråtveit, K., Bruland, A., & Brevik, O. (2016). Rock falls in selected Norwegian hydropower tunnels subjected to hydropeaking. *Tunnelling and Underground Space Technology*, *52*, 202–207. https://doi.org/10.1016/J.TUST.2015.10.003

Bredesen, H.-A. (2016). The Nord Pool Market Model. *Asean Energy Market Integration (Aemi)*, 20. http://www.asean-aemi.org/wp-content/uploads/2016/03/AEMI-Forum-November-2015-Bredesen-Feb2016.pdf

Broch, E. (1984a). The development of unlined pressure shafts and tunnels in Norway. *Underground Space*, *8*, 177–184.

Broch, E. (1984b). Unlined high pressure tunnels in areas of complex topography. *Int. Water Power Dam Constr.; (United Kingdom)*, 21–23.

Burdine, N. T. (1963). Rock Failure Under Dynamic Loading Conditions. *Society of Petroleum Engineers Journal*, *3*(01), 1–8. https://doi.org/10.2118/481-PA

Butterworth, S. (1930). On the Theory of Filter Amplifiers. *Experimental Wireless and the Wireless Engineer*, 536–541.

Bye, T., & Hope, E. (2005). Deregulation of Electricity Markets: The Norwegian Experience. *Economic and Political Weekly*, *40*(50), 5269–5278.

Cerfontaine, B., & Collin, F. (2018). Cyclic and Fatigue Behaviour of Rock Materials: Review, Interpretation and Research Perspectives. *Rock Mechanics and Rock Engineering*, *1*, 3. https://doi.org/10.1007/s00603-017-1337-5

Chaudhry, H. (2014). *Applied Hydraulic Transients Third Edition*. Springer.

Choi, S. O., Chung, S.-K., Xing, Y., Wang, J., Zhao, Z., Gao, A., & Lamberg, M. S. M. (2004). Stability Analysis of Jointed Rock Slopes with the Barton-Bandis Constitutive Model in UDEC. *International Journal of Rock Mechanics and Mining Sciences*, *41*(3).

Costin, L. S., & Holcomb, D. J. (1981). Time-dependent failure of rock under cyclic loading. *Tectonophysics*, *79*(3–4), 279–296. https://doi.org/10.1016/0040-1951(81)90117-7

Dolphin, R. (2020). *LSTM Networks | A Detailed Explanation |* . Towards Data Science. https://towardsdatascience.com/lstm-networks-a-detailed-explanation-8fae6aefc7f9

Energifakta. (2021). *KRAFTPRODUKSJON*. https://energifaktanorge.no/norsk-energiforsyning/kraftforsyningen/

Erarslan, N., Alehossein, H., & Williams, D. J. (2014). Tensile Fracture Strength of Brisbane Tuff by Static and Cyclic Loading Tests. *RMRE*, *47*(4), 1135–1151. https://doi.org/10.1007/S00603-013-0469-5

Erarslan, N., & Williams, D. J. (2012). Investigating the effect of cyclic loading on the indirect tensile strength of rocks. *Rock Mechanics and Rock Engineering*, *45*(3), 327–340. https://doi.org/10.1007/S00603-011-0209-7/FIGURES/18

Eurelectric. (2011). Hydro in Europe: Powering Renewables. In *Brussels, Belgium, 2011*.

Fathi, A., Moradian, Z., Rivard, P., & Ballivy, G. (2016). Shear mechanism of rock joints under pre-peak cyclic loading condition. *International Journal of Rock Mechanics and Mining Sciences*, *83*, 197–210. https://doi.org/10.1016/J.IJRMMS.2016.01.009

Fei, F., & Choo, J. (2023). Extended Barton–Bandis model for rock joints under cyclic loading: Formulation and implicit algorithm. *International Journal for Numerical and Analytical Methods in Geomechanics*, *47*(3), 349–369. https://doi.org/10.1002/NAG.3472

Ghamgosar, M., & Erarslan, N. (2016). Experimental and Numerical Studies on Development of Fracture Process Zone (FPZ) in Rocks under Cyclic and Static Loadings. *Rock Mechanics and Rock Engineering*, *49*(3), 893–908. https://doi.org/10.1007/S00603-015-0793-Z/FIGURES/15

Gischig, V., Preisig, G., & Eberhardt, E. (2016). Numerical investigation of seismically induced rock mass fatigue as a mechanism contributing to the progressive failure of deep-seated landslides. *Rock Mechanics and Rock Engineering*, *49*(6), 2457–2478. https://doi.org/10.1007/S00603-015-0821-Z/FIGURES/16

Goodman, R. E. (1989). *Introduction to Rock Mechanics* (2nd Editio). John Wiley & Sons.

Gudmundsson, A. (2000). Fracture dimensions, displacements and fluid transport. *Journal of Structural Geology*, *22*(9), 1221–1231. https://doi.org/10.1016/S0191-8141(00)00052-3

Gudmundsson, A., Berg, S. S., Lyslo, K. B., & Skurtveit, E. (2001). Fracture networks and fluid transport in active fault zones. *Journal of Structural Geology*, *23*(2–3), 343–353. https://doi.org/10.1016/S0191-8141(00)00100-0

Halliwell, A. R. (1963). Velocity of a Water-Hammer Wave in an Elastic Pipe. *Journal of the Hydraulics Division*, *89*(4), 1–21. https://doi.org/10.1061/JYCEAJ.0000897

Hashash, Y. M. A., Hook, J. J., Schmidt, B., & I-Chiang Yao, J. (2001). Seismic design and analysis of underground structures. *Tunnelling and Underground Space Technology*, *16*(4), 247–293. https://doi.org/10.1016/S0886-7798(01)00051-7

Helwig, P. C. (1987). A theoretical investigation into the effects of water hammer pressure surge on rock stability of unlined tunnels. *Hydropowers'87*, 881–828.

Hoek, E. (1994). Strength of rock and rock masses. *ISRM News Journal*, *2*, 4–16.

Hoek, E. (2006). *Practical Rock Engineering*. https://doi.org/10.2113/gseegeosci.14.1.55

Hoek, E., Carranza-Torres, C., & Corkum, B. (2002). Hoek-Brown failure criterion - 2002 Edition. *NARMS-TAC Conference*, 267–273.

Holmøy, K. H. (2008). *Significance of geological parameters for predicting water leakage in hard rock tunnels*. Norwegian University of Science and Technology.

Hudson, J. A., & Harrison, J. P. (1997). Engineering Rock Mechanics. In *Elsevier Science*.

IRENA. (2018). Global energy transformation, A roadmap to 2050. In *Global Energy Transformation: Four Necessary Steps to Make Clean Energy the Next Success Story*. https://doi.org/10.1057/9780230244092

IRENA. (2022). *Renewable Energy Statistics 2022*. www.irena.org

ISRM. (1978). Suggested methods for the quantitative description of discontinuities in rock masses: International Society for Rock Mechanics. *International Journal of Rock Mechanics and Mining Science & Geomechanics*, *15*, 319–368.

ITASCA. (2011). *UDEC Version 5.0 User's Guide*.

ITASCA. (2023a). *Choice of Material Properties*. https://docs.itascacg.com/flac3d700/flac3d/docproject/source/theory/interfaces/choiceofproperties.html

ITASCA. (2023b). *UDEC*. https://www.itascacg.com/software/udec

Jaeger, C. (1953). *Present Trends in Surge Tank Design*.

Jafari, M. K., Pellet, F., Boulon, M., & Hosseini, K. A. (2004). Experimental Study of Mechanical Behaviour of Rock Joints Under Cyclic Loading. *Rock Mechanics and Rock Engineering*, *37*(1), 3–23. https://doi.org/10.1007/S00603-003-0001-4/METRICS

Jing, L. (2003). A review of techniques, advances and outstanding issues in numerical modelling for rock mechanics and rock engineering. *International Journal of Rock Mechanics and Mining Sciences*, *40*(3), 283–353. https://doi.org/10.1016/S1365-1609(03)00013-3

Lee, M., & Barr, B. (2004). An overview of the fatigue behaviour of plain and fibre reinforced concrete. *Cement and Concrete Composites*, *26*(4). https://doi.org/10.1016/S0958-9465(02)00139-7

Lees, T., Reece, S., Kratzert, F., Klotz, D., Gauch, M., De Bruijn, J., Kumar Sahu, R., Greve, P., Slater, L., & Dadson, S. J. (2022). Hydrological concept formation inside long short-term memory (LSTM) networks. *Hydrology and Earth System Sciences*, *26*(12), 3079–3101. https://doi.org/10.5194/HESS-26-3079-2022

Lévesque, L. (2014). Nyquist sampling theorem: Understanding the illusion of a spinning wheel captured with a video camera. *Physics Education*, *49*(6), 697–705. https://doi.org/10.1088/0031-9120/49/6/697

Liu, X. R., Kou, M. M., Lu, Y. M., & Liu, Y. Q. (2018). An experimental investigation on the shear mechanism of fatigue damage in rock joints under pre-peak cyclic loading condition. *International Journal of Fatigue*, *106*, 175–184. https://doi.org/10.1016/J.IJFATIGUE.2017.10.007

Lyons, R. G. (2011). *"Infinite Impulse Response Filters," Understanding Digital Signal Processing* (3rd ed.). Pearson.

Maklin, C. (2019). *Fast Fourier Transform*. Towards Data Science. https://towardsdatascience.com/fast-fourier-transform-937926e591cb

Mosonyi, E. (1991). *High-Head Power Plants: Vol. Two/A*. Akadémiai Kiadó.

Nemcik, J., Mirzaghorbanali, A., & Aziz, N. (2014). An Elasto-Plastic Constitutive Model for Rock Joints Under Cyclic Loading and Constant Normal Stiffness Conditions. *Geotechnical and Geological Engineering*, *32*(2), 321–335.

https://doi.org/10.1007/S10706-013-9716-5/FIGURES/13

Neupane, B. (2021). *Long-term impact on unlined tunnels of hydropower plants due to frequent start/stop sequences*. Norwegian University of Science and Technology.

Neupane, B., & Panthi, K. K. (2018). Effect of Pressure Fluctuations in Long-term Stability of Unlined Pressure Shaft at Svandalsflona Hydropower Project, Norway. *10th Asian Rock Mechanics Symposium*.

Neupane, B., & Panthi, K. K. (2021). Evaluation on the Effect of Pressure Transients on Rock Joints in Unlined Hydropower Tunnels Using Numerical Simulation. *Rock Mechanics and Rock Engineering*, *54*(6), 2975–2994. https://doi.org/10.1007/s00603-021-02418-x

Neupane, B., Panthi, K. K., & Vereide, K. (2020). Effect of Power Plant Operation on Pore Pressure in Jointed Rock Mass of an Unlined Hydropower Tunnel: An Experimental Study. *Rock Mechanics and Rock Engineering*, *53*(7), 3073–3092. https://doi.org/10.1007/s00603-020-02090-7

Neupane, B., Panthi, K. K., & Vereide, K. (2021). Cyclic fatigue in unlined hydro tunnels caused by pressure transients. In *Article in International Journal on Hydropower and Dams*. https://www.researchgate.net/publication/356264255

Neupane, B., Vereide, K., & Panthi, K. K. (2021). Operation of Norwegian hydropower plants and its effect on block fall events in unlined pressure tunnels and shafts. *Water (Switzerland)*, *13*(11). https://doi.org/10.3390/w13111567

NFF. (2013). *Norwegian Hydropower Tunnelling II*. *22*.

Nilsen, B., & Thidemann, A. (1993). *Rock Engineering*. Norwegian Institute of Technology, Division of Hydraulic Engineering.

Nordpoolgroup. (2023). *Price Formation*. https://www.nordpoolgroup.com/en/the-power-market/Day-ahead-market/Price-formation/

Odling, N. E. (1997). Scaling and connectivity of joint systems in sandstones from western Norway. *Journal of Structural Geology*, *19*(10), 1257–1271. https://doi.org/10.1016/S0191-8141(97)00041-2

Olsson, R., & Barton, N. (2001). An improved model for hydromechanical coupling during shearing of rock joints. *International Journal of Rock Mechanics and Mining Sciences*, *38*(3), 317–329. https://doi.org/10.1016/S1365-1609(00)00079-4

Palmström, A., & Broch, E. (2017). The design of unlined hydropower tunnels and shafts: 100

years of Norwegian experience. *Hydropower & Dams*, *3*. www.RockMass.net

Panthi, K. K. (2006). Analysis of engineering geological uncertainties related to tunnelling in Himalayan rock mass conditions. In *Norwegian University of Science and Technology*.

Panthi, K. K. (2017). Review on the prevailing methods for the prediction of potential rock burst / rock spalling in tunnels. *Norsk Forening for Fjellsprengningsteknikk, Norsk Bergmekanikkgruppe Og Norsk Geoteknisk Forening Oslo*, 572.

Panthi, K. K., & Basnet, C. B. (2016). Review on the Major Failure Cases of Unlined Pressure Shafts/Tunnels of Norwegian Hydropower Projects. *Hydro Nepal: Journal of Water, Energy and Environment*, *18*, 6–15. https://doi.org/10.3126/HN.V18I0.14637

Panthi, K. K., & Basnet, C. B. (2018). State-of-the-art design guidelines in the use of unlined pressure tunnels / shafts for hydropower scheme. *ISRM International Symposium - 10th Asian Rock Mechanics Symposium, ARMS 2018, March 2019*.

Panthi, K. K., & Basnet, C. B. (2021). Fluid Flow and Leakage Assessment Through an Unlined/Shotcrete Lined Pressure Tunnel: A Case from Nepal Himalaya. *Rock Mechanics and Rock Engineering*, *54*(4), 1687–1705. https://doi.org/10.1007/S00603-020-02350-6/FIGURES/17

Parmakian, J. (1963). *Waterhammer Analysis*. Dover Publications, Inc.

Patton, F. D. (1966, September 25). Multiple Modes of Shear Failure In Rock. *1st Congress of International Society for Rock Mechanics*.

Pitorac, L., Vereide, K., & Lia, L. (2020). Upgrading hydropower plants to pump storage plants: A hydraulic scale model of the tunnel system. *Proceedings of the 8th IAHR International Symposium on Hydraulic Structures, ISHS 2020*. https://doi.org/10.14264/uql.2020.602

Preisig, G., Eberhardt, E., Smithyman, M., Preh, A., & Bonzanigo, L. (2016). Hydromechanical rock mass fatigue in deep-seated landslides accompanying seasonal variations in pore pressures. *Rock Mechanics and Rock Engineering*, *49*(6), 2333–2351. https://doi.org/10.1007/S00603-016-0912-5/FIGURES/13

Pröll, S. (2022). *Finding peaks in noisy signals (with Python and JavaScript)*. https://www.samproell.io/posts/signal/peak-finding-python-js/

Rancourt, A. J. (2010). *Guidelines for preliminary design of unlined pressure tunnels* (Issue May). McGill University.

Rocscience. (2023). *Geotechnical Finite Element Analysis, Rocscience*. https://www.rocscience.com/software/rs2

Schijve, J. (2009). Fatigue of structures and materials. In *Fatigue of Structures and Materials*. Springer Netherlands. https://doi.org/10.1007/978-1-4020-6808-9/COVER

Selmer-Olsen, R. (1970). Experience with unlined pressure shafts in Norway. *Int. Symposium On Large Permanent Underground Openings, Oslo*.

Selmer-Olsen, R. (1974). Underground openings filled with high-pressure water or air. *Bulletin of the International Association of Engineering Geology-Bulletin de l'Association Internationale de Géologie de l'Ingénieur*, *9*(1), 91–95. https://doi.org/10.1007/BF02635310/METRICS

Serafim, J. ., & Pereira, J. P. (1983). Considerations on the Geomechanical Classification of Bieniawski. Proceedings of International Symposium on Engineering Geology and Underground Openings. *Roceedings of International Symposium on Engineering Geology and Underground Openings, Lisbon, Portugal, 1983*, 1133–1144.

Shrestha, G. L. (2021). *Rock Engineering Handbook on Design of Tunnel and Other Underground Structures*.

Solak, T., & Schubert, W. (2004). *Influence of block size and shape on the deformation behavior and stress development around tunnels* (pp. 695–700). VGE.

Stephansson, O., & Zang, A. (2012). ISRM suggested methods for rock stress estimation-part 5: Establishing a model for the in situ stress at a given site. *Rock Mechanics and Rock Engineering*, *45*(6), 955–969. https://doi.org/10.1007/S00603-012-0270-X/FIGURES/8

Tøndevold, E. (2002). Use of the rock mass as a structural component in underground projects. *Hydropower Tunnelling, NFF Publication no. 3*.

Trivedi, C., Gandhi, B., & Michel, C. J. (2013). Effect of transients on Francis turbine runner life: a review. *Journal of Hydraulic Research*, *51*(2), 121–132. https://doi.org/10.1080/00221686.2012.732971

Tsubota, Y., Kunishi, T., Iwakoke, Y., Yoshinaka, R., & Yamaguchi, K. (2013). Fundamental studies on dynamic properties of rock joint under cyclic loading using mortar and Ryoke gneiss. *Rock Dynamics and Applications - State of the Art*, 225–232. https://doi.org/10.1201/B14916-24

Voznesenskii, A. S., Kutkin, Y. O., Krasilov, M. N., & Komissarov, A. A. (2015). Predicting

fatigue strength of rocks by its interrelation with the acoustic quality factor. *International Journal of Fatigue*, *77*, 194–198. https://doi.org/10.1016/J.IJFATIGUE.2015.02.012

Wang, Z., Li, S., Qiao, L., & Zhang, Q. (2015). Finite element analysis of the hydro-mechanical behavior of an underground crude oil storage facility in granite subject to cyclic loading during operation. *International Journal of Rock Mechanics and Mining Sciences*, *73*, 70–81. https://doi.org/10.1016/J.IJRMMS.2014.09.018

Witherspoon, P. A., Wang, J. S. Y., Iwai, K., & Gale, J. E. (1980). Validity of Cubic Law for fluid flow in a deformable rock fracture. *Water Resources Research*, *16*(6), 1016–1024. https://doi.org/10.1029/WR016I006P01016

Wylie, E. B., & Streeter, V. L. (1978). *Fluid Transients*. McGraw-Hill Inc.

Yang, Z. Y., Taghichian, A., & Li, W. C. (2010). Effect of asperity order on the shear response of three-dimensional joints by focusing on damage area. *International Journal of Rock Mechanics and Mining Sciences*, *47*(6), 1012–1026. https://doi.org/10.1016/J.IJRMMS.2010.05.008

Zang, A., Yoon, J. S., Stephansson, O., & Heidbach, O. (2013). Fatigue hydraulic fracturing by cyclic reservoir treatment enhances permeability and reduces induced seismicity. *Geophysical Journal International*, *195*(2), 1282–1287. https://doi.org/10.1093/GJI/GGT301

Zhou, H., Abdelaziz, A., & Grasselli, G. (2018). Rock Dilation and Its Effect on Fracture Transmissivity. *SPE/AAPG/SEG Unconventional Resources Technology Conference 2018, URTC 2018*. https://doi.org/10.15530/URTEC-2018-2903018

Personal Communication

Alfredsen, Knut (2023), Professor in Hydrology, Department of Hydraulic and Environmental Engineering, a meeting at his office.

Bøe, Susanne (2023), Engineering Geologist in Norconsult AS, two mail correspondences.

Neupane, Bibek (2023), Senior Engineering Geologist, Ramboll, several mail correspondences and one meeting.

Panthi, Krishna Kanta (2023), Professor of Geological Engineering, IGP, NTNU, several meetings at his office.

Vereide, Kaspar (2023), Associate Professor, Department of Civil and Environmental Engineering, NTNU: several mail correspondences and two meetings.

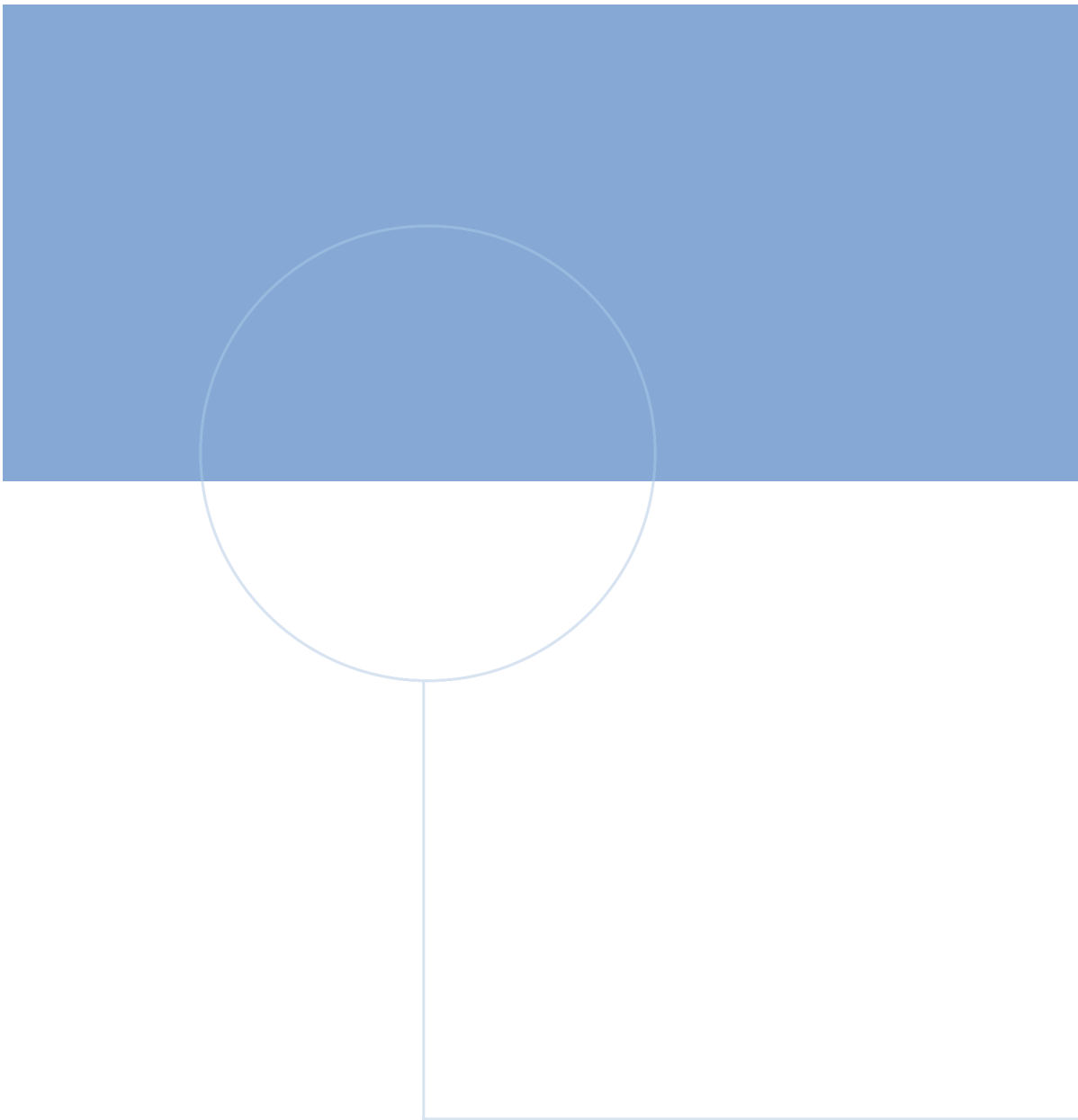

NTNU

Norwegian University of
Science and Technology